Uncertainty Quantification and Representativity Analysis of the LWR-PROTEUS Phase II Experimental Campaign

Thesis · August 2015

DOI: 10.13140/RG.2.1.2168.4240

1 author:

Daniel Siefman

École Polytechnique Fédérale de Lausanne

10 PUBLICATIONS **1** CITATION

SEE PROFILE

Ecole Polytechnique Fédérale de Lausanne

Eidgenössische Technische Hochschule Zürich

For Obataining the degree of Master's of Science in Nuclear Engineering

Uncertainty Quantification and Representativity Analysis of the LWR-PROTEUS Phase II Experimental Campaign

Author:
Daniel J. Siefman

Supervisors:
Professor Andreas Pautz
Dr. Mathieu Hursin

August 14, 2015

Abstract

The LWR-PROTEUS Phase II experimental program was conducted at the Proteus research reactor at the Paul Scherrer Institute (PSI) in the early 2000s. One of its purposes was to gain more insight into the reactivity changes caused by fuel burnup and to develop a sense of confidence in modern codes' ability to predict these changes. The presented project reexamines the experimental campaign using SHARK-X. SHARK-X is a set of Perl-based tools developed at PSI and built around the lattice physics code CASMO-5. It is used to perform sensitivity analysis (SA), uncertainty quantification (UQ), and representativity analysis (RA). This report discusses how SHARK-X was used to quantify the effect of input uncertainties when modeling the LWR-PROTEUS Phase II experiments and to evaluate the representativity of the experiments to a spent fuel pool of the nuclear power plant Gösgen (KKG).

The first objective of the analysis was to apply and assess the performance of SHARK-X for UQ analysis using the stochastic sampling and direct perturbation methods. This process involved modeling the experimental campaign in CASMO-5 and then evaluating the uncertainties in calculated criticality-relevant parameters (e.g. k_{eff}, reactivity) due to input uncertainties. These input uncertainties are associated with nuclear data and fuel compositions. The results of the UQ analysis gave a quantification of the statistical spread about the mean of these calculated criticality parameters. The mean values and statistical spreads were then compared to their respective experimentally measured values to calculate the bias and bias uncertainty of CASMO-5 for this application. CASMO-5 was then validated by using the bias and bias uncertainty in a z-score comparison analysis. Of the eleven samples from the H_2O moderated portion of the experimental campaign analyzed, only one did not have a successful validation.

The second objective was to apply SHARK-X to do uncertainty-based, RA of the experimental campaign to the application of an industrial spent fuel pool. This tested the abilities of SHARK-X to validate a CASMO-5 model of a given application, which in this project was the spent fuel pool of the nuclear power plant Gösgen. Additionally this analysis can help to allow for burnup credit to be taken in the design of spent fuel pools and thus ameliorate financial penalties that can occur due to conservative assumptions applied during criticality safety. The representativity of the experiment to the spent fuel pool was evaluated using a representativity index calculated from the UQ and SA for absolute reactivity worth. When this representativity index has a value of 0.9 or greater, there is a high degree of similarity between an application and an experiment. This means that the experiment can be used as a benchmark for establishing the bias and bias uncertainty of CASMO-5 for a given application which can then be used to validate the application's model. For the spent fuel pool and the LWR-PROTEUS Phase II experimental campaign, the representativity index was calculated for a UO_2 and MOX sample of intermediate

burnup. With H_2O moderation conditions the representativity indices were 0.761 and 0.861 for the UO_2 and MOX samples respectively. With an H_2O moderator containing 2,023 ppm of boric acid, the representativity indices were calculated to be 0.847 and 0.780 respectively. Therefore no sample had the sufficiently high representativity value of 0.9 to be declared representative of the KKG spent fuel pool.

Keywords: Proteus, uncertainty quantification, sensitivity analysis, representativity, validation, spent fuel pool

Contents

List of Figures

List of Tables

Chapter 1

Introduction

This report summarizes an application of the uncertainty quantification and sensitivity analysis (UQ/SA) tool SHARK-X developed at the Paul Scherrer Institut (PSI). SHARK-X was applied to an experiment and an application: the LWR-PROTEUS Phase II experimental campaign and the spent fuel pool of the nuclear power plant Gösgen (KKG, or Kernkraftwerk Gösgen). First SHARK-X was used to validate the lattice physics code CASMO-5 with the experiments done at the Proteus research reactor. Additionally SHARK-X was used to perform representativity analysis with UQ/SA, which is a quantitative method for evaluating the similarity of Proteus' reactivity experiments to one of KKG's spent fuel pools. The main purpose of this work was to successfully apply the SHARK-X tool and create practices and methodologies for validation and representativity analysis. Additionally, the results allow for conclusions to be made concerning the validation of CASMO-5 and the representativity of the experimental campaign to the KKG spent fuel pool.

The first chapter of the report gives an introduction into the concepts of UQ/SA, validation, bias, and representativity analysis. The second chapter describes the LWR-PROTEUS Phase II experimental campaign. Chapter 3 describes SHARK-X's UQ methods called stochastic sampling (SS) and direct perturbation (DP) along with representativity analysis (RA) using representativity indices. Chapter 4 describes the SHARK-X's SS and DP utilities and the CASMO-5 models of Proteus and the KKG spent fuel pool. Chapter 5 presents the results of the UQ analysis for the parameters k_{inf}, k_{eff}, absolute reactivity worth, and relative reactivity worth. Additionally this chapter contains a discussion of the bias and bias uncertainty of the relative reactivity worth parameter and a validation study based on these results. Chapter 6 presents the representativity analysis of the KKG spent fuel pool based on the use of representativity indices. Chapter 7 gives a conclusion and summary of the report along with recommendations for future improvements.

1.1 Validation

A key part of the design and safety assessment of nuclear systems is computer modeling. The modern trend in nuclear engineering modeling is based upon *best-estimate* codes. Best-estimate codes are desirable because they allow to reduce the costs of redundant safety margins, to improve the quality of safety analysis, to help extend the operation of existing nuclear power plants, and to ease the design of complicated Generation IV systems. A best-estimate code must

1. Avoid the purposeful introduction of conservatism.
2. Minimize the use of expert judgement to tune models.
3. Use state-of-the-art methods.

To help objectively classify a code as best-estimate, the accuracy of the code must be proven by *validation* against experiments. Validation is the process in which a code's outputs are compared to experimental results to assess the code's accuracy. The necessity of validation can be seen in many state-of-the-art neutron transport codes (e.g. SCALE [1], MCNP [2], CASMO [3]). These codes can predict k_{eff} with a high degree of precision, or with repeatability and reproducibility. However problems exist with these codes' accuracies, or how close the value they calculate is to the true value in experiment, that is, there is always a difference between the calculated and true value. Thus when modeling critical systems (e.g. spent fuel pools) with one of these codes, it is impossible to perfectly and consistently calculate the criticality of systems.

The accuracy of the simulation, or the difference between the calculated value and the real-world value measured in application, is called the *bias* and is due to different contributions:

- Uncertainties of the input parameters (e.g. geometry, compositions, and especially nuclear data)
- Computational methods used to solve the neutron transport equation (e.g. diffusion theory, Monte Carlo method)
- Modeling approximations (e.g. homogenizing regions or simplifying geometry)

This bias is why standards for nuclear criticality safety analysis (e.g. ANSI/ANS-8.1-1998 [4] and ANSI/ANS-8.24-2007 [5]) require the validation of the analytical methods and nuclear data used in calculations. Validation establishes the credibility of a code for an application by quantifying the bias and the bias' uncertainty. Often when simulating a given application, experimental results do not exist and thus cannot be used to calculate the bias of the code system for the application. In instances like this, validation is done by comparing computed results with critical *benchmarks*, which are based on experimental data from critical systems[1].

Choosing a benchmark for validation is typically undertaken using similarity studies between the benchmark and the application of interest. Traditionally the benchmark choice is based off of finding its physical characteristics that are similar to the application. These characteristics can be the fissile elements present, the fissile concentration, the moderator type, the geometrical configuration, the hydrogen-to-fissile atom ratio, the average energy of neutrons causing fission, or the average neutron lethargy causing fission [8]. A series of benchmarks are then selected and trending analysis applied to their biases as a function of the previously described physical characteristics (fissile concentration, etc.). Once a benchmark is found to be suitable, it is then chosen as the basis for establishing the application's bias [6]. The next step in validation is to model the chosen benchmark in the same code with the same cross-section data as the application. Then the difference between the experimental quantity (e.g. k_{eff}) of the benchmark is compared

[1]There is a difference between critical benchmarks and critical experiments. Critical benchmarks are critical experiments that have been peer reviewed. They have relatively detailed descriptions of experimental conditions and can be repeatedly and consistently modeled by qualified specialists. In other words, all critical benchmarks are critical experiments, however not all critical experiments are critical benchmarks.

to the benchmark's calculated value with the code. This establishes the computational bias for the experimental benchmark. Next the benchmark's bias is used to calculate the application's computational bias.

Modern approaches used in SHARK-X and the TSUNAMI sequence of SCALE-6 [1] use advanced tools to assess the similarity of applications to benchmarks. The basis of these tools is that the computational biases seen are mainly caused by uncertainties in nuclear data. The nuclear data uncertainties are propagated through the system to find the uncertainty in the computed value. Sensitivity coefficients are also calculated and used with uncertainties to compute correlation coefficients between the benchmark and the application, which are used as the basis for choosing a given benchmark. This technique of quantifying the similarity between a benchmark and the application is called *representativity analysis* (RA) and is discussed further in Section 1.3.

1.2 Bias

The bias, b_c, between a calculated value, C, and an experimental value, E, is quantified as shown in Equation 1.1. A perfectly unbiased result (i.e. the code perfectly predicts the experimental value) would have a b_c value of 1.0.

$$b_c = \frac{C}{E} \tag{1.1}$$

Left out of this calculation of the bias in Equation 1.1 is the fact there are uncertainties associated with both C and E. In criticality safety analysis, the uncertainties associated with C could be the composition of the fissile material input into the code, or the nuclear data used in the neutron transport calculations. The experimental value will always have experimental uncertainties associated with it, which in nuclear systems can come from many sources (e.g. detector efficiencies and statistics). This means that C and E really exist with associated uncertainties as $C \pm \sigma_C$ and $E \pm \sigma_E$ and thus the uncertainty of bias between the calculated and experimental result is given by Equation 1.2.

$$\sigma_{b_c} = b_c \sqrt{\left(\frac{\sigma_C}{C}\right)^2 + \left(\frac{\sigma_E}{E}\right)^2} \tag{1.2}$$

Without access to UQ, and thus without knowledge of σ_C, the validation procedure has three possible outcomes [7]:

1. *Complete success*: C is within a number of standard deviations (often two standard deviations of σ_E) from the experimental result,

$$|C - E| \leq 2\sigma_E \tag{1.3}$$

2. *Partial success*: C is within some expert defined tolerance, ε, but outside the previous two-standard-deviation bounds,

$$|C - E| \leq \varepsilon \tag{1.4}$$

3. *Failure*: C is outside the defined tolerance ε,

$$|C - E| > \varepsilon \tag{1.5}$$

A major problem with this procedure is the definition of ε. This tolerance is based on expert experience with the given type of prediction. The subjectivity involved in defining this parameter violates the "no expert judgement" criteria for best-estimate codes. The degree of subjectivity necessary in choosing a benchmark can be decreased with the use of UQ/SA. By using UQ/SA, the calculation uncertainty, σ_C, is quantified and then used for calculating σ_{b_c}. Then b_c and σ_{b_c} are used in a different validation test, where the calculation is validated to a z-score tolerance, ε_z, as shown in Equation 1.6 [7].

$$\frac{|b_c - 1|}{\sigma_{b_c}} \leq \varepsilon_z \tag{1.6}$$

The meaning of a z-score for a normal distribution is shown in Figure 1.1 in relation to standard deviations, cumulative percentages, and percentiles. A two standard deviation level of validation, or a z-score of 2.0 level of validation, means that ε_z is equal to 2.0 and the term seen in Equation 1.6 must be less than or equal to 2.0. The advantage of this z-score tolerance approach is fast validation and easy comparison between many cases because the methodology is straightforward and the comparison between cases is relative.

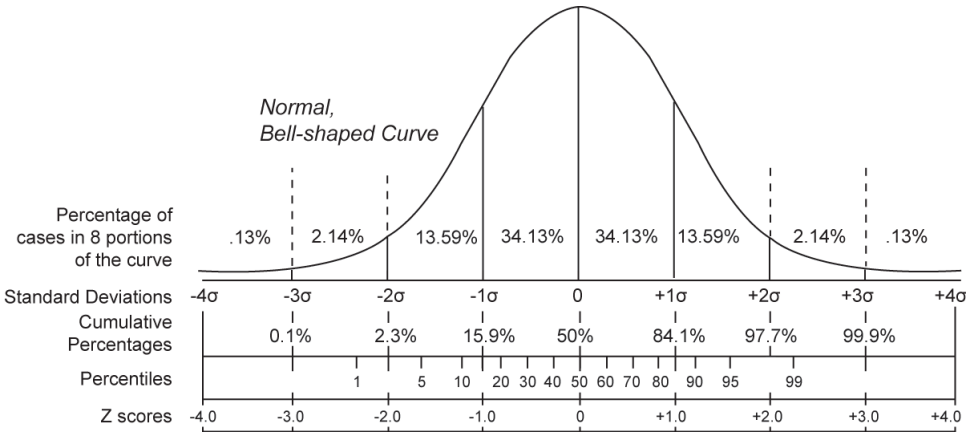

Figure 1.1 – Relation of z-scores to other grading methods for a normal distribution [9].

The importance of knowing σ_{b_c} can be seen when examining the validation of a hypothetical critical system both with and without UQ: Measurements by engineers show that the system is critical, that the measured value, E, of k_{eff} is equal to 1.00000. Calculations by engineers with their favorite code show that the system is not critical, that C of k_{eff} is equal to 0.97000. If b_c is evaluated without considering uncertainties (Equation 1.1), the engineers may derive the conclusion that the bias is significant, that b_c is far from 1.0.

But what if the uncertainty associated with C and E is large? There can be significant uncertainties associated with the nuclear data (e.g. cross sections, $\bar{\nu}$, fission spectra) that are used in computational simulations. There can also be significant uncertainties associated with the experimental value. If these uncertainties are accounted for, error bars could be placed on b_c that indicate that its value could be 1.0 given its own statistical spread. This means that what the engineers previously believed was a significant bias, may not be significant due to inherent uncertainties in the inputs of the calculation and the experiment.

1.3 Representativity Analysis

Representativity analysis is employed in validation to discern how representative an integral experiment, like the LWR-PROTEUS Phase II campaign, is of a NPP application, e.g. a spent fuel pool. In other words, it helps to determine the applicability of an experiment as a benchmark in validating code systems for a given application. When an experiment is deemed representative of an application, it is then possible to validate the application's model in a given code system by determining the application's bias and bias uncertainty by using the experiment as a benchmark [8].

To quantitatively determine the representativity of an experiment to an application, it is necessary to use *integral indices* based UQ/SA. Validation could be done without integral indices using vectors of sensitivity coefficients for a given response to nuclear data. These vectors however are cumbersome and the large volume of information associated with them is often too large for general use. Therefore the integral indices are used as a parameter to synthesise this information and turn it into an easily understood and calculated value [6].

The integral index used in this report is uncertainty and sensitivity based and represented by the variable c_{res}, where res is a given response. Typically in criticality analyses k_{eff} is used as the response that leads to the calculation of c_k. Other responses can be used as well, which in this analysis includes reactivity coefficients, $c_{\Delta\rho}$. This is the preferred index for representativity quantification and is excellent for reducing the use of expert judgement, a requirement in the use of best-estimate code systems. A value of zero for c_{res} represents no correlation between the systems. A value of 1.0 indicates full correlation. For benchmark selection purposes, if c_{res} has a value greater than 0.9, the experiment is considered to be highly representative of the given application.

Chapter 2

The LWR-PROTEUS Phase II Experiments

Phase II of the LWR-PROTEUS campaign was dedicated to experimentally investigating the reactor physics of well-characterised, high-burnup fuel samples from Swiss NPPs. Reactivity measurements were performed with samples cut from the fuel rods of these Swiss NPPs to investigate the effect of burnup upon reactivity. The reactivity worth of each sample was measured by inserting it into the core of Proteus. Afterwards, chemical assays were done at the PSI hot laboratory to identify the concentrations of actinides and fission products in the irradiated fuel. The results were and are now, in this report, being used to validate codes for predicting the composition and reactivity of fuel with burnup [13] [10].

2.1 Proteus Description

Proteus is a zero-power (maximum 1 kW and flux of 5×10^9 n/s-cm^2) nuclear research reactor that operated from 1968 to 2011 at PSI [11]. During its operation history, it was used for several experimental campaigns investigating reactor concepts like the gas-cooled fast reactor, the high-conversion light water reactor, the high temperature reactor, and the light water reactor (LWR). Its use in the 21st century was mainly devoted to studying fuels used in LWRs. These groups of experiments are called the LWR-PROTEUS campaigns, of which the second campaign, Phase II [13], is investigated in this report.

Proteus in Greek mythology is the son of Poseidon and a god of seas, rivers, and in general water. Often he was ascribed to be the god of "elusive sea change", suggesting that he was behind the capriciousness of the sea. The adjective "protean" is derived from Proteus, with the general meaning of "versatile," "mutable," or "capable of assuming many forms" [12]. "Protean" has positive connotations of flexibility, versatility and adaptability and is thus a excellent derivation of the moniker for this research reactor. This is because the reactor has a cavity at its center (1.2 m in diameter) which can be filled with the desired experimental configuration. Around the cavity, seen in Figure 2.1, is a graphite region with 5 w.% enriched UO_2 pins that drive the criticality of the reactor.

Figure 2.1 – Proteus' configuration during the LWR-PROTEUS programs [11].

2.2 The Experimental Campaign

Proteus was configured during this experimental campaign to represent a LWR. In the reactor's central cavity was a test zone consisting of an Al tank in which there were nine full-length assemblies arranged in a 3×3 matrix. Eight of these were full-sized, Optima2, BWR assemblies (10×10 pins, 5 w.% enriched UO_2) and the central assembly was an 11×11 array of fresh, 4.3 w.% enriched, UO_2, PWR fuel rods. The center pin of the PWR assembly was removed and existed as a guide tube through which the previously discussed samples were inserted and withdrawn to vary reactivity. This central core region can be seen in Figure 2.2.

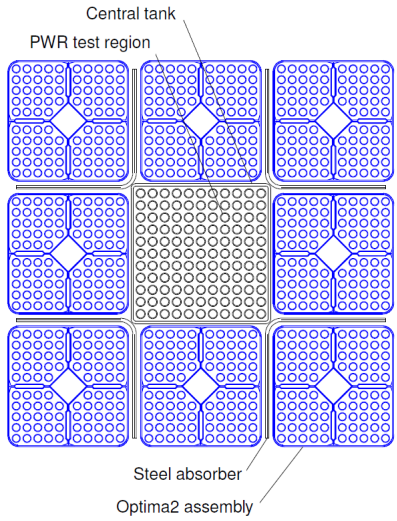

Figure 2.2 – Central test region during the experimental campaign [10].

The PWR assembly was placed in a stainless steel tank allowing for different moderating conditions to exist there than in the BWR assemblies. The moderating conditions of the PWR assembly investigated in the experiment were

- Full-density H_2O at atmospheric temperature and pressure (ATP),

- A mixture of H_2O and D_2O (37.0 w% D_2O at ATP),
- And borated H_2O (2,023 ± 46 ppm of boric acid) at ATP.

The full-density H_2O moderator was used to produce a standard neutron spectrum that might be seen in criticality safety situations at ATP. The D_2O/H_2O moderator was used to simulate the H number density that exists during PWR operations, and thus the harder neutron spectrum at these conditions. The BWR assemblies were all moderated by pure H_2O at ATP.

2.2.1 Sample Compositions

This report discusses eleven burnt fuel rod samples (seven UO_2, four MOX) that were taken from the Gösgen-Däniken PWR (KKG). The samples varied in their degree of burnup, ranging from ∼21 to ∼121 MWd/kg, and provided a spectrum of burnups for which experimental data could be obtained. The samples were prepared at the PSI hot laboratory and enclosed in a Zircaloy over-clad. Each sample was approximately 40 cm long and cut from the center of the fuel rods to avoid gradients in burnup that may exist at the axial rod extremities.

In this document, the samples are identified either as "U" for the UO_2 samples or "M" for the MOX samples. Each sample within a class (U or M) then has a corresponding identification number that corresponds to increasing values of burnup. Thus for the seven U samples, 1 indicates the lowest burnup and 7 the highest. A summary of the samples in this identification system is given in Table 2.1. A different nomenclature is used with Proteus' documentation, where each sample is named UR and then a number (e.g. UR1) with the numbers based on the chronological order of the sample's use in the experiment. The problem with this system is that it gives no indication of fuel type or burnup and makes the analyses harder to understand. A complete history of each sample's irradiation can be found in Ref. [10].

Table 2.1 – Descriptions of the fuel samples [14].

ID	Proteus ID	Type	# of Cycles	Burnup (MWd/kg)
U1	UR7	UO_2	3	∼38
U2	UR3	UO_2	3	∼54
U3	UR5	UO_2	5	∼71
U4	UR4	UO_2	5	∼75
U5	UR2	UO_2	3	∼91
U6	UR1	UO_2	7	∼92
U7	UR11	UO_2	10	∼121
M1	UR6	MOX	1	∼21
M2	UR8	MOX	2	∼44
M3	UR9	MOX	3	∼64
M4	UR10	MOX	4	∼72

2.2.2 Radiochemical Analyses

Radiochemical, post-irradiation analytical investigations on the fuel samples were performed in the PSI hot laboratory during the experimental campaign. The experiments measured the concentrations of the 17 actinides and 40 fission products seen in Table 2.2.

The data gained by these studies has been and will be used to validate computer codes for high burnup and MOX fuels [10] [14].

Table 2.2 – Nuclides selected for radiochemical analysis [14].

Major Actinides:	
	^{234}U, ^{235}U, ^{236}U, ^{238}U
	^{238}Pu, ^{239}Pu, ^{240}Pu, ^{241}Pu, ^{242}Pu
Minor Actinides:	
	^{237}Np
	^{241}Am, ^{242m}Am, ^{243}Am
	^{242}Cm, ^{243}Cm, ^{244}Cm, ^{245}Cm, ^{246}Cm
Fission Products:	
Volatiles:	^{133}Cs, ^{134}Cs, ^{135}Cs, ^{137}Cs
Metallics:	^{90}Sr, ^{95}Mo, ^{99}Tc, ^{101}Ru, ^{106}Ru, ^{103}Rh, ^{109}Ag, ^{125}Sb
Lanthanides:	^{144}Ce, ^{147}Pm, ^{155}Gd
	^{142}Nd, ^{143}Nd, ^{144}Nd, ^{145}Nd, ^{146}Nd, ^{148}Nd, ^{150}Nd
	^{147}Sm, ^{148}Sm, ^{149}Sm, ^{150}Sm, ^{151}Sm, ^{152}Sm, ^{154}Sm
	^{151}Eu, ^{153}Eu, ^{154}Eu, ^{155}Eu

The chemical analyses were done using a combination of high-performance liquid chromatography (HPLC) and multicollector inductively coupled plasma mass spectrometry (MC-ICP-MS). The chromatography was done to separate chemical elements and mass spectroscopy was done to analyze the isotopic compositions of the elements. Mass spectroscopy cannot be used alone because it cannot separate isobars (nuclides having the same mass number, but different atomic numbers). The nuclides ^{106}Ru, ^{125}Sb, ^{144}Ce, and ^{243}Cm existed in small concentrations in the fuel samples and needed to be measured with γ-ray spectroscopy using a high-purity germanium detector. The uncertainty associated with the experimental measurement of the nuclides using MC-ICP-MS and HPLC is 0.3-1%. The uncertainty of the isotopes measured with γ-ray spectroscopy is 5-10% [13].

The burnup of each sample was measured using the ^{148}Nd technique. This isotope is a fission product and its concentration increases with burnup. By measuring its concentration in the fuel samples, it is possible to approximate a sample's burnup. The assumption made in this technique is that the only phenomenon affecting the concentration of ^{148}Nd is the fission reaction. In reality, there is a significant amount of ^{148}Nd produced by neutron capture in ^{147}Nd and a significant amount of ^{148}Nd destroyed by its own reactions with neutrons. The concentration of ^{148}Nd generated by neutron capture is approximately independent of burnup (but dependent on the magnitude of the flux) because ^{147}Nd reaches saturation quickly as its half-life is $\sim$11 days. The fraction of ^{148}Nd destroyed however increases linearly with burnup. This means that with the previously stated assumption, samples with low burnups have their burnups overestimated and those with high burnups have their values underestimated. The net uncertainty therefore associated with the burnups of the samples is $\pm$2.3-2.5% for the UO_2 samples and less than 1% for the MOX samples [10].

2.3 Reactivity Worth Measurements

The reactivity worth of each sample was experimentally measured by inserting them one-by-one into the center of the PWR assembly. For each measurement, the reactivity worths were measured against a fresh, 3.5 w.% enriched, UO_2 reference sample. The

enrichment of this sample is the same as the initial value for all of the U samples, except U1. The experimental results obtained with this method show the effect on reactivity of replacing a reference sample with a burnt sample. It allows to directly measure the reactivity loss of fuel due to exposure in a reactor.

The reactivity was measured by using the compensation method with an automatically-driven fine control rod and the inverse kinetics method. The two methods provide complementary results, but the compensation method is more precise. Therefore during the experiment, the compensation technique was primarily used, with the inverse kinetics method used as a cross check. The experimental precision of the compensation technique measurements was approximately 0.5% at one standard deviation [15].

Relative Reactivity

In each measurement, the absolute reactivity worth, $\Delta\rho$, of a sample was evaluated against that of the reference sample (U_{ref}) of fresh, 3.5 w.% enriched UO_2 as calculated in Equation 2.1. In addition, $\Delta\rho$ of a naturally enriched sample (U_{nat}) was also evaluated with this method. This $\Delta\rho$ of U_{nat} is then used to create a ratio of reactivity worths called *relative reactivity* as seen in Equation 2.2. This parameter, $\Delta\rho_{rel}$ was used and not $\Delta\rho$ so that accurate comparisons can be made between calculated values from CASMO[1] and measured experimental values. Two things are accomplished by using $\Delta\rho_{rel}$. The first is to cancel out possible inherent errors in the experimental design and measurement techniques. The second is to help correct for a neglected importance shift that occurs in CASMO when measuring $\Delta\rho$ by being independent of the size of the system, which the $\Delta\rho$ is not.

$$\Delta\rho = \frac{1}{k_{ref}} - \frac{1}{k_{pert}} \tag{2.1}$$

$$\Delta\rho_{rel} = \frac{\Delta\rho(U_{ref} \rightarrow sample)}{\Delta\rho(U_{ref} \rightarrow U_{nat})} \tag{2.2}$$

The importance shift can be conceptualized when considering the effects that occur when a sample is inserted into PROTEUS. The k_{eff} response calculated during the experiment is the result of global effects in the reactor; Neutron production and neutron losses in all regions of the core determine k_{eff}. Each region can then be thought of as contributing with varying degrees of importance to the resulting global k_{eff}. For example a fuel pin at the center of the core has a higher importance to the measured k_{eff} than a piece of steel at the core extremity.

Upon insertion of the sample, a global shift in the reactor's flux and the energy spectrum of the flux occurs. In other words, this alteration of the flux is not isolated locally in the PWR assembly. The issue is then that in the CASMO simulations, global changes in the reactor's flux are not taken into account due to the 2D, infinite-assembly calculation. Virtually inserting the sample into the PWR assembly in CASMO effects the change in k_{eff} due to changes in the flux in that assembly alone. In reality the situation is different. The PWR assembly is coupled neutronically to the whole core and the importance of each region shifts relative to each other due to the insertion of a sample.

[1] When the code system in general is referenced, with no specificity on its version number, the term "CASMO" will be used. When content is version specific, the code system will be referred to as either "CASMO-5" or "CASMO-4E."

In addition to the use of relative reactivity to account for the importance shift, a 2D whole core simulation was made in the code BOXER [16]. The ratio of the fission reaction rate in the PWR assembly to the whole core was calculated for the reference case with the reference sample ands the given experimental sample, seen in Equation 2.3. This was then used as an importance correction factor by which each reactivity coefficient is multiplied. Overall this effect is very small, but has been included in this analysis for completeness in its comparison to previous work done with CASMO-4E [10].

$$\Delta F^s = \frac{\int_{PWR} \Phi \Sigma_f^s dV}{\int_{Proteus} \Phi \Sigma_f^s dV} \tag{2.3}$$

2.4 CASMO-4E Analyses

The fuel composition analyses and reactivity worth data acquired during the experimental campaign were compared in previous analyses [10][14] to calculations done with the CASMO-4E fuel assembly code with the ENDF/B-VI nuclear data library. This comparison was done to test the ability of CASMO-4E to predict the changes in fuel that occur during exposure and how these changes affect the fuel's reactivity worth.

First burnup calculations were done with CASMO-4E version 2.10.13. Each sample was depleted to the experimentally measured burnup with their appropriate state parameters, i.e. specific power, water temperature and density, fuel temperature, and soluble boron concentration. The outputs of these calculations were the fuel compositions after exposure, which were then used as the sample compositions in the reactivity analyses. The decay of radioactive nuclides was calculated until a time point which was in the middle of the experiment, which was either July 2002 or March 2003 depending on the sample.

The results were deemed to be satisfactory with an average bias, or calculated to experiment ratio, of 1.00 ± 0.02. Here the uncertainty quoted is the sample uncertainty based off of the sample size of eleven. It does not include any uncertainty quantification. The bias for each sample that was calculated in the previous analysis is shown in Figure 2.3 along with the sample's burnup. These results showed a slight trend of biases increasing towards 1.0 with increased burnup.

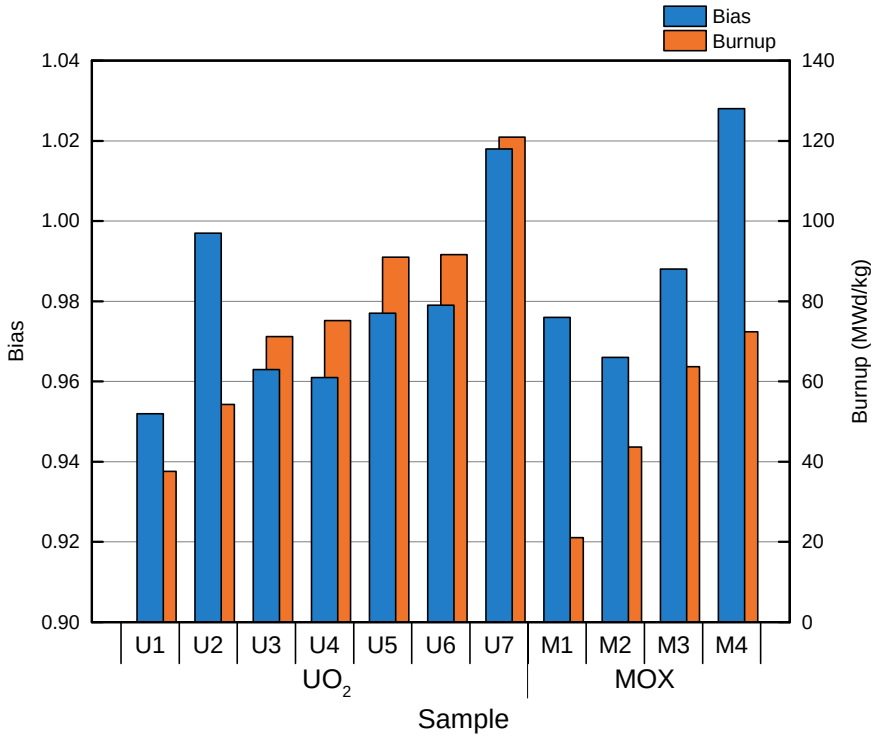

Figure 2.3 – CASMO-4E bias values for relative reactivity [10].

Chapter 3

Uncertainty Quantification and Sensitivity Analysis Methods

Several uncertainty quantification and sensitivitiy analysis (UQ/SA) methods are applicable for use in reactor physics codes and can be generally divided into statistical and deterministic methods. In the SHARK-X utility a version of each of these methods is implemented for use with CASMO-5. The statistical method is called *stochastic sampling* (SS) and the deterministic method is called *direct perturbation* (DP) [23]. Each of these methods is applied in this analysis to quantify the uncertainty associated with criticality parameters due to nuclear data and technological parameter input uncertainties. Furthermore, the methods are used in sensitivity analysis which provides input for representativity analysis (see Sections 1.3 and 3.6).

The use of multiple UQ/SA methods is an important part of the methodology and calculation scheme applied in this project. A single UQ/SA method cannot satisfactorily satisfy every need for UQ/SA, which includes the ability to

- Handle any uncertain inputs and outputs.
- Generate output variance-covariance matrices (VCM) from input VCMs.
- Decompose the output uncertainty into its contributions from individual inputs.
- Include (or estimate) greater than first-order effects.

By using multiple methods concurrently, it is possible to compensate for weaknesses in one method with the strengths of another. The DP method for example has weaknesses modeling higher than first-order effects. SS compensates for this weakness by being able to evaluate highly non-linear systems. This is detailed with example functions in Appendix A. Similarly SS is efficient and expeditious for quantifying total uncertainties, but has difficulties in calculating the contributions to output uncertainty due to its individual inputs. DP, being a local method, perturbs each input individually and is thus better suited for identifying individual contributions to total uncertainty because of its ease of use.

3.1 Stochastic Sampling (SS)

Stochastic sampling (SS) is a global UQ/SA method based on the assignment of probability density functions (PDFs) to uncertain inputs. These PDFs are based on the knowledge of the actual distribution of the given parameter or are approximated when not available. In the sampling scheme implemented in SHARK-X, simple random

sampling (SRS) is used to sample the PDFs of uncertain inputs to create a number, N, of independent input samples. For the N samples created, the model is run N times with these samples' inputs and N outputs are generated. Then the output is interpreted in terms of its sample distribution and its statistical properties are calculated (e.g. the sample mean and standard deviation). This method is often known by other names such as *statistical sampling*, *sampling-based UQ*, or *Monte Carlo*.

With the SS method, the standard deviation of the given output sample set is estimated from sample statistics using the unbiased, standard deviation estimator seen in Equation 3.1, where N is the number of samples, $y^{(i)}$ is the i^{th} output of y, and $\bar{y}$ is the sample mean which is directly available from the nominal, unperturbed case.

$$\sigma_{y_c} \approx \sqrt{\frac{1}{N-1}\sum_{i=1}^{N}(y^{(i)}-\bar{y})^2} \tag{3.1}$$

The SS method can be applied to both nuclear data and technological parameter (e.g. material composition) uncertainty quantification. SS is considered to be a global method because all of the uncertain inputs are concurrently perturbed for each simulation.

3.2 Direct Perturbation (DP)

The deterministic method for UQ, direct perturbation (DP), is based on the calculation of sensitivity coefficients. A sensitivity coefficient, S_{ij}, is a measure of the change in an output y_j with respect to a relative change in an input x_i with the superscript (0) being the reference state of the parameter.

$$S_{ij} = \frac{x_i^{(0)}}{y_j^{(0)}}\frac{\delta y_j}{\delta x_i}\Big|_{x_i=x_i^{(0)}} = \frac{\delta q_j}{\delta p_i}\Big|_{p_i=1} \tag{3.2}$$

where q_j is the relative change in the output y,

$$q_j = \frac{y_j}{y_j^{(0)}} \tag{3.3}$$

and p_i is the relative change in the input x, or the perturbation applied to input,

$$p_i = \frac{x_i}{x_i^{(0)}} \tag{3.4}$$

A single sensitivity coefficient thus describes the change in a response relative to changes in an input parameter. A single sensitivity coefficient (not the entire matrix) in criticality analyses can be thought of as a triplet. The triplet is the given nuclide, the cross section for the given reaction, and the neutron energy group for which it is calculated. For the response of k_{eff}, the sensitivity coefficient describes the importance of the nuclide-reaction-energy group triplet to the computed k_{eff} [6].

Once a set of sensitivity coefficients, S_{ij}, is obtained, it can be combined with variance-covariance data, in the form of VCMs, to quantify the uncertainty in the outputs to the first-order. This calculation is done using the Taylor-series-derived *sandwich rule* seen in Equation 3.5, where $\boldsymbol{V}_{in}$ is the input (relative) VCM, $\boldsymbol{S}$ is the matrix of sensitivity coefficients, $\boldsymbol{V}_{out}$ is the output (relative) VCM, and T denotes the transpose.

$$\boldsymbol{V}_{out} = \boldsymbol{S}^T \boldsymbol{V}_{in} \boldsymbol{S} \tag{3.5}$$

For the propagation of nuclear data uncertainty, the number of neutron energy groups (N_G) dictates the dimensions of the VCM and sensitivity coefficient matrix. Thus for a single input reaction and N_R output responses, $\boldsymbol{S}$ has dimensions of $N_G \times N_R$, $\boldsymbol{V}_{in}$ is $N_G \times N_G$, and $\boldsymbol{V}_{out}$ is $N_R \times N_R$. The standard deviation of the output is given as $\sigma_{\vec{y}_c}$, a vector of standard deviation of size N_R.

$$\sigma_{\vec{y}_c} = \sqrt{diag(\boldsymbol{V}_{out})} \tag{3.6}$$

The size of the problem increases proportionally to the number of nuclides. Thus for 44-energy groups, 200 nuclides, and approximately three reactions per nuclide, $\boldsymbol{V}_{in}$ will have dimensions of approximately 26,400×26,400. A normal sensitivity coefficient calculation requires three points, or transport calculations with corresponding outputs, and thus roughly 80,000 inputs would be required for nuclear data uncertainty propagation for this problem [7].

The definition of the sandwich rule (Equation 3.5) is derived with a Taylor series expansion truncated to the first order, which can create problems in nonlinear systems to which the DP method is applied. This means that for lattice physics codes (which can be non-linear), Equation 3.5 is a first-order approximation. Although the neutron transport equation is linear with respect to the angular flux, lattice physics codes are difficult to linearize especially with resonance self-shielding and depletion calculations. In this analysis however, the UQ/SA skips resonance treatment and is not applied to depletion calculations and therefore does not present problems in terms of linearity. In fact, the multiplication factor, k, is a linear response, while the responses absolute reactivity and relative reactivity are not. The effect of non-linearities on absolute reactivity worth and relative reactivity worth are discussed in Appendix B. For simple and general cases, these first-order problems are discussed with example problems in Appendix A.

3.3 Implementation of SS and DP in SHARK-X

The SS method's sequence in SHARK-X begins with each input being sampled N times according to the input's underlying probability distribution. This sampling is done with respect to correlation that may exist to other inputs if it exists. For nuclear data, the probability distributions come from the SCALE-6.0 VCMs and for the non-nuclear data the PDFs come from user defined distributions. For example in this report's analysis, UQ is performed for uncertainty associated with fuel composition. The PDFs for the fuel composition are normal distributions based off of experimental analyses of the fuel compositions [13].

The DP method as implemented in SHARK-X begins with a perturbation of unity, or $p = 1.0$, for the nominal calculation. This finds the nominal value of the response, y_0, used in calculating sensitivity coefficients. The DP driver then selects and performs additional perturbed cases to create a perturbed response that is neither too big nor too small to calculate the sensitivity coefficient, S. Once sensitivity coefficients are available, UQ may be performed using standard, first-order uncertainty propagation via the sandwich rule and with the SCALE-6.0 VCMs described in Section 3.4. More detailed explanations of this implementation can be found in Ref. [23].

The SS method implemented in SHARK-X is very similar to the DP method's framework. The major differences between the implementations are

1. In SS, all input parameters are varied simultaneously. The DP method varies a single input parameter at a time.
2. The DP method is a sensitivity analysis technique which then allows for UQ with the sandwich rule. The SS method is first a UQ technique which can later be used to calculate sensitivity coefficients.
3. The SS method is inherently parallel. Meanwhile the adaptive nature of the DP method limits the degree to which the calculation of a sensitivity coefficient can be parallelized. The sensitivities of different inputs however can be found simultaneously and therefore parallelization can be implemented there.

3.4 Nuclear Data Input Uncertainties

Uncertainties associated with group-wise nuclear data are typically described by variance/covariance matrices (VCMs). A VCM has variance terms along the diagonal of the matrix and covariance terms at the off-diagonal elements. The VCM allows for the interpretation of variance in multiple dimensions, showing how a given variables varies itself and with other variables.

When used with nuclear data uncertainties, a VCM implies a normal distribution of the data. For a single nuclide and single reaction with G energy groups, the VCM matrix's size is $G \times G$. The diagonal elements of the matrix give the group-wise variance and the off-diagonal elements give the covariance between two groups. Uncertainty data for the ENDF/B-VII.R0, 586-group nuclear data library used in CASMO-5 was not available at the time that SHARK-X was developed. Therefore this uncertainty data in the current implementation is borrowed from the SCALE-6.0 VCM library [1],[23]. This data exists for 401 nuclides/materials and in 44 energy groups. Nuclides are described by ZAID numbers and reactions are described by ENDF-style MT numbers.

3.5 Variance Decomposition

Part of UQ/SA involves reducing the sandwich rule, or decomposing the variance, to compute the variance on a given response due to just a single nuclide/reaction pair. By decomposing the variance, it is then possible to identify the varying degrees which input parameters contribute to the total variance. For the DP method, the sensitivity coefficient for this decomposition is then S_{X_i} where X_i is a given input parameter. The sandwich rule is used serially for each X_i with an input VCM, V_α, to calculate the output variance, V_{X_i} as shown in Equation 3.7.

$$V_{X_i} = S_{X_i}^T V_\alpha S_{X_i} \tag{3.7}$$

Because this expression calculates V_{X_i} individually, one at a time, it calculates only covariance between energy groups within a given input parameter (e.g. nuclear data) and ignores possible covariance between two or more input parameters. In reality covariance between variables is possible, meaning that the decomposed variance calculated in Equation 3.7 may be over or underestimated to a certain degree. To illustrate the problem of neglecting covariances, Equation 3.7 is shown for the total variance, V_{tot}, calculated for two input parameters X_1 and X_2. The variances of V_{X_1} and V_{X_2} as individually calculated with Equation 3.7 are shown in Equations 3.9 and 3.10 [19]. If V_{X_1} and V_{X_2} were added together to calculate V_{tot}, the $2S_{X_1}S_{X_2}\sigma_{X_1,X_2}$ would be missing. This shows the possible error that neglecting covariance may cause with this variance decomposition method.

$$V_{tot} = S_{X_1} S_{X_1} \sigma^2_{X_1} + S_{X_2} S_{X_2} \sigma^2_{X_2} + 2 S_{X_1} S_{X_2} \sigma_{X_1, X_2} \tag{3.8}$$

$$V_{X_1} = S_{X_1} S_{X_1} \sigma^2_{X_1} \tag{3.9}$$

$$V_{X_2} = S_{X_2} S_{X_2} \sigma^2_{X_2} \tag{3.10}$$

A set of MATLAB scripts are used to decompose the SS-calculated variance into its component parts. The scripts infer from input parameter samples and the corresponding response samples the sensitivity coefficient of a given response due to the individual input parameters. The sensitivity coefficients are computed using the least square solver in MATLAB. These sensitivity coefficients are then used with the sandwich rule as described in Equation 3.7 [19].

The performance of the least square solver is improved by limiting the number of input parameters. This is done by integrating the energy dependence of the neutron flux. Because this is done in SHARK-X after the CASMO-5 calculation, the local neutron flux cannot be used and 1/E dependence is approximated. This approximation introduces further errors in the variance decomposition for the SS method. Additionally, because of the stochastic nature of the calculation, each sensitivity coefficient has an uncertainty associated with it. The combination of these two effects leads to the variance decomposition with the SS method to be less reliable than with the DP method. Therefore the DP variance decomposition is used in parts of the analyses presented later in this report.

Part of the variance decomposition done in SHARK-X includes computing the *variance fraction*. The variance fraction is simply the fraction of the total variance that the variance from a single input contributes. The variance fraction from a given input parameter, X_i, is computed as seen in Equation 3.11.

$$\text{Variance} - \text{Fraction} = \frac{V_{X_i}}{\sum_{n=1}^{N} V_{X_n}} \tag{3.11}$$

3.6 Representativity Analysis

The quantification of the representativity of a benchmark to an application is done in this analysis with *representativity indices*. These indices are useful because they provide a single quantity which summarizes the similarity between two systems. These can be based off of sensitivity coefficients or the combination of sensitivity coefficients and uncertainty. In this analysis, the indices based off of both sensitivity coefficients and uncertainty are preferred. The other indices that are based solely on sensitivity coefficients and not uncertainty are not used. This is because previous studies [17] have shown that they are not effective for systems containing Pu due to the anti-correlation between certain components in its cross-section data. As some of the samples used in the LWR-PROTEUS Phase II campaign contain high quantities of Pu, these sensitivity-based indices were avoided.

The uncertainty and sensitivity-based index used in this study, c_{res}, is useful because it is calculated from both uncertainty and sensitivity information. The benefit of deriving c_{res} like this is that the correlation in the bias between systems tends to mimic the correlation between the uncertainties of the systems, with the assumption that the bias is mainly due to uncertainties in nuclear data [18]. The sensitivity-based indices can be

useful to determine the underlying reasons why poor representativity to an application exists. By comparing the sensitivity coefficients, the responsible nuclide-reaction pair can be identified.

To compute c_{res}, the sandwich rule as presented in Equation 3.5 is used with expanded sensitivity coefficient matrices of the response of interest, $\boldsymbol{S}_{res}$. The matrix $\boldsymbol{S}_{res}$ has dimensions of $N \times L$, where L is the number of systems considered in the representativity analysis and N is the number of nuclear data parameters considered. Usually N is the number of nuclide-reaction pairs times the number of energy groups. The input VCM, $\mathbf{V}_\alpha$ is a $N \times N$ matrix. When $\boldsymbol{S}_{res}$ and $\mathbf{V}_\alpha$ are used in the sandwich rule, the result is a symmetrical $L \times L$ response matrix $\mathbf{V_{res}}$, as shown in Equation 3.12.

$$\boldsymbol{V}_{res} = \boldsymbol{S}_{res}^T \boldsymbol{V}_\alpha \boldsymbol{S}_{res} \tag{3.12}$$

The diagonal elements of the $\boldsymbol{V_{res}}$ matrix are the variance values, σ_i^2 for each of the critical systems in the representativity analysis. The off-diagonal terms are the covariance between the systems, $\sigma_{i,j}$. The covariances, $\sigma_{i,j}$, are then divided by the product of the standard deviations of the responses of each system, σ_i and σ_j, to obtain a correlation coefficient matrix, or the representativity matrix, $\boldsymbol{c_{res}}$. This is shown for a single index, c_{res}^{ij}, in Equation 3.13.

$$c_{res}^{ij} = \frac{\sigma_{i,j}}{\sigma_i \sigma_j} \tag{3.13}$$

Each c_{res}^{ij} value is a correlation coefficient between input parameters of systems i and j and the response res. A typical response is k_{eff} and thus the integral index is c_k. Additionally in this analysis, the response of reactivity, $\Delta\rho$, will be considered and its integral index is $c_{\Delta\rho}$

Chapter 4

CASMO-5 and SHARKX Calculations

This chapter discusses the implementation of the SS and DP methods in the utility SHARK-X along with the input parameters considered when using the utility. Additionally it discusses the two reactivity responses that were considered during the LWR PROTEUS Phase II campaign, that of absolute reactivity worth and relative reactivity worth. Additionally, the Proteus and spent fuel rack models are discussed, which are used in UQ/SA and representativity analyses.

4.1 CASMO-5 and SHARK-X Simulation Parameters

The calculations for UQ/SA and RA for all samples and the spent fuel pool models were carried out using the CASMO-5 fuel assembly code driven by SHARK-X. SHARK-X uses a modified version of CASMO-5 version 1.07.01 and is part of the SHARK-X utility [23]. It uses the E7R0 125 cross-section library, 586-group cross-section library (file e7r0.125.586.bin), based on ENDF/B-VII release 1 nuclear data [20].

For all UQ/SA results presented in Chapter 5, the neutron transport calculations in CASMO-5 are done with the CASMO-5, 19-energy-group structure [3]. The spent fuel pool calculations for RA use 95-energy-groups because this is the default calculation in CASMO-5 for spent fuel pools and is the structure that would be used in industrial applications. For the UQ/SA with both the SS and DP methods, the uncertainties come from 19-energy-group VCMs for all nuclides. Originally the VCMs are in a 44-energy-group structure, but they are then collapsed in 19-energy groups (see Ref. [23] for more information).

Significant Digits on SHARK-X Results

CASMO-5 has numerical precision to the fifth digit after the decimal point, or at 1 pcm if the given value is k_{eff} or k_{inf}. Sensitivity coefficients and the representativity indices are derived from k_{eff}, which has this said numerical uncertainty below 1 pcm. Therefore these numerical uncertainties have to be considered when results are reported. If a uniform distribution from [0,1E-6] is assumed to exist that describes the uncertainty of k_{eff} below 1E-5, the uncertainty below the fifth digit after the decimal point can be propagated. When this is done, it is seen that for sensitivity coefficients, numerical accuracy is given only to the fourth digit after the decimal and for representativity indices, only to the third digit. A detailed summary of this analysis is given in Appendix C.

4.2 The Uncertain Inputs

Currently the SHARK-X utility allows for nuclear data perturbations to the following parameters (ENDF MT numbers shown in parentheses):

1. Elastic scattering, $\sigma_{s,el}$ (MT = 2)
2. Inelastic scattering, $\sigma_{s,in}$ (MT = 4)
3. The (n,2n) reaction, $\sigma_{n,2n}$ (MT = 16)
4. Fission, σ_f (MT = 18)
5. Capture, σ_c (MT = 101)
6. Average number of neutrons per fission, $\bar{\nu}$ (MT = 452)
7. Average fission spectrum, χ (MT = 1018)

In this analysis, the uncertainty associated with nuclear data of 41 isotopes is investigated. For low atomic number nuclides (e.g. H, O, Zr, Nd) only σ_s and σ_c uncertainties are considered. No distinction was made between inelastic and elastic scattering, only total scattering, or MT = 13, was used. For fissile and fertile nuclides, all of the previously enumerated reactions are considered for UQ/SA.

Additionally, UQ was performed with SS for uncertainties associated with the composition of the fuel samples inserted and removed from the core. The experimentally measured compositions of the samples were used as the nominal values of the sample input composition. The uncertainties associated with their experimental measurement were then used as the PDFs for sampling in the SS method. The uncertainty associated with the isotopic compositions of elements comes from the post-irradiation measurements in the hot laboratory (see Section 2.2.2). For very rare isotopes, this number can be larger. For elemental concentrations, and therefore isotopic concentrations, the uncertainties range between 0.3% and 1% for most isotopes. For isotopes that could only be measured with γ-ray spectroscopy, uncertainties are as large as 5%. For elements measured with MC-ICP-MS without chromatographic separation, uncertainties are $\sim$10%. These isotopes are the metallic fission products and ^{237}Np [14].

4.3 CASMO Models of LWR-PROTEUS Phase II

The CASMO models of Proteus simulate only the PWR assembly, which is formally defined as a BWR assembly. This means that the CASMO feature that allows modeling of a BWR channel box can be used to represent the stainless steel tank containing the BWR assembly.

The model is seen in Figure 4.1 consists of, in addition to the central PWR assembly,

- The stainless steel tank,
- The moderator between the outermost pins and the tank,
- And the moderator that exists in the one-half distance between the PWR and BWR peripheral pins (ignoring the BWR assemblies' Zircaloy boxes).

The model is 2D and uses reflective boundary conditions upon its outer surfaces. The effect of this modeling approximation on the bias of reactivity responses may be significant for the borated water and D_2O/H_2O moderated Proteus configurations. This is because in the real experiment only the central assembly has this adaptable moderating condition and there are seven BWR assemblies surrounding the central assembly with an unchangeable H_2O moderator. By using the reflective boundary condition for the borated

water and D_2O/H_2O moderated configurations, the whole system is simulated as having this moderator, while in reality it is only the central assembly. Therefore the neutron flux in the CASMO model is not truly representative of what existed during the experimental campaign. The effect that this has upon bias is investigated in Chapter 5.

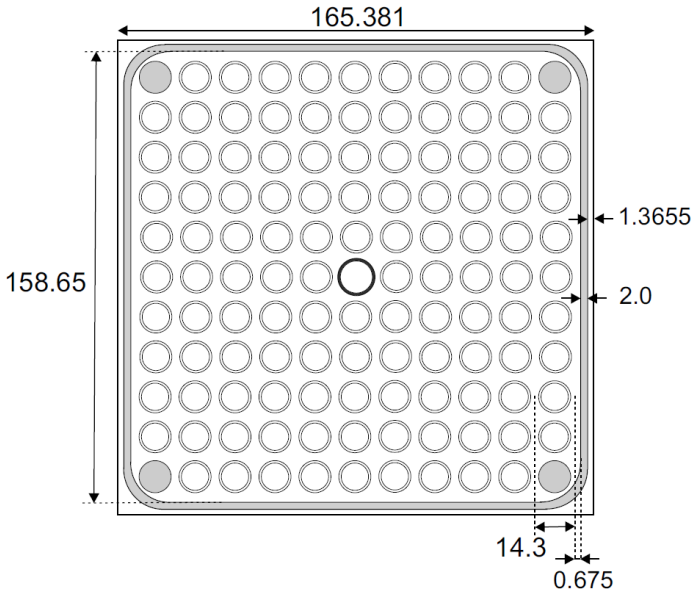

Figure 4.1 – CASMO-5 model of the PWR test region (dimensions in mm) [10].

The samples compositions in the models use experimental values measured at the PSI hotlab for the composition of each sample in the CASMO input decks. Due to technical limitations at the hotlab, experimental compositions were only available for 72 isotopes. For isotopes where experimental values were not available, the values from the CASMO-4E calculations were used. The effect of using experimental compositions the CASMO-5 input decks versus compositions from burnup calculations with CASMO-4E was investigated and is presented in Section 5.4.

Criticality is achieved ($k_{eff} = 1.0$) for the reference sample of 3.5%-enriched UO_2 by searching for the critical axial buckling. This buckling is then fixed constant and used as input for the rest of the models where the various samples are inserted into the core. The buckling is also fixed for the perturbations to input parameters that occur during UQ/SA with SHARK-X. These inputs were made for previous analyses with CASMO-4E [10] and were slightly adapted for compatibility with CASMO-5.

4.4 Spent Fuel Rack Model

The model of the spent fuel rack is for the Kompaktlager spent fuel pool, one of three spent fuel pools at KKG. The model was based off of previous analyses done at PSI [21] and direct communications done with the KKG fuel management division. The previous study was a criticality safety analysis using 2D calculations. Figure 4.2 shows a horizontal cross-section of a quarter of the spent fuel rack.

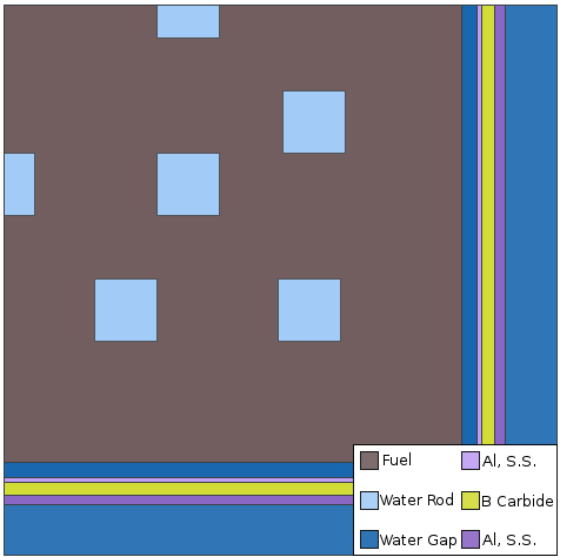

Figure 4.2 – Depiction of one quarter of the KKG spent fuel rack.

The fuel assembly is 15×15 array with water rods dispersed through the lattice. After the assembly is a 0.475 cm thick inner water gap channel which is surrounded by the following zones, going from inside to outside:

- A 0.1 cm thick zone of stainless steel SS-304,
- A 0.025 cm thick zone of Al,
- A 0.43 cm thick Boral plate with a B concentration of 60 mg/cm^2,
- A 0.025 cm thick zone of Al,
- A 0.3 cm thick zone of SS-304,
- And the outermost zone, a water channel gap, whose thickness is 1.42 cm.

The model is developed in CASMO-5 using the FSS and FSC cards that allow the modeling of spent fuel racks. With these cards, only full symmetry is allowed in modeling [3]. Additionally, CASMO-5 automatically used its 95-energy-group structure for these calculations. While this energy-group structure can be overridden and changed back to the 19 groups typically used in its lattice physics calculations, this was not done for the representativity analyses. This is because it was desired to keep the simulation conditions as similar as possible to those that would be used in industrial applications of CASMO-5. Therefore the results of the representativity analysis would be most interesting and applicable to these types of analyses.

The SHARK-X utility is incompatible with the M×N functionality in CASMO-5, which allows for modeling of an array of assemblies of different compositions. In this SFP model, reflective boundary conditions are used on the rack's outer surfaces. This means that effectively being modeled is an infinite array of identical fuel racks. The composition of the fuel assembly takes the exact form of that of the samples in Proteus models. The entire assembly is either the reference, 3.5 w.% enriched UO_2, or it is the given sample composition. Therefore, when absolute or relative reactivity worth is calculated, what is being measured is the change in reactivity that occurs when an infinite pool of fresh assemblies becomes an infinite pool of burnt assemblies. While this modeling is unrealistic, it serves as a starting point for developing the RA methodology during a six-month masters thesis.

For consistency with the Proteus CASMO models, criticality is achieved ($k_{eff} = 1.0$) for the assembly of 3.5 w.% enriched UO_2 by searching for the critical axial buckling. This buckling is then used as an input parameter for the given burned assembly. The buckling from the 3.5 w.% enriched UO_2 assembly is fixed constant for the fuel rack neutron transport calculations and thus allows for the determination of deviations from criticality when the hypothetical assembly is inserted into the spent fuel pool. In other words, it assumed that axial leakage is not modified when a fresh assembly is replaced by a burned assembly because the axial buckling is fixeds for the simulations.

Chapter 5

UQ/SA and Validation Results

The results for the UQ/SA and validation analyses of LWR-PRTOEUS Phase II campaign are summarized and analyzed in this chapter. First the SS results with H_2O moderating conditions are presented. The UQ/SA is presented by response type starting with k_{inf} and k_{eff}, then $\Delta\rho$, and finally $\Delta\rho_{rel}$. Then the nuclear data, technological parameter, and experimental uncertainties are combined to quantify the bias uncertainty of $\Delta\rho_{rel}$ and conclusions are drawn concerning the validation of CASMO-5. Next the SS and DP results are compared and their similarities and differences are analyzed. The difference between CASMO-4 and CASMO-5 bias results is then discussed along with the effect of using the experimentally measured isotopic inventory of the samples vs. compositions from CASMO-4 burnup calculations. Finally the results for borated and D_2O/H_2O moderating conditions are summarized to highlight the differences in UQ/SA results resulting from different moderators and thus different neutron flux spectra.

In summary, UQ analysis was performed for the following response parameters:

- k_{inf} : Infinite multiplication factor
- k_{eff} : Effective multiplication factor
- $\Delta\rho$: Absolute reactivity worth, calculated with k_{eff} (Equation 2.1)
- $\Delta\rho_{rel}$: Relative reactivity worth, calculated with k_{eff} (Equation 2.2)
- b_c : Computational bias, calculated with $\Delta\rho_{rel}$

Each response's uncertainty value is presented for all eleven samples to highlight how its magnitude may change with burnup and fuel composition (i.e. UO_2 vs. MOX). The mean values for k_{inf}, k_{eff}, ρ_{inf}, $\Delta\rho$, and $\Delta\rho_{rel}$ are omitted because they are proprietary. Only their relative standard deviations are given.

5.1 H_2O Moderator UQ/SA With SS

5.1.1 k_{inf} and k_{eff} UQ/SA

The nuclear data UQ results for the responses of k_{inf} and k_{eff} were calculated with the SS method, using 1,000 samples of the input parameters. The samples' relative standard deviations, $1\sigma_{rel}$, for each response do not vary between samples; $1\sigma_{rel}$ is equal to 0.46% for each and every sample's k_{inf} response and is constant for k_{eff} as well at 0.55%. This indicates that the uncertainty associated with k_{inf} and k_{eff} is driven by the fuel pins surrounding the sample pin, not the sample pin itself.

A noticeable and interesting phenomenon seen in the results is a large difference in $1\sigma_{rel}$ between k_{inf} and k_{eff}, increasing from 0.46% to 0.55%. This behavior is thought to be

the result of leakage effects and the concurrently harder spectra that exist in each samples' criticality flux in comparison to their infinite-medium fluxes[1]. Shown in Stammler and Abbate [22] is that for $k_{inf} > 1$, the critical spectrum for a given calculation is harder than that of the infinite-medium spectrum. Concurrently, for $k_{inf} < 1$, the critical spectrum is softer.

To understand these differences, the $1\sigma_{rel}$ values of k_{inf} and k_{eff} for a representative sample of intermediate burnup, U2, are analyzed. To test for a spectral shift and to quantify its change, the spectrum index, r, was used as in Equation 5.1 where ϕ_2 is the thermal flux integrated over all energies from 0 eV to the thermal energy boundary and ϕ_1 is the fast flux integrated over all energies from the thermal energy boundary to higher.

$$r = \frac{\phi_2}{\phi_1} \tag{5.1}$$

Larger values of r indicate that a larger portion of the neutron flux is in the thermal region, or in other words, that the ϕ_2 term in the numerator is larger. Equation 5.1 was applied to data taken from CASMO-5 results to analyse the spectral effects in sample U2. The calculated spectrum indices for the critical spectrum, r_{crit}, and the infinite-medium spectrum, r_∞, were calculated to be 0.1738 and 0.1885 respectively. The smaller value of r_{crit} indicates that indeed the critical neutron-flux spectrum is harder than that of the infinite-medium spectrum.

To explain what spectral changes do to affect the total uncertainty, U2's DP-calculated[2] $1\sigma_{rel}$ values are decomposed into each of its contributing nuclide/reaction pairs. This decomposition is ordered in Table 5.1 as the top five nuclide/reaction pairs contributing to the responses' total uncertainty, along with each of these nuclide/reaction pair's sensitivity coefficient. First seen in Table 5.1 is the appearance in the top five of the nuclide/reaction pair $^{238}U/\sigma_{s,in}$ for k_{eff}; its sensitivity coefficient (SC) increases from -3.2E-3 for k_{inf} to 1.34E-2 and its $1\sigma_{rel}$ increases from 0.06% to 0.23% for k_{inf} to k_{eff} respectively. Additionally, the $^{235}U/\chi$ pair's SC increases from -4E-4 to 3.5E-3 and its $1\sigma_{rel}$ value increases from 0.06% to 0.17% for k_{inf} to k_{eff} respectively.

Table 5.1 – U2 decomposition of DP $1\sigma_{rel}$ sensitivity coefficients (SC) for k_{inf} and k_{eff}. Nuclear data UQ only.

Nuc./Reac.	k_{inf} $1\sigma_{rel}$	SC	Nuc./Reac.	k_{eff} $1\sigma_{rel}$	SC
$^{235}U/\bar{\nu}$	0.28%	0.9421	$^{235}U/\bar{\nu}$	0.27%	0.9417
$^{238}U/\sigma_c$	0.25%	-0.1895	$^{238}U/\sigma_c$	0.25%	-0.1818
$^{235}U/\sigma_c$	0.21%	-0.1338	$^{238}U/\sigma_{s,in}$	0.23%	0.0134
$^{235}U/\sigma_f$	0.13%	0.2970	$^{235}U/\sigma_c$	0.21%	-0.1295
$^{235}U/\chi$	0.06%	0.0004	$^{235}U/\chi$	0.17%	0.0035

Beginning with the effect seen for $^{238}U/\sigma_{s,in}$, its change is thought to be the result of the harder spectrum seen in the criticality flux in comparison to the infinite-medium flux. A harder spectrum has such a significant effect because of two factors:

1. The input relative variance for $^{238}U/\sigma_{s,in}$ is large at 16%, which is approximately

[1] Uncertainty in the axial buckling is not considered in this study, which could also introduce spectral differences from sample to sample.

[2] The DP method's decomposition is used instead of SS's because its higher accuracy, because of reasons explained in Section 3.5.

one order of magnitude larger than the other nuclide/reaction pairs seen in Table 5.1.

2. The energy dependence of $^{238}U/\sigma_{s,in}$ behaves such that its cross section increases with increasing energy, as seen in Figure 5.1.

The combination of these two factors means that $^{238}U/\sigma_{s,in}$ is extremely important when considering spectral changes in the multiplication factor. This is because a harder spectrum, or the average neutron having a higher energy, compounds the effect of the larger input variance. The higher neutron energies mean higher magnitudes of $\sigma_{s,in}$, which have high relative uncertainties. This makes this nuclide/reaction pair's effect on the uncertainty associated with k_{eff} sensitive to changes in the neutron flux spectrum. This higher sensitivity in harder spectra conditions can be seen in the increase in the nuclide/reaction pair's SC from -3.0E-3 to 1.3E2 for k_{inf} to k_{eff} respectively.

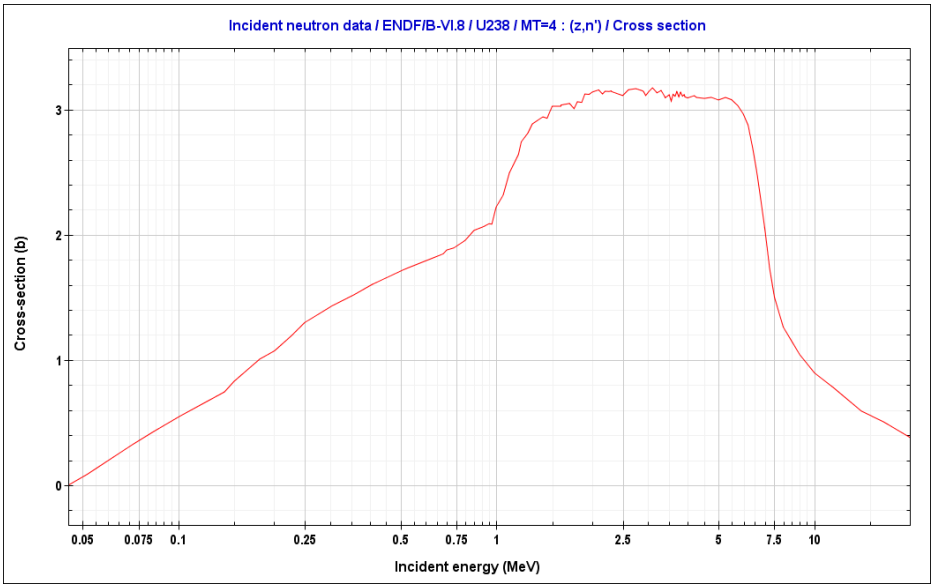

Figure 5.1 – Cross section vs. incident inergy for $^{238}U/\sigma_{s,in}$ [24].

Returning to the $^{235}U/\chi$ pair's increased $1\sigma_{rel}$, this effect can be explained by the introduction of leakage to the system in the calculation of k_{eff}. When there is no leakage in the system, the distribution of the fission neutrons' energy is not as important to the overall neutron balance. In the infinite system, neutron deaths only occur by parasitic absorption while down-scattering to lower energies during the moderation process. Thus the spectrum of energies does not matter greatly when scattering down through the resonance absorption regions. However when the system does have leakage, the spectrum of fast neutron energies is important because it is predominantly fast neutrons that are lost from leakage. Therefore if a fission neutron has more or less than a given energy, it can greatly affect the probability that it leaks from the system, and thus greatly increase the importance of $^{235}U/\chi$ to k_{eff}. This can be seen in its SC increase from -4.0E-4 to 3.5E-3.

5.1.2 Absolute Reactivity Worth ($\Delta\rho$) UQ/SA

Nuclear Data UQ

UQ results for absolute reactivity worth, $\Delta\rho$ (as defined in Equation 2.1), are summarized in Table 5.2 for nuclear data input uncertainty. First comparing the $\Delta\rho$ UQ results to those for k_{inf} and k_{eff}, the magnitude of $1\sigma_{rel}$ now varies from sample to sample and with burnup. This indicates a dependence upon burnup and fuel type. Furthermore, the uncertainty associated with $\Delta\rho$ is larger, varying from ∼0.9% to ∼4.1%.

Table 5.2 – $\Delta\rho$ relative standard deviations, $1\sigma_{rel}$. For nuclear data UQ.

Sample ID	$1\sigma_{rel}$	Burnup (MWd/kg)
U1	1.45%	∼38
U2	1.11%	∼54
U3	0.94%	∼71
U4	0.95%	∼75
U5	0.88%	∼91
U6	0.89%	∼92
U7	0.95%	∼121
M1	4.12%	∼21
M2	2.63%	∼44
M3	1.94%	∼64
M4	1.66%	∼72

The decomposition of sample U2 and M1's DP-calculated $1\sigma_{rel}$ values was inspected to determine the origin of the differences in σ_{rel} values between the ranges of samples' burnup and between fuel type. These samples were chosen because they are considered to be representative examples of the UO_2 and MOX samples. This decomposition, seen in Table 5.3[3], revealed that for $\Delta\rho$, σ_{rel} is dominated by reactions involving the isotopes ^{235}U and ^{239}Pu.

Table 5.3 – Decomposition of sample U2 and M1's DP-calculated σ_{rel} for $\Delta\rho$. Nuclear data UQ only .

U2			M1		
Nuc./Reac.	$\Delta\rho$ $1\sigma_{rel}$	Variance Fraction	Nuc./Reac.	$\Delta\rho$ $1\sigma_{rel}$	Variance Fraction
$^{239}Pu/\bar{\nu}$	0.80%	38%	$^{239}Pu/\bar{\nu}$	3.02%	65%
$^{235}U/\bar{\nu}$	0.66%	26%	$^{235}U/\bar{\nu}$	1.39%	14%
$^{238}U/\sigma_{s,in}$	0.56%	18%	$^{239}Pu/\sigma_f$	0.86%	5%
$^{239}Pu/\sigma_f$	0.25%	4%	$^{239}Pu/\sigma_c$	0.82%	5%
$^{239}Pu/\sigma_c$	0.24%	3%	$^{235}U/\chi$	0.62%	3%

The average number of neutrons per fission, $\bar{\nu}$, is particularly important for both ^{235}U and ^{239}Pu making up 38% and 26% of the relative variance for U2 respectively and 65% and 14% of the variance for M1 respectively. Here the variance fraction is calculated

[3]The $1\sigma_{rel}$ and variance fraction data reported for each nuclide reaction pair are equivalent, i.e. the variance fraction is derived from $1\sigma_{rel}$. Variance fraction is shown to emphasize the proportion that a given nuclide/reaction pair contributes to the total $1\sigma_{rel}$ value.

as seen in Equation 3.11. The $^{238}U/\sigma_{s,in}$ nuclide/reaction pair appears in U2's ranking, but not in the M1's. The absence in the M1's ranking is likely due to the much lower concentration of ^{238}U, which is about 5 w.% less in the MOX sample.

The large influence of ^{239}Pu content on reactivity is interesting considering that no ^{239}Pu/reaction pair appeared in the top five of contributors to σ_{rel} for k_{inf} and k_{eff}, seen in Table 5.1. These contributors were composed of only nuclide/reaction pairs involving ^{235}U and ^{238}U. The differences seen are the result of the nature of the different responses. For both k_{inf} and k_{eff} the uncertainty is mainly driven by the unburnt fuel pins within the assembly, not the inserted sample. This is because the given sample is only a small component of the system contributing to the overall integral value of k. In contrast $\Delta\rho$ is a response measuring the difference in two systems, or the difference in k caused by the sample. This response is therefore sensitive to differences between the systems, which in this case is primarily the difference in sample compositions (which thus cause differences in k).

When this is considered in context of the sandwich rule, it explains the high uncertainties associated with ^{239}Pu and ^{235}U nuclide reaction pair: $\Delta\rho$ is sensitive to differences in sample compositions, especially those important to criticality. Additionally input uncertainties are high with nuclide/reaction pairs like $^{239}Pu/\bar{\nu}$ and $^{235}U/\bar{\nu}$. When large sensitivity coefficients and large input uncertainties are used in the sandwich rule, the result is large output uncertainties, as is seen in Table 5.3.

With reactions with ^{235}U and ^{239}Pu identified as being large contributors to the uncertainty associated with $\Delta\rho$, the differences in their compositions and the effect of these differences on σ_{rel} was investigated and is presented in Figure 5.2. A strong trend is visible between the magnitude of the weight percent of both ^{235}U and ^{239}Pu and the size of $1\sigma_{rel}$ for $\Delta\rho$. Higher quantities of both ^{235}U and ^{239}Pu lead to larger σ_{rel} values. The UO_2 samples have approximately equivalent ^{239}Pu concentrations (^{239}Pu saturates with burnup) but the concentration of ^{235}U decreases as it is consumed with burnup. The UO_2 samples thus show decreasing $1\sigma_{rel}$ values with increased burnup as ^{235}U is consumed, and then approximately constant σ_{rel} at high burnups when most of the fissile material is ^{239}Pu. The small variations in σ_{rel} for the high burnup samples (U5, U6, and U7) are likely due to small variations in the ^{239}Pu content due to varying conditions seen by the samples during their irradiation histories.

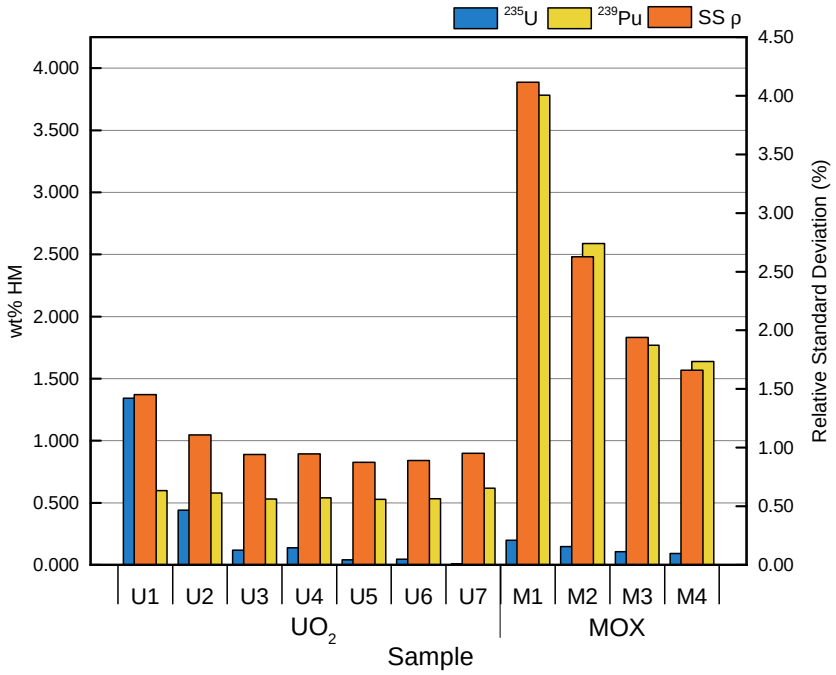

Figure 5.2 – ^{235}U and ^{239}Pu weight percents and $\Delta\rho$ $1\sigma_{rel}$ values.

The MOX samples also show a strong trend towards decreasing σ_{rel} values with increased burnup, due to decreased ^{239}Pu content as it is consumed during fission. Sample M1 with the largest ^{239}Pu content correspondingly has the largest $1\sigma_{rel}$ value at 4.12%. The MOX values have uniformly larger σ_{rel} values than UO_2 as their ^{239}Pu contents are larger. Thus the quantity of fissile material (either ^{235}U or ^{239}Pu) in a sample can be identified as a determining factor in the uncertainty associated with $\Delta\rho$.

Sample Composition UQ

Sample composition UQ is presented in Table 5.4 for $\Delta\rho$. The uncertainty associated with sample compositions is smaller than that from nuclear data, with relative standard deviations of 0.31 to 0.59%. The uncertainty is dominated largely by one isotope, ^{103}Rh, which makes up ∼75% of the total uncertainty. The cause of the large dominance of ^{103}Rh is founded in its large capture cross section at thermal energies and its large input uncertainty at 10%. This can be seen in Figure 5.3 where the nuclide/reaction pair ^{103}Rh/(n,γ) is plotted. This reaction makes up most of ^{103}Rh's total capture cross section. Because this cross section is so large, especially in the thermal region, uncertainties in its value will have large effects on the total response's uncertainty.

Table 5.4 – $\Delta\rho$ sample composition relative standard deviations, $1\sigma_{rel}$, values.

Sample ID	$1\sigma_{rel}$	Burnup (MWd/kg)
U1	0.42%	~38
U2	0.47%	~54
U3	0.44%	~71
U4	0.45%	~75
U5	0.44%	~91
U6	0.46%	~92
U7	0.45%	~121
M1	0.31%	~21
M2	0.42%	~44
M3	0.39%	~64
M4	0.59%	~72

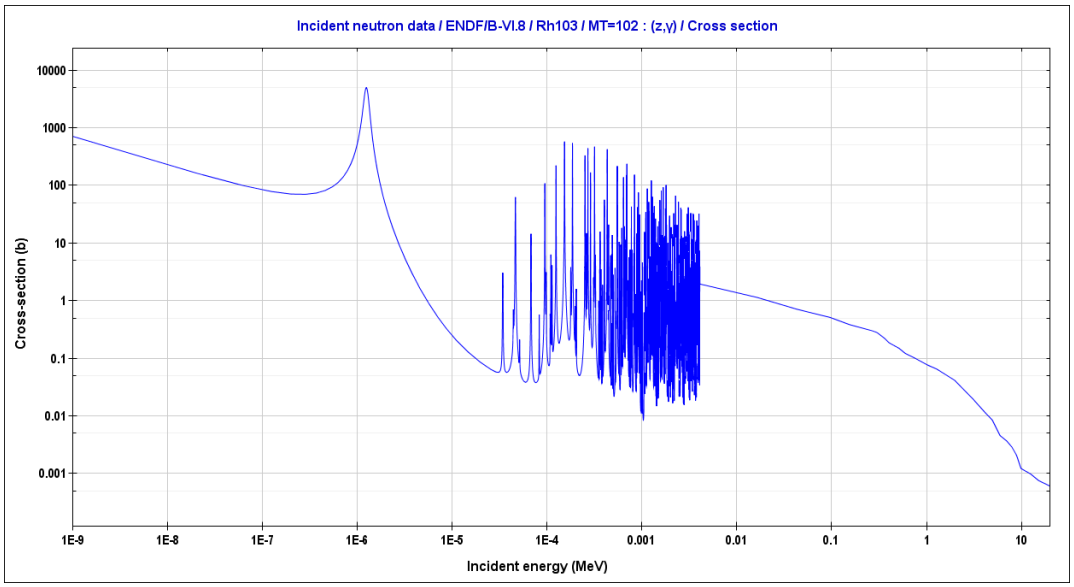

Figure 5.3 – Cross section vs. incident energy for ^{103}Rh/(n,γ) [24].

Table 5.4 shows a slight trend of increasing σ_{rel} with increasing burnup, but the relation is deeper than just a dependency on the magnitude of burnup. Figure 5.4 shows an investigation into the effect that the concentration of two isotopes, ^{103}Rh and ^{237}Np, have upon σ_{rel}. ^{237}Np is important because it has a large uncertainty at 10%, it changes with burnup, and has a significant capture cross section. Here the samples are organized by fuel type and by increasing burnup. The concentrations of ^{103}Rh and ^{237}Np are compared between samples by using their normalized number densities. The number density of the lowest burnup sample for each fuel type, U1 for UO_2 samples and M1 for MOX samples, of ^{103}Rh or ^{237}Np is used as the normalization factor for each sample's ^{103}Rh or ^{237}Np number density. Real number densities cannot be shown because they are proprietary information.

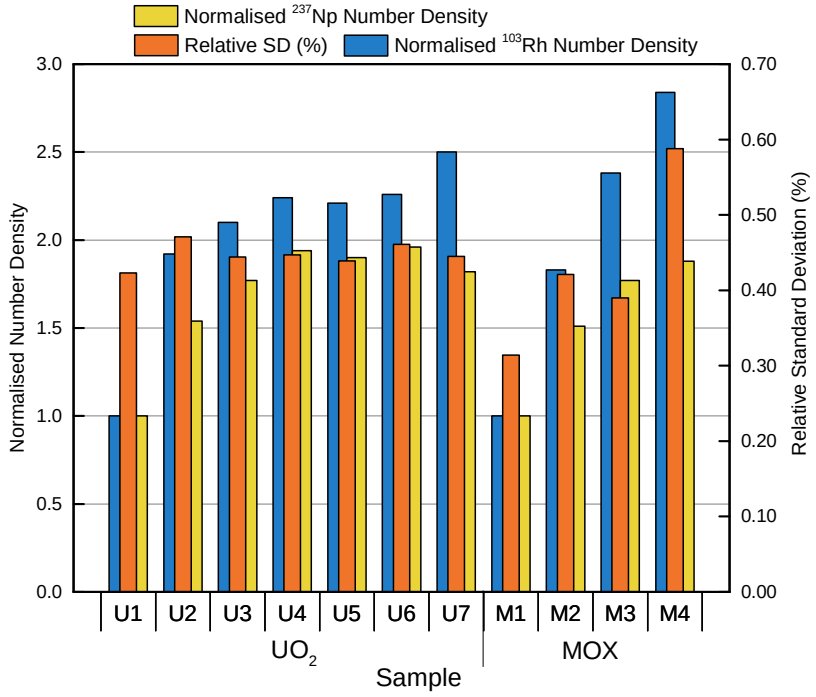

Figure 5.4 – ^{103}Rh and ^{237}Np normalized number densities and $\Delta\rho$ σ_{rel} values from technological input UQ.

The general trend seen is that with increased burnup, more ^{103}Rh and ^{237}Np is yielded from fission and decay processes. With higher concentrations of these isotopes, the σ_{rel} increases. For samples U3 to U7 whose burnups range from ∼71 to ∼121 MWd/kg, the concentration of these isotopes plateaus as their creation by fission and their destruction by neutron absorption reaches equilibrium. The result of this concentration equilibrium is a plateau of σ_{rel}. Small variations in σ_{rel} are likely due to variations in conditions that each sample saw during its exposure periods, causing small variations in their compositions. The MOX samples which have lower burnup values never reach equilibrium in their concentration of ^{103}Rh and ^{237}Np and therefore show continually increasing σ_{rel} values with increased burnup.

The concentration of ^{103}Rh is likely a first-order effect, as it contributes most to the total uncertainty, at around 55% for the UO_2 samples and around 43% for the MOX. The ^{237}Np concentration is likely a second-order effect, accounting for some of the differences in σ_{rel} seen between samples with similar ^{103}Rh concentrations.

5.1.3 Relative Reactivity Worth ($\Delta\rho_{rel}$) UQ

Nuclear Data UQ

UQ results for relative reactivity worth, $\Delta\rho_{rel}$ (as defined in Equation 2.2), are summarized in Table 5.5 for nuclear data input uncertainty. Comparing the $\Delta\rho_{rel}$ UQ in Table 5.5 to the $\Delta\rho$ UQ in Table 5.2 the magnitudes of $1\sigma_{rel}$ have increased by approximately 0.5 to 0.6%.

Table 5.5 – SS-calculated $\Delta\rho_{rel}$ relative standard deviations, $1\sigma_{rel}$. For nuclear data UQ only.

Sample ID	SS $1\sigma_{rel}$	Burnup (MWd/kg)
U1	1.93%	∼38
U2	1.61%	∼54
U3	1.47%	∼71
U4	1.48%	∼75
U5	1.44%	∼91
U6	1.45%	∼92
U7	1.54%	∼121
M1	4.58%	∼21
M2	3.17%	∼44
M3	2.53%	∼64
M4	2.28%	∼72

The decomposition of sample U2 and M1's $1\sigma_{rel}$ values show behavior similar to that of $\Delta\rho$'s, presented in Table 5.3, with $\bar{\nu}$ of ^{235}U and ^{239}Pu dominating the uncertainty associated with $\Delta\rho_{rel}$ for all of the samples. For U2, $^{235}\mathrm{U}/\bar{\nu}$ and $^{239}\mathrm{Pu}/\bar{\nu}$ make up 47% and 9% of σ_{rel} respectively. For M1, $^{235}\mathrm{U}/\bar{\nu}$ and $^{239}\mathrm{Pu}/\bar{\nu}$ make up 29% and 46% of σ_{rel} respectively.

The response $\Delta\rho_{rel}$ shows a similar trend to $\Delta\rho$ between the magnitude of the weight percent of both ^{235}U and ^{239}Pu and the size of the σ_{rel}. Higher quantities of both ^{235}U and ^{239}Pu lead to larger σ_{rel} values. The UO_2 samples have approximately equivalent ^{239}Pu concentrations (^{239}Pu saturates with burnup) but the concentration of ^{235}U decreases as it is consumed with burnup. The UO_2 samples thus show an approximately decreasing σ_{rel} values with increased burnup as ^{235}U is consumed, and then approximately constant σ_{rel} at high burnups when most of the fissile material is ^{239}Pu.

Sample Composition UQ

Sample composition UQ of $\Delta\rho_{rel}$ is identical to that of $\Delta\rho$ presented in Section 5.1.2. The $\mathrm{U_{ref}}$ and $\mathrm{U_{nat}}$ samples were references and thus their compositions were exactly known, unlike that of the samples. The uncertainty associated with their composition is zero and thus uncertainty on all responses associated with them is zero. Therefore in the calculation of $\Delta\rho_{rel}$ seen in Equation 2.2, there is no uncertainty associated with the $\Delta\rho(U_{ref} \rightarrow U_{nat})$ term in the denominator, uncertainty only comes from the $\Delta\rho(U_{ref} \rightarrow sample)$ term. When the uncertainty is calculated for $\Delta\rho_{rel}$, only uncertainty from $\Delta\rho_{sample}$ is propagated, and thus is identical that of $\Delta\rho_{sample}$.

5.2 Bias (b_c) UQ and Validation

Finally the bias, b_c, and bias uncertainty, σ_{b_c}, of the response $\Delta\rho_{rel}$ was calculated with Equations 1.1 and 5.2 respectively. Equation 5.2 is used to propagate the uncertainties from nuclear data ($\sigma_{NuclearData}$), sample composition ($\sigma_{composition}$), and experimental measurement (σ_E) to find a final, total uncertainty associated with b_c. Additionally, the validation procedure outlined in Section 1.2 was done with a z-score tolerance, ε_z, of 2.0 as the validation criteria.

$$\sigma_{b_c} = b_c \sqrt{\left(\frac{\sigma_{NuclearData}}{C}\right)^2 + \left(\frac{\sigma_{composition}}{C}\right)^2 + \left(\frac{\sigma_E}{E}\right)^2} \tag{5.2}$$

Table 5.6 is presented as a summary of SS UQ for b_c. First presented is $1\sigma_{rel}$ of σ_{b_c} due to only nuclear data input uncertainties. Therefore in these results the σ_E and $\sigma_{composition}$ terms in Equation 5.2 were assumed to be zero. This illustrates the magnitude of σ_{b_c} that is made up of nuclear data input uncertainties. Next in Table 5.6, total uncertainty is given, which is the combination of nuclear data, sample composition, and experimental uncertainties. The $1\sigma_{rel}$ uncertainty associated with the experimental $\Delta\rho_{rel}$ measurements is 0.5% [15], and is thus the value used in the σ_{b_c} uncertainty propagation.

Table 5.6 – SS $1\sigma_{b_c}$ values. For nuclear data UQ and for total UQ.

Sample ID	$1\sigma_{b_c}$ Nuc. Data	$1\sigma_{b_c}$ Total	Burnup (MWd/kg)
U1	1.93%	2.03%	∼38
U2	1.61%	1.75%	∼54
U3	1.47%	1.62%	∼71
U4	1.48%	1.55%	∼75
U5	1.45%	1.60%	∼91
U6	1.44%	1.59%	∼92
U7	1.54%	1.68%	∼121
M1	4.58%	4.62%	∼21
M2	3.17%	3.23%	∼44
M3	2.53%	2.61%	∼64
M4	2.28%	2.41%	∼72

Bias is a derived quantity of $\Delta\rho^{rel}$, which is itself derived from $\Delta\rho$, and thus shows very similar UQ behavior with burnup and fuel type to each of those responses described in Sections 5.1.2 and 5.1.3 respectively. At low burnups for both the UO_2 and MOX samples, the higher quantities of fissile material and thus the $\bar{\nu}$ nuclear data uncertainty contributes to larger uncertainties. For the UO_2 samples, increased burnup leads to a flattening out of fissile material content and very similar σ_{b_c} values for the high burnup samples of U3 to U7. The MOX samples have larger uncertainties than the UO_2 samples due to their larger ^{239}Pu content. The MOX samples also show decreasing σ_{b_c} values with the decreased fissile content that accompanies increased burnup.

5.2.1 Comparison of CASMO-4E and CASMO-5 b_c Values Without and With UQ

Figure 5.5 helps to summarize the accomplishment of using UQ in the analysis of b_c. Here the original CASMO-4E simulations for b_c done in [10] are compared to simulations done with CASMO-5. Each simulation used identical input parameters, particularly identical input sample compositions. When the CASMO-4E and CASMO-5 b_c results are compared in this figure without UQ, the conclusion could be made that they differ significantly from each other, especially for the MOX samples. With only the experimental uncertainty available there is no explanation as to why the differences in b_c exist. Is it because of changes made in the methods used from CASMO-4E to CASMO-5? Is it because of different cross-section libraries used in CASMO-4E and CASMO-5? Or, are the differences due to simply uncertainties associated with cross-section data?

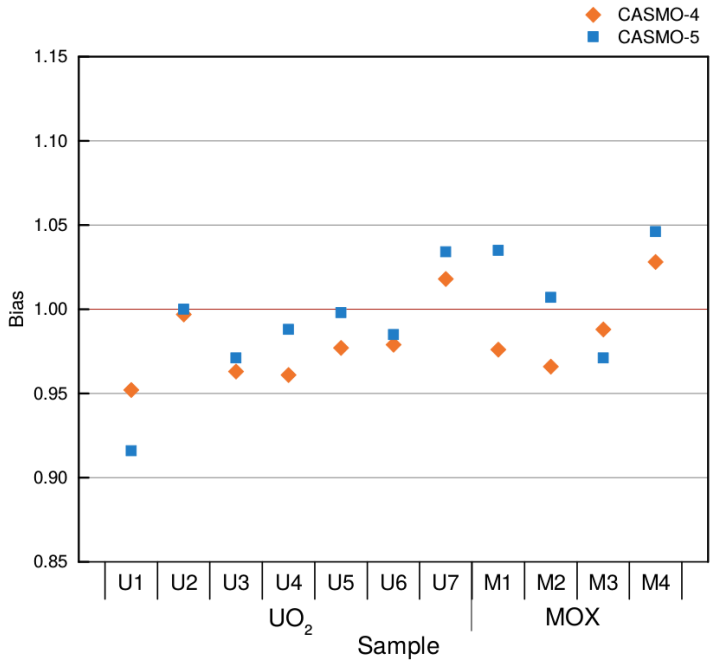

Figure 5.5 – Comparison of CASMO-4E and CASMO-5 b_c without UQ.

With the use of UQ, these questions can be answered. Figure 5.6 shows total $2\sigma_{b_c}$ (two standard deviations of b_c) associated with nuclear data, sample compositions, and experiment. The size of the spread of each b_c data point is such that it is not possible to eliminate the possibility that the CASMO-5 results agree well with those of CASMO-4E. In other words, the CASMO-5 b_c statistical spreads each contain the CASMO-4E b_c values, meaning that statistically the two values could be equivalent. If the uncertainty spread from these input data was small and there was significant discrepancies in the comparisons, one could conclude that there are inherent differences between the two CASMO versions. Now with the aid of UQ it is concluded that the differences between the results of CASMO-4E and CASMO-5 are likely due to input uncertainties and experimental uncertainty, not due to inherent differences in their methodologies. This conclusion provides a good example of the power of UQ in bias analysis.

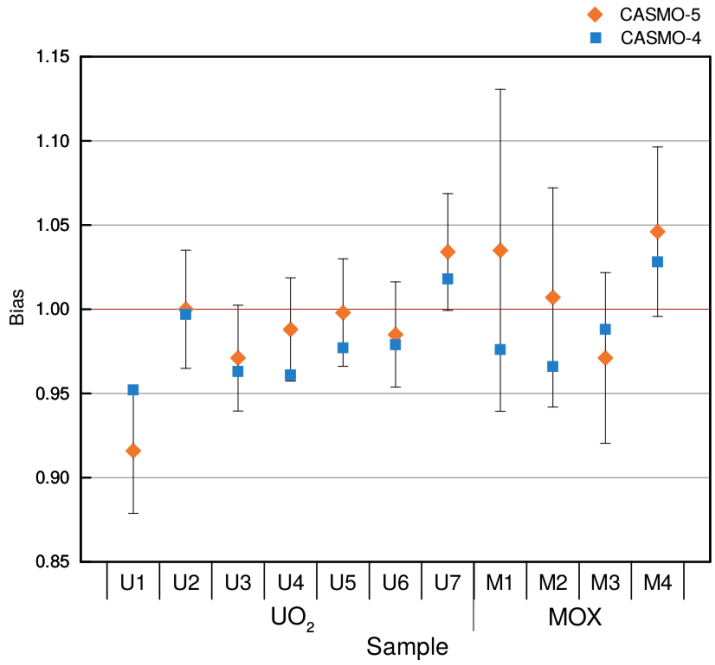

Figure 5.6 – Comparison of CASMO-4E and CASMO-5 b_c with UQ.

Validation

With UQ/SA giving σ_{b_c} values, validation was then performed using Equation 1.2 to see if a b_c of 1.0 was covered within each sample's two standard deviation uncertainty spread. This validation procedure is summarized in Table 5.7. Every sample succeeds the validation test except for U1, which has a large bias of 0.916 and validation score of 4.5. This means that a bias of 1.0 is included in U1's distribution only at 4.5 standard deviations, or that only 4.22E-4% of the time is the bias' distribution including the value of 1.0.

Table 5.7 – Validation procedure for H_2O moderated samples.

Sample ID	b_c	$\leq \varepsilon_z$	Burnup (MWd/kg)
U1	0.916	4.5	~38
U2	1.000	0.0	~54
U3	0.971	1.8	~71
U4	0.988	0.8	~75
U5	0.998	0.1	~91
U6	0.985	1.0	~92
U7	1.034	2.0	~121
M1	1.035	0.7	~21
M2	1.007	0.2	~44
M3	0.971	1.1	~64
M4	1.046	1.8	~72

The validation failure of U1 is not the result of a very small uncertainty associated with b_c. In fact as seen in Table 5.6, this sample has the largest uncertainty of the U

samples at 2.03%. Furthermore the large bias of 0.916 for sample U1 is not likely due to a method bias that is particularly strong for this sample composition. In previous analyses done with CASMO-4E [10], burnup calculations were done to calculate the composition of each sample. When the CASMO-4E calculated U1 composition was used in the CASMO-5 input, a b_c of 0.952 was calculated. This lead to a much smaller validation score of 2.5 with this input's respective σ_{b_c}. This indicates that the low b_c seen for this sample is likely due to the experimental sample composition used in the input. Furthermore, the uncertainty in the experimental composition does not explain the low bias because, if the uncertainty was large, it would be represented by larger σ_{b_c} values and a better validation score.

With methodology bias and composition uncertainty eliminated as the causes of the low b_c value for U1, the likely explanation lies in the experimental values used in the input. Perhaps there is an error in their measurement at the time of the experimental campaign. Perhaps there is an error in their enumeration in the ensuing documentation that this analysis was based off. Whatever errors that exist in this sample's composition's description lead to a combination of effects that skew the bias to this low value that is not seen in the other samples' results.

5.3 Comparison of SS and DP Results

DP is a first-order UQ method and therefore has known limits in its applications. Part of this analysis was to define where these limits are and determine the degree which this approximation affects the results. This section compares the SS and DP UQ results for $\Delta\rho$ and $\Delta\rho_{rel}$. Analytically the effects of these non-linearities on the responses are discussed in Appendix B. The responses k_{inf} and k_{eff} are not discussed because they are linear and the UQ by each was identical. Shown in the following Sections 5.3.1 and 5.3.2 is that the non-linearities of each response cause discrepancies between the uncertainty quantified by the SS and DP methods. The discrepancies are larger for the more non-linear response $\Delta\rho_{rel}$. Because of the higher degree of non-linearity of $\Delta\rho_{rel}$, it is not used in the representativity analysis (see Chapter 6) of this work as it would have affected the DP-computed sensitivity coefficients used in calculating representativity indices.

5.3.1 DP vs. SS for $\Delta\rho_{rel}$

UQ results for relative reactivity worth, $\Delta\rho_{rel}$, calculated with SS and DP are shown in Table 5.8. These results showed that the differences between the σ_{rel} values calculated by the SS and DP methods are large, particularly for the UO_2 samples. The average absolute difference between the SS and DP $1\sigma_{rel}$ values of the U samples was 0.57%. The MOX samples show smaller divergences, with the average absolute difference between the SS and DP $1\sigma_{rel}$ values of being 0.14%.

The differences between the SS and DP σ_{rel} values can be attributed to errors introduced by the first-order approximation used in the DP method, which is described in detail in Section B.1.2. The equation used to calculate $\Delta\rho_{rel}$, Equation 2.2, is non-linear and thus has higher than first-order terms. The application of the DP method ignores these higher-than-first-order terms and their contributions to the total uncertainty quantification. Variations between σ_{rel} values are therefore seen in Table 5.8, with the DP method sometimes over-predicting and other times under-predicting the SS σ_{rel} value. These discrepancies thus show a limitation when applying the DP method for UQ in a real-world application.

Table 5.8 – SS and DP $\Delta\rho_{rel}$ relative standard deviations, $1\sigma_{rel}$, and the difference between SS and DP $1\sigma_{rel}$ values. For nuclear data UQ only.

Sample ID	SS $1\sigma_{rel}$	DP $1\sigma_{rel}$	SS-DP	Burnup (MWd/kg)
U1	1.93%	2.65%	-0.72%	∼38
U2	1.61%	2.34%	-0.74%	∼54
U3	1.47%	2.16%	-0.69%	∼71
U4	1.48%	2.04%	-0.56%	∼75
U5	1.44%	1.62%	-0.18%	∼91
U6	1.45%	1.89%	-0.45%	∼92
U7	1.54%	2.20%	-0.66%	∼121
M1	4.58%	4.47%	0.12%	∼21
M2	3.17%	3.03%	0.14%	∼44
M3	2.53%	2.60%	-0.07%	∼64
M4	2.28%	2.50%	-0.22%	∼72

5.3.2 DP vs. SS for $\Delta\rho$

A comparison of the SS and DP UQ results for absolute reactivity, $\Delta\rho$, is given in Table 5.9 for nuclear data input uncertainty. Evident in Table 5.9 are the discrepancies between the DP and SS-calculated σ_{rel} values, however these are less than are seen for $\Delta\rho_{rel}$. The σ_{rel} values for the U samples calculated with the DP method over-predict σ_{rel} by an average absolute difference of 0.12%, smaller than 0.57% seen for $\Delta\rho_{rel}$. Meanwhile the M samples' DP-calculated σ_{rel} values under-predict σ_{rel} by and average absolute difference of 0.23%.

Table 5.9 – SS and DP $\Delta\rho$ relative standard deviations, $1\sigma_{rel}$, and the absolute difference between SS and DP $1\sigma_{rel}$ values. For nuclear data UQ only.

Sample ID	SS $1\sigma_{rel}$	DP $1\sigma_{rel}$	SS-DP	Burnup (MWd/kg)
U1	1.45%	1.63%	-0.18%	∼38
U2	1.11%	1.31%	-0.20%	∼54
U3	0.94%	1.07%	-0.13%	∼71
U4	0.95%	0.98%	-0.03%	∼75
U5	0.88%	1.00%	-0.12%	∼91
U6	0.89%	0.90%	-0.01%	∼92
U7	0.95%	1.12%	-0.17%	∼121
M1	4.12%	3.76%	0.36%	∼21
M2	2.63%	2.35%	0.28%	∼44
M3	1.94%	1.78%	0.16%	∼64
M4	1.66%	1.54%	0.12%	∼72

The smaller differences between SS and DP for $\Delta\rho$ occur because $\Delta\rho$ is less non-linear than $\Delta\rho_{rel}$. This means that the first-order approximation in the DP method introduces less error into σ_{rel} when applied to $\Delta\rho$. Because σ_{rel} is calculated from sensitivity coefficients in the DP method this means that the error exists in the sensitivity coefficients. Therefore in RA where the sensitivity coefficients are used to compute representativity indices, the $\Delta\rho$ response was used in this analysis, not the $\Delta\rho_{rel}$ response so that non-

linearity errors could be minimized.

5.4 Effect of Using Experimental Fuel Compositions

The results previously presented use experimental values measured at the PSI hotlab for the composition of each sample in the CASMO input decks. Due to technical limitations at the hotlab, experimental compositions were only available for 72 isotopes. For isotopes where experimental values were not available, the values from the CASMO-4E calculations were used. To test the effect of using the experimental isotopic values, three different sets of calculations for the b_c of $\Delta\rho_{rel}$ were compared:

1. CASMO-4E/CASMO-4E: CASMO-4E is used as the transport code and the isotopic inventory of the samples comes from CASMO-4E burnup calculations.
2. CASMO-5/CASMO-4E: CASMO-5 is used as the transport code and the isotopic inventory of the samples comes from CASMO-4E burnup calculations.
3. CASMO-5/Experiment: CASMO-5 is used as the transport code and the isotopic inventory of the samples comes from PSI hotlab experimental measurements.

The CASMO-4E/CASMO-4E calculations were done during previous analyses at PSI [10]. These analyses are included and compared to CASMO-5/CASMO-4E calculations to highlight changes in b_c that can be seen from code to code. These changes can occur from the different nuclear data libraries used or changes in methodologies. The CASMO-5/CASMO-4E and CASMO-5/Experiment calculations are compared to investigate the effect that using experimental isotopic compositions has upon b_c and σ_{b_c}. This comparison is shown in Figure 5.7 where the uncertainties are $1\sigma_{b_c}$ and from nuclear data input uncertainties only, no isotopic or experimental uncertainties are included.

First examining the b_c values of CASMO-4E/CASMO-4E vs. CASMO-5/CASMO-4E, the difference in b_c ranges from -2.7% to 0.6%. Considering the $2\sigma_{b_c}$ error bars for CASMO-5/CASMO-4E, these differences cannot be judged to be significant as the $2\sigma_{b_c}$ values associated with σ_{b_c} range from 2.7% to 9.2% and thus include the CASMO-4E/CASMO-4E b_c mean values. Therefore it is concluded that the difference between CASMO-4E and CASMO-5 do not significantly affect the bias of $\Delta\rho_{rel}$ in comparison to the effect of uncertainties of input nuclear data.

For CASMO-5/CASMO-4E vs. CASMO-5/Experiment calculations, the differences σ_{b_c} values are large ranging from -4.9% to 4.5%, however the uncertainties associated are also large. The $2\sigma_{b_c}$ values range from 3.10% to to as high as 9.24% for sample M1. The conclusion drawn from this data is that differences between the three calculation sets likely exist, but they are not significant when considering the uncertainties due to input nuclear data alone. Thus the use of the experimental data as the fuel sample composition input is considered to be a consistent modeling choice in comparison to other modeling methodologies. Because of this, the experimental fuel compositions were used in all of the simulations done in the project.

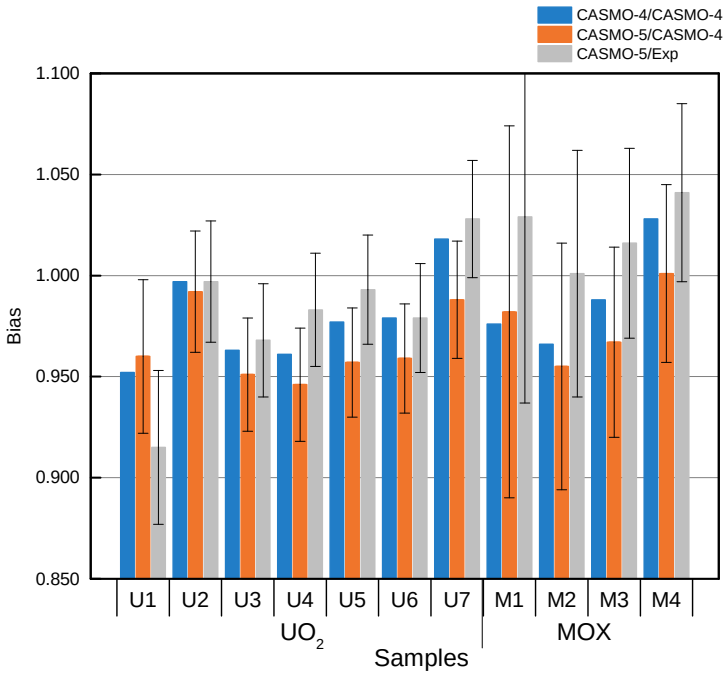

Figure 5.7 – Comparison of b_c for each calculation type. Error bars seen are $2\sigma_{rel}$ and are from nuclear data UQ only.

5.5 Borated (H_2O/H_3BO_3) and D_2O/H_2O Moderator Validation Results

This section summarizes the validation results (i.e. the calculation of bias, bias uncertainty, and then subsequent z-score analysis) for the other two moderating conditions that existed during the experimental campaign: H_2O with 2,023 ppm of boric acid (H_2O/H_3BO_3) and a D_2O/H_2O mixture. UQ results for k_{inf}, k_{eff}, $\Delta\rho$, and $\Delta\rho_{rel}$ are not given. For k_{inf} and k_{eff}, the results are not given because they are very similar to the H_2O results; The calculated relative standard deviations for k_{inf} and k_{eff} are equal from sample to sample and the k_{eff} relative standard deviations are slightly larger than the k_{inf} values, as summarized for H_2O results in Section 5.1.1.

The $\Delta\rho$, and $\Delta\rho_{rel}$ UQ results are not given because their behavior is similar to that of bias' (see Section 5.2). Therefore a summary of the bias UQ results is considered akin to that of $\Delta\rho$ and $\Delta\rho_{rel}$ UQ results. All results presented are calculated with the SS method and with sample compositions based off the experimental values.

5.5.1 σ_{b_c} UQ Results

The bias uncertainties, σ_{b_c}, of the response $\Delta\rho^{rel}$ for each sample with each moderating condition are given in Table 5.10. No measurements were done with U4 during the H_2O/H_3BO_3 moderated part of the experimental campaign and thus data are omitted for U4.

Table 5.10 – SS-calculated total (nuclear data + sample composition + experiment) $1\sigma_{b_c}$ values for each moderator.

Sample ID	H_2O/H_3BO_3 $1\sigma_{b_c}$	D_2O/H_2O $1\sigma_{b_c}$	H_2O $1\sigma_{b_c}$	Burnup (MWd/kg)
U1	1.74%	1.73%	2.03%	∼38
U2	1.37%	1.16%	1.75%	∼54
U3	1.19%	1.13%	1.62%	∼71
U4	-	1.13%	1.55%	∼75
U5	1.58%	1.14%	1.60%	∼91
U6	1.14%	1.12%	1.59%	∼92
U7	1.24%	1.19%	1.68%	∼121
M1	7.82%	2.74%	4.62%	∼21
M2	4.10%	2.09%	3.23%	∼44
M3	2.80%	1.75%	2.61%	∼64
M4	2.42%	1.66%	2.41%	∼72

First examining the UO_2 samples results in Table 5.10, the $1\sigma_{b_c}$ values are very similar from moderator to moderator, with the H_2O results being generally higher. Additionally they all show similar trends with burnup, with the highest $1\sigma_{b_c}$ values at low burnup for U1 and U2 and then a flattening of values at increased burnup due to saturation of ^{239}Pu content and consumption of ^{235}U. The MOX samples in contrast show different behavior between the moderators especially for samples M1 and M2, with the H_2O/H_3BO_3 moderated M1 having a particularly high $1\sigma_{b_c}$ of 7.82%. Meanwhile for the D_2O/H_2O moderating conditions, samples M1 and M2 have smaller $1\sigma_{b_c}$ values at 2.74% and 2.09% respectively. The cause of the different σ_{b_c} values for M1 was investigated by decomposing its variance into its respective nuclide/reaction pairs in Table 5.11.

Table 5.11 – Decomposition of M1's DP-calculated $1\sigma_{b_c}$ for each moderating condition. Nuclear Data UQ Only.

H_2O/H_3BO_3		D_2O/H_2O		H_2O	
Nuc./Reac.	$1\sigma_{b_c}$	Nuc./Reac.	$1\sigma_{b_c}$	Nuc./Reac.	$1\sigma_{b_c}$
$^{239}Pu/\bar{\nu}$	5.69%	$^{239}Pu/\bar{\nu}$	1.95%	$^{239}Pu/\bar{\nu}$	3.02%
$^{235}U/\bar{\nu}$	2.05%	$^{235}U/\bar{\nu}$	0.78%	$^{235}U/\bar{\nu}$	2.40%
$^{235}U/\sigma_c$	1.83%	$^{239}Pu/\sigma_c$	0.72%	$^{239}Pu/\sigma_f$	0.86%
$^{239}Pu/\sigma_f$	1.77%	$^{238}U/\sigma_c$	0.63%	$^{238}U/\sigma_c$	0.84%
$^{239}Pu/\sigma_c$	1.42%	$^{239}Pu/\sigma_f$	0.60%	$^{235}U/\sigma_c$	0.82%

The differences in variance can be largely attributed to $^{239}Pu/\bar{\nu}$. For H_2O/H_3BO_3 its individual decomposed $1\sigma_{b_c}$ is 5.69%, or 65% of the total variance. Meanwhile with H_2O moderating conditions, its individual decomposed $1\sigma_{b_c}$ is 3.02%, or 46% of the total variance. Meanwhile the D_2O/H_2O decomposition shows the bias uncertainity from $^{239}Pu/\bar{\nu}$ to be only 1.95%. Shifts can be seen in the other nuclide/reaction pairs as well, especially for H_2O/H_3BO_3 results, where the other four nuclide/reaction pairs are all above 1.4%. A likely source of the different UQ for each moderator is a shift in the neutron flux spectrum that exists between each system. The different neutron flux spectra affect the sensitivity of the system to these nuclide/reaction pairs, especially $^{239}Pu/\bar{\nu}$, and cause the different UQ values seen.

The existence of a spectral shift was investigated and is presented in Figure 5.8 along with the sensitivity coefficient per unit lethargy of $^{239}Pu/\bar{\nu}$ for each system. Here the normalized flux per unit lethargy inside sample M1 is presented for each moderating condition. Figure 5.8 shows that the H_2O spectrum is the softest, i.e. in the thermal energy range there is a larger portion of its neutron population. The next hardest spectrum is that of H_2O/H_3BO_3 which is caused by the large thermal absorption cross section of B, which decreases the thermal neutron population. The D_2O/H_2O system has the hardest spectrum caused by poorer moderation with the D_2O/H_2O mixture.

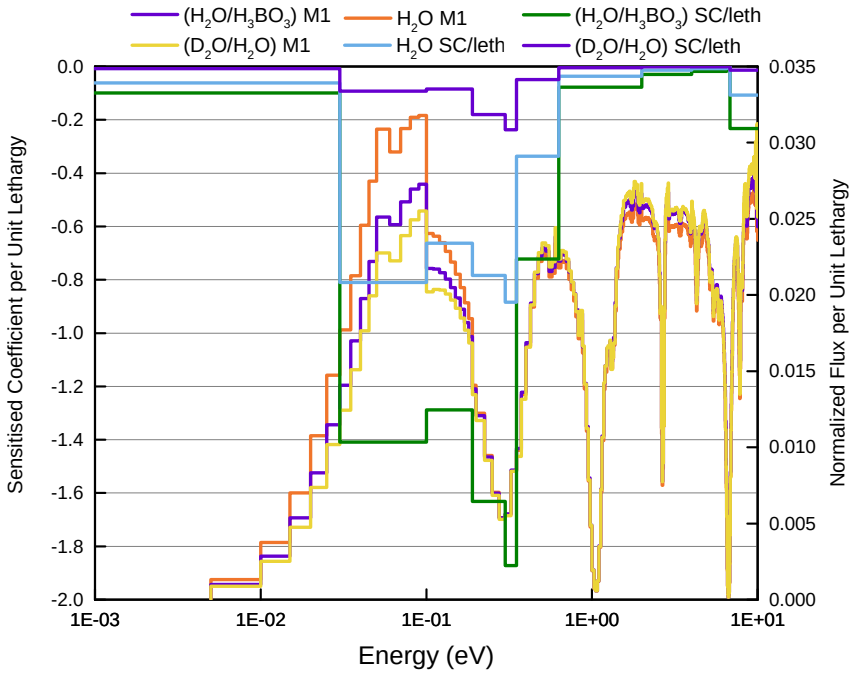

Figure 5.8 – M1 neutron flux spectra for all moderating conditions and their respective sensitivity coefficients of $^{239}Pu/\bar{\nu}$ for the response $\Delta\rho_{rel}$.

The sensitivity profiles of $^{239}Pu/\bar{\nu}$ are largest in the thermal range, which is where the majority of fissions in ^{239}Pu occur. The sensitivity coefficient from 0.3 to 0.35 eV is particularly large, where all neutron flux spectra show a large dip. The H_2O/H_3BO_3 sensitivity profile is largest in magnitude (more negative) and the D_2O/H_2O sensitivity profile is the smallest. The effect that larger in magnitude sensitivity coefficients has on UQ can be considered with respect to the sandwich rule. H_2O/H_3BO_3 had larger sensitivity coefficients than H_2O and D_2O/H_2O, but each system has equal input VCMs. Therefore larger sensitivity coefficients being input into the sandwich rule with equal input VCMs resulted in larger output uncertainties being calculated. Likewise the D_2O/H_2O sensitivity profile being the smallest resulted in the smallest UQ calculated with the sandwich rule.

Focusing on the thermal energy range (especially at 0.3 to 0.35 eV), the higher sensitivity coefficients are believed to be related to the ^{239}Pu fission cross section resonance. The fission cross section resonance of ^{239}Pu is quite large, with its peak being ~3,250 barns. Therefore neutrons in this energy range are very important to the fission chain reaction, or to criticality, because they are very likely to cause fission. Because these

neutrons are so important, this means that criticality parameters are very sensitive to differences in the neutron flux spectra in this energy range. The sensitivity in this energy range is reflected in the sensitivity profiles of $^{239}Pu/\bar{\nu}$. Each moderator's sensitivity profile for $^{239}Pu/\bar{\nu}$ is plotted in Figure 5.9 along with the fission cross section of ^{239}Pu. The sensitivity profiles peak in the cross section's resonance, indicating the importance of the energy range in the profile.

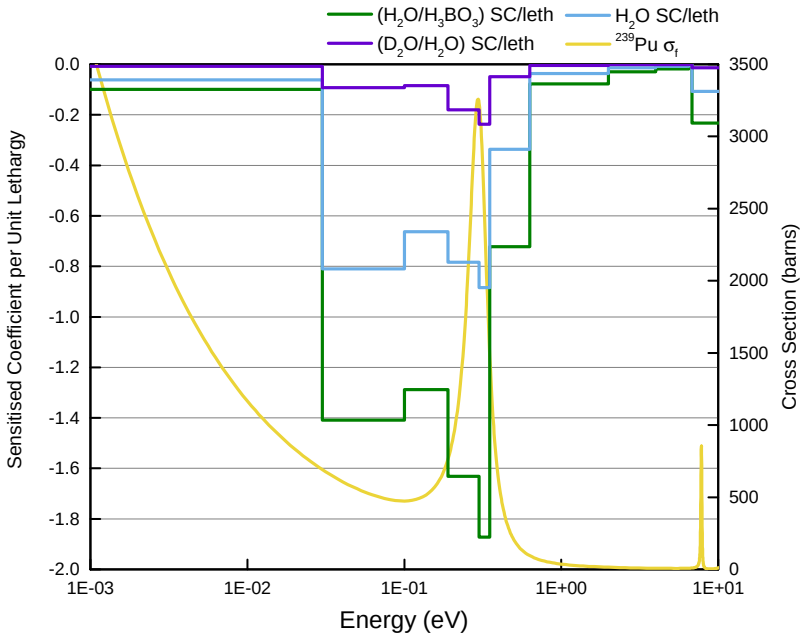

Figure 5.9 – $^{239}Pu/\sigma_f$. Sensitivity coefficient of $^{239}Pu/\bar{\nu}$ for each moderator for the response $\Delta\rho_{rel}$.

The cause of the different $^{239}Pu/\bar{\nu}$ sensitivity profiles in the ^{239}Pu fission cross section resonance was investigated by comparing each system's neutron flux spectrum within that energy range. The comparison between spectra is done by calculating the difference in normalized neutron flux spectra between the systems. The normalized flux per unit lethargy inside sample M1 moderated by H_2O/H_3BO_3 or D_2O/H_2O is subtracted from the normalized flux per unit lethargy inside sample M1 moderated by H_2O. If there is no difference between the spectra, this value is zero for the given energy group. If the value is greater than unity, it means that for this energy group the H_2O moderator's spectra has a higher normalized flux per unit lethargy at that energy range. By subtracting the two spectra, small differences between them are easier to find which cannot be distinguished in plots like Figure 5.8.

The difference between the two moderator's normalized neutron flux spectra in the fission cross section energy range is shown in Figure 5.10. The H_2O/H_3BO_3 moderated sample, in comparison to the H_2O sample, has a greater portion of its neutron flux spectrum (i.e. the difference in spectra is less than 0) in the energy range between the high energy tail of the resonance and up to its peak. This means that a larger number of its fissions are occurring in this energy and in particular, a larger number of fissions are occurring in ^{239}Pu in general because of the large cross section at the energy range. Because more fissions are occurring in ^{239}Pu, criticality parameters like $\Delta\rho_{rel}$ are more

sensitive to nuclear data associated with ^{239}Pu, of which $\bar{\nu}$ is particularly important. This higher sensitivity caused by a larger proportion of the neutron density being in the ^{239}Pu fission cross section resonance is reflected in the larger sensitivity coefficients for H_2O/H_3BO_3. These large sensitivity coefficients lead to larger uncertainties (when considered with respect to the sandwich rule). Therefore the larger σ_{b_c} values in the H_2O/H_3BO_3 moderated system's MOX samples are likely associated with a fine spectral shift around the ^{239}Pu fission cross section's resonance.

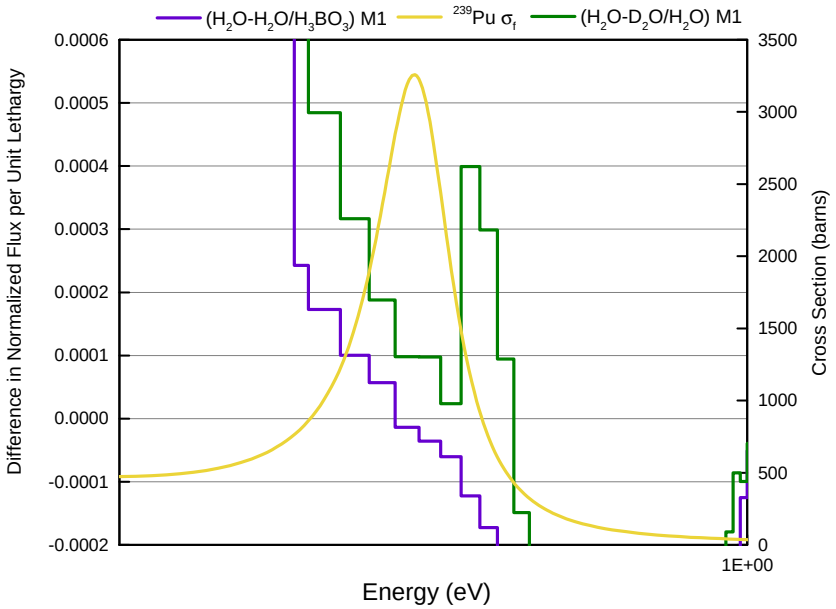

Figure 5.10 – Difference in M1 neutron flux spectra between moderators. Sensitivity coefficient of ^{239}Pu/$\bar{\nu}$ for each moderator for the response $\Delta\rho_{rel}$.

In contrast to the difference between H_2O and H_2O/H_3BO_3, the difference with D_2O/H_2O is greater than 0.0 at the entrance of and into the resonance. This means that in comparison to the H_2O spectrum, a smaller portion of its neutron population is in the energy range of this resonance. This means that less of its fissions are occurring here and its criticality parameters are less sensitive to uncertainties in ^{239}Pu/$\bar{\nu}$. The total effect is then smaller sensitivity coefficients for ^{239}Pu/$\bar{\nu}$ that were seen in Figure 5.8 and ultimately the smaller σ_{b_c} values seen in Table 5.10. The spectral shift also affected other nuclide/reaction pairs (as seen in Table 5.11) but these are secondary effects compared to ^{239}Pu/$\bar{\nu}$ and are not discussed here.

Bias and Validation Results

The validation results for the H_2O/H_3BO_3 and D_2O/H_2O moderated samples are presented in Figure 5.12. First examining b_c, all CASMO-5 simulations or each moderator over-predict the experimental value (i.e. $b_c > 1.0$) for relative reactivity except for U1. For the H_2O/H_3BO_3 moderator, the average b_c for this moderator is 1.061 ± 0.017 with the quoted uncertainty being that of the distribution of ten b_c values in the sample set. The average b_c for the D_2O/H_2O and H_2O moderators is 1.034 ± 0.009 and 0.996 ± 0.011 respectively.

Table 5.12 – Validation procedure for Proteus with H_2O/H_3BO_3 and D_2O/H_2O moderating conditions.

	H_2O/H_3BO_3		D_2O/H_2O		
Sample ID	b_c	$\leq \varepsilon_z$	b_c	$\leq \varepsilon_z$	Burnup (MWd/kg)
U1	0.990	0.6	0.963	2.2	∼38
U2	1.042	3.0	1.043	3.5	∼54
U3	1.025	2.0	1.020	1.8	∼71
U4	N/A	N/A	1.056	4.7	∼75
U5	1.056	3.4	1.051	4.2	∼91
U6	1.030	2.6	1.015	1.3	∼92
U7	1.045	3.5	1.041	3.3	∼121
M1	1.184	2.0	1.068	2.3	∼21
M2	1.130	2.8	1.059	2.7	∼44
M3	1.021	0.7	1.004	0.3	∼64
M4	1.089	3.4	1.051	2.9	∼72

The larger biases seen for the H_2O/H_3BO_3 and D_2O/H_2O moderating conditions may be the result of modeling approximations described in Section 4.3. The reflective boundary condition on the outer surfaces of the central PWR assembly means that for the H_2O/H_3BO_3 or D_2O/H_2O models, the simulated Proteus core is moderated entirely by H_2O/H_3BO_3 or D_2O/H_2O respectively. In reality it is only the central assembly that has this moderator, the others are moderated by pure H_2O. This means that for this configuration, the neutron flux spectrum in the core is harder than it is in reality. The harder spectrum means that more parasitic absorptions by the fission products and actinides in the inserted samples will occur during the thermalization of neutrons. This causes an over-prediction of the $\Delta\rho_{rel}$ with respect to the experimental value and leads to the $b_c > 1.0$ seen here.

Concerning the validation tests, only four out of ten samples passed for H_2O/H_3BO_3 and three out of eleven for D_2O/H_2O. This means that in a 2.0 z-score tolerance interval, only four and three samples respectively contain a perfect b_c of 1.0 with their statistical spread. U1, which for the H_2O conditions had a b_c of 0.916 and a validation score of 4.5, now has a b_c of 0.990 and a passing validation score of 0.6 for H_2O/H_3BO_3, and a b_c of 0.963 and a failing validation score of 2.2 for D_2O/H_2O. With an identical sample composition, the b_c results improve greatly just by the spectral shift with a new moderator. This further supports the explanation that the low b_c for U1 with the H_2O moderator is likely a combination of effects related to the experimental sample composition that uniquely stacked up to give this outlying result. Samples U4 and U5 with the D_2O/H_2O moderator show particularly large validation scores for the D_2O/H_2O cases at 4.7 and 4.2 respectively as a result of their small σ_{b_c} values (0.98% and 0.97% respectively).

Overall the conclusion of the validation test for this moderator is that with this system, the differences between experiment and CASMO-5 calculation are significant even when the effect of input uncertainties is considered. In other words, the difference between calculation and experiment cannot be explained only by uncertainties associated with nuclear data, sample composition, and experimental methods because a majority of the samples failed the validation test.

For the H_2O/H_3BO_3 moderated samples, another possible source of bias comes from neglecting the uncertainty in the concentration of boric acid measured during the experi-

mental campaign. During the experiment there was an uncertainty of ±46 ppm associated with the boric acid. As the absolute reactivity worth of the samples is low at ∼150 to ∼300 pcm, this uncertainty could have significant effects in the calculated $\Delta\rho$ and $\Delta\rho_{rel}$ values.

To improve the bias results for this moderator, an M×N model of the Proteus configuration in CASMO-5 could be created to eliminate the reflective boundary conditions on the PWR assembly and to assess its effect upon the bias. To address the boric acid uncertainty, modifications could be made to SHARK-X. In the SS method, the boric acid concentration could be treated identically to the sample composition uncertainty that was presented in this report. A PDF could be assigned to the boric acid concentration and this PDF could be randomly sampled to see how this uncertainty would contribute to σ_{b_c}.

5.5.2 Summary

The three moderating conditions delivered differing results for their UQ and validation studies. The H_2O/H_3BO_3 moderating conditions in particular gave high calculated σ_{b_c} values for samples M1 and M2. The higher uncertainty is related to larger sensitivity coefficients for $^{239}Pu/\bar{\nu}$ in this sample. These larger sensitivity coefficients are believed to result from the harder neutron flux spectrum in the H_2O/H_3BO_3 moderated samples around the energy range of the resonance of the fission cross section of ^{239}Pu. The D_2O/H_2O moderated samples show smaller σ_{b_c} values which is believed to related to the comparatively softer neutron spectrum at the resonance of the fission cross section of ^{239}Pu.

The validation results with a 2.0 z-score criteria showed that for H_2O/H_3BO_3 4/10 samples passed the test and for D_2O/H_2O 3/11 samples passed the test. The likely cause of the higher number of failures for these moderators (where with H_2O 9/11 samples passed) was their larger b_c values, which the averages are 1.061 ± 0.017 and 1.034 ± 0.009 for H_2O/H_3BO_3 and D_2O/H_2O respectively. The larger biases for these moderating conditions may result from the reflective boundary conditions placed on the central assembly in the CASMO model. This modeling approximation can cause artificially harder neutron flux spectra and an over-prediction of $\Delta\rho$. Creating an M×N model for these configurations may help to improve the bias by eliminating this modeling approximation. Additionally for the H_2O/H_3BO_3 models, performing UQ/SA for the uncertainty in input boric acid concentration may reveal that a large part of the bias between experiment and calculation comes from this source.

Chapter 6

Representativity Analysis Results

This chapter describes the results of the representativity analysis (RA) between a model of KKG's spent fuel pool (SFP) and the Proteus research reactor. It uses the methodology and theory described in Sections 1.3 and 3.6. Two representativity indices were calculated: c_k and $c_{\Delta\rho}$, which correspond to the responses k_{eff} and $\Delta\rho$. Relative reactivity worth, $\Delta\rho_{rel}$, was not used because representativity analysis must be done with the DP method to obtain accurate sensitivity coefficients. Because the DP method is used, the response $\Delta\rho_{rel}$ cannot be used because it is too highly non-linear and would lead to non-negligible errors in the sensitivity coefficients used to calculate the representativity index. This non-linearity was seen in the comparison between the SS and DP methods in Section 5.3. Additionally in Appendix B there are further discussions of the non-linearity of $\Delta\rho_{rel}$ with its derivation given and a discussion of the implications of using it with UQ/SA.

The c_k and $c_{\Delta\rho}$ results are shown for the reference sample U_{ref} and samples U2 and M2 for H_2O and H_2O/H_3BO_3 moderating conditions. Samples U2 and M2 were chosen because they have intermediate burnups of ∼54 MWd/kg and ∼44 MWd/kg respectively, which are the burnups most likely to be seen of fuel in a SFP. These samples' compositions were used as the burned assemblies' compositions in the CASMO-5 model of the KKG SFP. Representativity indices for D_2O/H_2O moderating conditions were not calculated because this moderating condition is unrealistic for the given application, a SPF. Next the $c_{\Delta\rho}$ results are presented for each moderating condition, where $\Delta\rho$ is the difference in reactivity between the U_{ref} system and the U2/M2 systems.

In the following sections, first the representativity indices are presented for k_{eff}, c_k, for each moderating condition. Then representativity indices results are given for $\Delta\rho$, $c_{\Delta\rho}$, along with a breakdown of $c_{\Delta\rho}$ into the major nuclide/reaction pair players. Finally, conclusions are made considering the representativity of the LWR-PROTEUS Phase II experimental campaign to KKG's spent fuel pool.

6.1 k_{eff} Representativity Index, c_k

First c_k of the samples is evaluated for each of the experimental campaign's moderating conditions. Each c_k value is given in Table 6.1. No sample with any of the moderating conditions satisfies the requirement of $c_k > 0.9$ for high representativity. The low representativity is expected for k_{eff} because of how different the Proteus and SPF models are. The Proteus model has only one pin with the sample composition at the center of the PWR assembly. The rest of the pins are 4.3 w.% enriched, fresh pins. Meanwhile in the SFP model, every pin has the given sample's composition with the addition of the fuel

rack surrounding the material. The higher c_k values of the U_{ref} systems are related to the similarity of the U_{ref} pin to that of the 4.3 w.% enriched pins in the Proteus model. The fresh 3.5 w.% enriched SFP assembly is more similar in composition to the 4.3% enriched Proteus assembly (with the exception of the sample) than the burnt assembly, leading to higher c_k values for the U_{ref} SFP assembly.

Table 6.1 – c_k for U_{ref} and U2 with each moderating condition.

Moderator	U_{ref} c_k	U2 c_k	M2 c_k
H_2O	0.565	0.130	0.017
H_2O/H_3BO_3	0.500	0.234	0.127

6.2 Absolute Reactivity Worth Representativity Index, $c_{\Delta\rho}$

The next step in the analysis was to quantify $c_{\Delta\rho}$ for $\Delta\rho$. The response $\Delta\rho$ is calculated as seen in Section 2.3 with Equation 2.1. The k_{eff} value from a given system with a given sample composition (e.g. U2 or M2) is compared to that of a reference composition, U_{ref}, of 3.5% enriched UO_2 to measure the change in reactivity. This was done for each moderating condition and is shown in Table 6.2.

Table 6.2 – $c_{\Delta\rho}$ of U2 for each moderating condition.

Moderator	U2 $c_{\Delta\rho}$	M2 $c_{\Delta\rho}$
H_2O	0.762	0.861
H_2O/H_3BO_3	0.847	0.780

First evident is the much higher values of $c_{\Delta\rho}$ in comparison to c_k. The explanation of the higher $c_{\Delta\rho}$ is very similar to that of why $\Delta\rho$ has higher uncertainty than k_{eff} discussed in Section 5.1.2. The response $\Delta\rho$ is a parameter that effectively quantifies the difference between two systems, it is not a direct comparison of two systems. Therefore when measuring $c_{\Delta\rho}$, the similarity between the difference between the fresh and burnt SFP to the difference between the reference and sample-inserted Proteus system is being evaluated. In contrast c_k is a direct comparison between the entire SFP and Proteus models. Therefore the higher $c_{\Delta\rho}$ values come from the fact that what is different between the the fresh and burnt SFP (i.e. the presence of fission products and major and minor actinides) is very similar to what is different between the reference and sample-inserted Proteus systems (again the presence of fission products and actinides). In summary, because these differences between fresh/burnt SFP and reference/sample-inserted Proteus systems are similar, the corresponding $c_{\Delta\rho}$ value is much higher.

U2 and M2 $c_{\Delta\rho}$ values were then decomposed into their constituent nuclide/reaction pairs to determine from where the similarity between Proteus and the SFP originated. This decomposition is shown in Table 6.3 for H_2O and H_2O/H_3BO_3 moderated samples. These decomposition show that $^{239}Pu/\bar{\nu}$ dominates $c_{\Delta\rho}$ at 0.466 for U2 and 0.590 for M2 with H_2O moderation and 0.555 for U2 and 0.538 for M2 with H_2O/H_3BO_3 moderation. The other contributors are an order of magnitude smaller.

Table 6.3 – Decomposition of U2 and M2's $c_{\Delta\rho}$ by nuclide.

H_2O				H_2O/H_3BO_3			
U2		M2		U2		M2	
Nuc./Reac.	$c_{\Delta\rho}$	Nuc./Reac.	$c_{\Delta\rho}$	Nuc./Reac.	$c_{\Delta\rho}$	Nuc./Reac.	$c_{\Delta\rho}$
$^{239}Pu/\bar{\nu}$	0.466	$^{239}Pu/\bar{\nu}$	0.590	$^{239}Pu/\bar{\nu}$	0.555	$^{239}Pu/\bar{\nu}$	0.538
$^{235}U/\bar{\nu}$	0.072	$^{239}Pu/\sigma_f$	0.059	$^{239}Pu/\sigma_f$	0.102	$^{235}U/\bar{\nu}$	0.068
$^{239}Pu/\sigma_f$	0.065	$^{235}U/\bar{\nu}$	0.049	$^{238}U/\sigma_c$	0.031	$^{239}Pu/\sigma_f$	0.063
$^{238}U/\sigma_c$	0.055	$^{240}Pu/\sigma_c$	0.038	$^{238}U/\bar{\nu}$	0.025	$^{240}Pu/\sigma_c$	0.028
$^{239}Pu/\sigma_c$	0.022	$^{235}U/\sigma_c$	0.036	$^{235}U/\bar{\nu}$	0.018	$^{239}Pu/\sigma_c$	0.024

Interestingly these rankings of $c_{\Delta\rho}$ by nuclide/reaction pair are similar to the rankings of σ_{rel} seen in Chapter 5, that is the same sets of nuclide/reaction pairs are seen in each ranking. This is because $c_{\Delta\rho}$ is an uncertainty based index with its premise being that because the bias is mostly due to input uncertainties, evaluating the similarity between the bias two systems should be based off of how similar the effect of input uncertainties is upon each system. Thus because most of the bias for the SFP and Proteus models comes from the uncertainties in these nuclide/reaction pairs, the similarity of their biases is also driven by these as well.

The dominance of $^{239}Pu/\bar{\nu}$ in the total value of $c_{\Delta\rho}$ was investigated by comparing the sensitivity profiles per unit lethargy between the SFP and Proteus for $^{239}Pu/\bar{\nu}$ and the next highest contributor to $c_{\Delta\rho}$, $^{235}U/\bar{\nu}$. This is done for H_2O moderated U2 in Figure 6.1 for $^{239}Pu/\bar{\nu}$ and Figure 6.2 for $^{235}U/\bar{\nu}$. The sensitivity profiles of $^{239}Pu/\bar{\nu}$ for each system are very similar, especially in the thermal range where the sensitivity coefficients are largest. From 1.0E-5 eV to 0.62 eV, the average relative difference between the sensitivity coefficients of the SFP and Proteus is 37%. The $^{235}U/\bar{\nu}$ sensitivity profiles show much larger differences, especially in the range of 1.0E-5 eV to 0.62 eV where the average relative difference between the sensitivity coefficients is 156%.

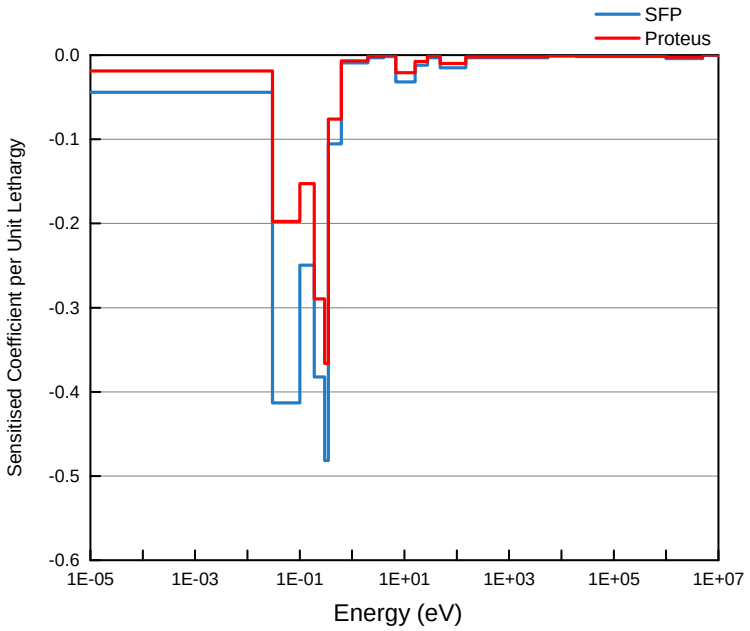

Figure 6.1 – Sensitivity coefficient of $^{239}Pu/\bar{\nu}$ for H_2O moderator for the response $\Delta\rho$.

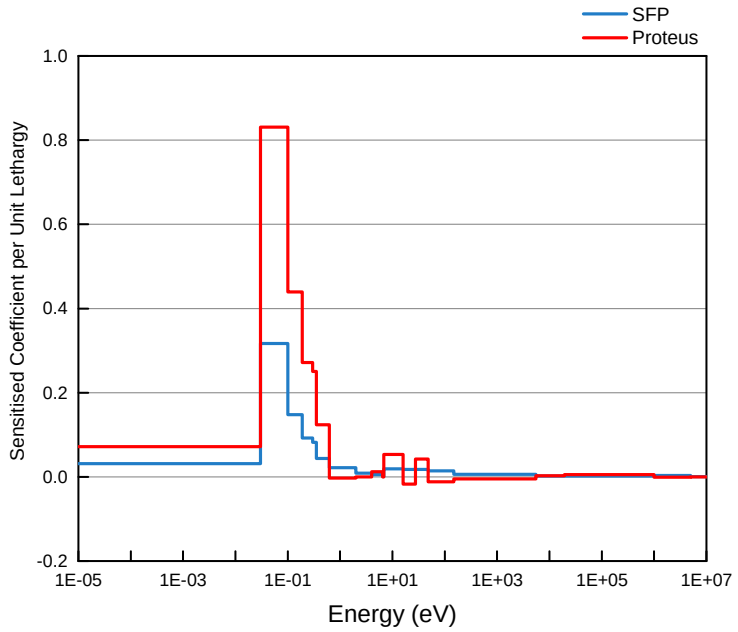

Figure 6.2 – Sensitivity coefficient of $^{235}U/\bar{\nu}$ for H_2O for the response $\Delta\rho$.

This sensitivity profile comparison highlights the second duality of $c_{\Delta\rho}$ as a representativity index: it is also sensitivity based. To have a high $c_{\Delta\rho}$, two systems must have similar sensitivities to a given input parameter as well, not only high uncertainties. The $1\sigma_{rel}$ uncertainties associated with $^{235}U/\bar{\nu}$ and $^{239}Pu/\bar{\nu}$ for H_2O moderated U2 are 0.66% and

0.80% (see Table 5.3). $^{239}Pu/\bar{\nu}$ does have higher uncertainty, but not significantly enough to explain the large difference in $c_{\Delta\rho}$. The large difference results from how dissimilar the sensitivity profiles of $^{235}U/\bar{\nu}$ are between the SFP model and the Proteus model. This illustrates how c_{res} behaves as both a sensitivity and uncertainty based representativity index: high representativity for evaluating similar bias behavior occurs when the systems have similar large uncertainties and similar sensitivities for a given parameter.

In summary different $c_{\Delta\rho}$ values from sample to sample and from nuclide/reaction pair to nuclide/reaction pair are caused by both varying magnitudes of uncertainty and by differences between sensitivity profiles. A nuclide/reaction pair that causes a high uncertainty in a given response for each system and of which each system has similar sensitivities will have a high c_{res} value. However nuclide/reaction pairs with high uncertainties for each systems but differing sensitivity profiles will have smaller c_{res} values, as was seen for $^{235}U/\bar{\nu}$.

Representativity Results for all H_2O Samples

The $c_{\Delta\rho}$ index was calculated for all H_2O moderated samples to illustrate how the index changes with burnup and with fuel type. Larger $c_{\Delta\rho}$ values are found for lower burnup samples and for the MOX samples in comparison to the UO_2 samples. This trend is similar to that of UQ, which is a logical result as $c_{\Delta\rho}$ is uncertainty based. The low burnup samples U1 and M1 have the highest uncertainties for their fuel types at 1.63% and 3.76% and also the largest $c_{\Delta\rho}$ values at 0.841 and 0.873 respectively.

Table 6.4 – $c_{\Delta\rho}$ for each sample with H_2O moderator.

Sample ID	$c_{\Delta\rho}$	DP σ_{b_c}	Burnup (MWd/kg)
U1	0.841	1.63%	∼38
U2	0.762	1.31%	∼54
U3	0.705	1.07%	∼71
U4	0.766	0.98%	∼75
U5	0.740	1.00%	∼91
U6	0.733	0.90%	∼92
U7	0.682	1.12%	∼121
M1	0.873	3.76%	∼21
M2	0.861	2.35%	∼44
M3	0.841	1.78%	∼64
M4	0.841	1.54%	∼72

For this moderating condition, none of the samples had sufficiently high $c_{\Delta\rho}$ values for Proteus to be deemed representative of the SFP model. Or in other words, no $c_{\Delta\rho}$ value was greater than 0.9. The conclusion is that based on this methodology, the LWR-PROTEUS phase II campaign currently cannot be used as a benchmark for the KKG SFP as both systems are modeled with CASMO-5 in the manner described in Chapter 4. This does not eliminate the possibility of the experimental campaign being able to be a benchmark for the SFP with a different code system or with CASMO-5 using a different modeling scheme.

If the M×N methodology was available for use in SHARK-X, a more realistic model of a SFP could be made without reflective boundary conditions on a single assembly. This could improve the representativity results by allowing the action that causes the change

in reactivity to be more similar to that in the Proteus system. In Proteus, a single pin is removed/inserted which introduces the change in reactivity. The rest of the system is static, i.e. it has a constant, fresh fuel composition. In the current SFP model, the reflective boundary conditions on the central fuel rack unit mean that when the fresh assembly is "replaced" with burnt assembly in the CASMO-5 models, what effectively occurs is a SFP of all fresh assemblies becomes all burnt assemblies, which is different behavior than is seen in Proteus. If an M×N model could be made, the models would simulate replacing a single fresh assembly with a single burnt assembly, the surrounding assemblies would be static with fresh composition. This modelling would more closely resemble the Proteus experiments. Additionally the modeling would be more realistic of fuel handling that would occur in the real SFP.

Chapter 7

Conclusions

This project successfully achieved many of the goals declared at its outset:

1. The literature concerning the SHARK-X utility, UQ/SA methodologies, and the LWR-PROTEUS Phase II experimental campaign were reviewed and synthesized.
2. CASMO-5 models of the LWR Proteus configuration were made by adapting existing CASMO-4E models. Additionally a comparison between their results was performed.
3. Stochastic sampling was applied to quantify the uncertainty due to input nuclear data and sample compositions uncertainties for all eleven samples and for each of the three moderating conditions.
4. Direct perturbation was successfully applied to quantify the uncertainty associated with input nuclear data for all experimental configurations.
5. Validation studies were done identifying that
   - Nine out of eleven H_2O moderated samples passed the validation test.
   - Four out of ten H_2O/H_3BO_3 moderated samples passed the validation test.
   - Three out of eleven D_2O/H_2O moderated samples passed the validation test.
6. A model of the KKG spent fuel pool was made based off of communications with the KKG fuel analysis team.
7. The UQ/SA results with DP calculations were successfully used to perform representativity analyses for evaluating the similarity of the Proteus experiments to the KKG spent fuel pool model.
8. The representativity analysis results for this modeling methodology were analyzed and found to be unsuccessful, but promising given the modeling approximations used.

Overall, the project was successful in its primary goal of applying the SHARK-X tool to a real world problem to perform UQ/SA for validation and representativity analysis. The validation studies showed good results for H_2O moderated samples and intimated that better results could be possible for the H_2O/H_3BO_3 and D_2O/H_2O moderated samples by using more accurate modelling methodologies. Likewise, the representativity analysis results could also be improved with more accurate modeling. A particularly interesting path for future work to improve the modeling would involve implementing compatibility in SHARK-X with the M×N feature in CASMO-5. If the representativity analysis results were sufficiently improved, the LWR-PROTEUS Phase II experimental campaign could then possibly be used as a benchmark for the KKG spent fuel pool or other spent fuel pools.

Bibliography

[1] "SCALE: A Modular Code System for Performing Standardized Computer Analyses for Licensing Evaluation." ORNL/TM-2005/39, Version 5.1, Vols. I–III, Oak Ridge National Laboratory, Oak Ridge, Tenn., November 2006.

[2] "MCNP–A General Monte Carlo N Particle Transport Code." Version 5, Vols. I–III, Oak Ridge National Laboratory, Oak Ridge, Tenn., February 2008.

[3] "CASMO-5 User's Manual Rev. 5." J. Rhodes, N. Gheorghiu, R.M. Ferrer, J. Hykes, T. Smed. SSP-07/431 Rev. 5, (2012)

[4] "American National Standard for Nuclear Criticality Safety in Operations with Fissionable Materials Outside Reactors, ANSI/ANS-8.1-1998." American Nuclear Society, La Grange Park, Ill., 1998.

[5] "American National Standard for Validation of Neutron Transport Methods for Nuclear Criticality Safety Calculations, ANSI/ANS-8.24-2007." American Nuclear Society, La Grange Park, Ill., 2007.

[6] "TSUNAMI Primer: A Primer for Sensitivity/Uncertainty Calculations with SCALE." B. T. Rearden, D. E. Mueller, S. M. Bowman, R. D. Busch, S. J. Emerson. ORNL/TM-2009/027. Oak Ridge National Laboratory, Oak Ridge, Tenn., January 2009.

[7] "CASMO-5MX: Tools for Sensitivity Analysis and Uncertainty Quantification with respect to Nuclear Data in CASMO-5M." W. Wieselquist. TM-41-12-09, Paul Scherrer Institut, Villigen, CH.

[8] "Application of Sensitivity/Uncertainty Methods to Burnup Credit Validation." D. E. Mueller and J. C. Wagner. Presented at the International Atomic Energy Agency (IAEA) Technical Committee Meeting on Advances in Applications of Burnup Credit to Enhance Spent Fuel Transportation, Storage, Reprocessing and Disposition. August 29 – September 2, 2005. London, UK

[9] Normal distribution and scales.gif. Wikipedia, The Free Encyclopedia. Wikimedia Foundation, Inc. 19 December 2005. Web. 1 June 2015. https://commons.wikimedia.org/wiki/File:Normal_distribution_and_scales.gif

[10] "CASMO-4E Analysis of Reactivity Worths of Burnt Fuel Samples Measured in LWR-PROTEUS Phase II." P. Grimm. TM-41-11–15, Paul Scherrer Institut, Villigen, CH. November 5, 2011.

[11] "PROTEUS FACILITY." Paul Scherrer Institut. 16 July 2012. Web. 18 June 2015. http://proteus.web.psi.ch/facility/

[12] "Proteus". Wikipedia, The Free Encyclopedia. Wikimedia Foundation, Inc. 3 June 2015. Web. 18 June 2015. https://en.wikipedia.org/?title=Proteus

[13] "LWR-PROTEUS PROGRAMME, PHASE II, FINAL REPORT." Ines Günther-Leopold, Judith Kobler Waldis, Niko Kivel, Hans-Peter Linder, Beat Wernli. TM-43-06-05, Paul Scherrer Institut, Villigen, CH. December, 2007.

[14] "Comparison of Calculated and Measured Isotopic Inventories for the LWR-PROTEUS Phase II Irradiated Fuel Samples." P. Grimm. TM-41-09-03, Paul Scherrer Institut, Villigen, CH. September 16, 2009.

[15] "LWR-PROTEUS PROGRAMME, Phase II Experimental Results." M.F. Murphy, G. Perret. TM-41-11-14, Paul Scherrer Institut, Villigen, CH. 26 July 2012.

[16] "ELCOS, The PSI Code System for LWR Core Analysis. Part II: User's Manual for the Fuel Assembly Code BOXER."J.M. Paratte, K. Foskolos, P. Grimm, J.M. Hollard. PSI Bericht Nr. 96-08 (1996).

[17] "Criticality Safety Applications of S/U Validation Methods." B. L. Broadhead, C. M. Hopper, K. R. Elam, B. T. Rearden, and R. L. Childs. Trans. Am. Nuc Winter Meeting, 2000, pp. 107–113.

[18] "Extended Interpretation of Sensitivity Data for Benchmark Areas of Applicability." S. Goluoglu, C. M. Hopper, and B. T. Rearden. Trans. Am. Nuc. "The Nuclear Technology Expansion: Unlimited Opportunities," 2003, pp. 77–79.

[19] "Uncertainty Quantification and Representativity Analysis of LWR-PROTEUS Phase III Experiments using CASMO-5MX." M. Hursin, M. Scriven. TM-41-13-26, Paul Scherrer Institut, Villigen, CH. 2013.

[20] "ENDF/B-VII.1 nuclear data for science and technology: cross sections, covariances, fission product yields and decay data." M.B. Chadwick et al. Nuclear Data Sheets, 112, 2887–2996 (2011).

[21] "Bestimmung der höchstuzlässigen Anreicherung im Kompaktlager des KKW Gösgen-Däniken mit Uran-Brennelementen." S. Pelloni. TM-41-00-30, Paul Scherrer Institut, Villigen, CH. October, 24 2000.

[22] "Methods of Steady-State Reactor Physics in Nuclear Design.' 'Stammler A.J.J., Abbate M.J.. Academic Press, 1983.

[23] "PSI Methodologies for Nuclear Data Uncertainty Propagation with CASMO-5M and MCNPX: Results for OECD/NEA UAM Benchmark Phase I." W. Wieselquist, T. Zhu, A. Vasiliev, H. Ferroukhi. Science and Technology of Nuclear Installations, Volume 2013.

[24] "Janis — A New Java-based Nuclear Data Display Program," OECD Nuclear Energy Agency (2001).

Appendix A: Uncertainty Quantification Example Exercise

An exercise is presented in this chapter to help develop an understanding of the SS and DP methods and where and why discrepancies between their results arise. Two example functions are used to highlight what happens when the methods are applied to linear and non-linear systems both with and without covariance between their variables. The variance of the functions is calculated in three ways:

1. Analytically,
2. With direct perturbation (DP),
3. And with stochastic sampling (SS).

The chosen example functions are Equations 1 and 2. Equation 1 is a linear application of the methods and Equation 2 is a non-linear application. The variables x_1 and x_2 are implemented as both fully correlated and fully uncorrelated random variables of uniform distributions. Fully uncorrelated variables means that their covariance is zero. With non-zero covariance, the calculations are more complex and the differences between SS and DP become more prominent.

$$f_1(x_1, x_2) = x_1 + x_2 \tag{1}$$

$$f_2(x_1, x_2) = x_1 * x_2 \tag{2}$$

A.1 Mean, Variance, and Covariance of x_1 and x_2

The expected value (mean) and variance of any continuous random variable are given by Equations 3 and 4 respectively, where x is a given random variable and $p(x)$ is that variable's probability density function (PDF).

$$E(x) = \int_{-\infty}^{\infty} xp(x)dx \tag{3}$$

$$Var(x) = \Delta_x^2 = E\Big[\big(x - E(x)\big)^2\Big] \tag{4}$$

Equations 3 and 4 can then be applied to a hypothetical uniform distribtuion, $f(x)$, seen in Figure A.1 and defined with the PDF given by Equation 5. The random variables x_1 and x_2 in Equations 1 and 2 are defined with α_{x_1} and β_{x_1} being equal to 1.0 and 2.0 respectively, and α_{x_2} and β_{x_2} 3.0 and 5.0 respectively.

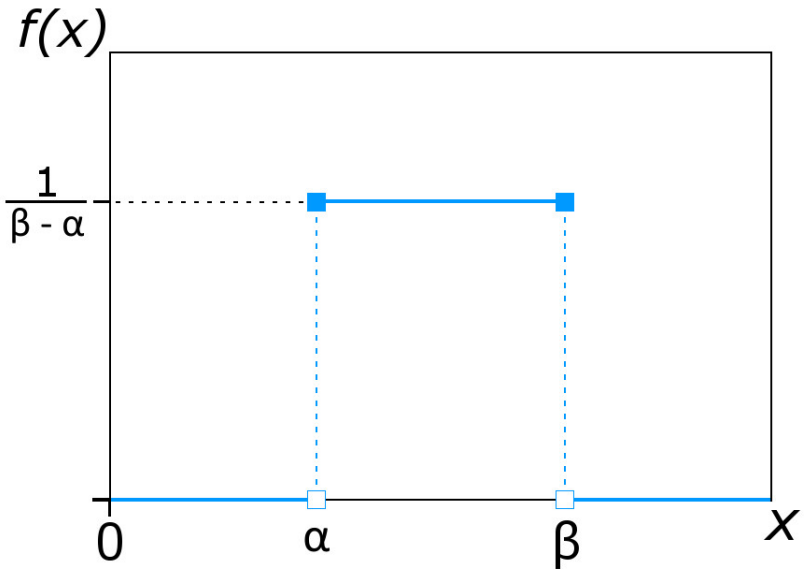

Figure A.1 – Hypothetical uniform distribution.

$$f(x) = \begin{cases} \frac{1}{\beta-\alpha}, & \text{if } \alpha \leq x \leq \beta. \\ 0, & \text{otherwise.} \end{cases} \tag{5}$$

In the case where there are two or more variables like in Equations 1 and 2, a *covariance* between any two of these variables exists, which is a measure of how much the two variables change together. For two random variables x and y, their covariance is given by Equation 6. If their covariance is positive, the variables show similar behavior, i.e. greater values in one variable correspond to greater values in the second variable, or vice versa. Negative covariance indicates greater values in one variable correspond to smaller values in the second variable. The degree of this correlation between the variables is described by a *correlation coefficient*, $\rho_{x,y}$, seen in Equation 7. Here $\Delta_{x,y}$ is the covariance between x and y and Δ_x and Δ_y are the standard deviations of x and y respectively. If $\rho_{x,y}$ is equal to 1.0 there is a total positive correlation between the variables, if it is 0 there is no correlation, and 1.0 there is total negative correlation. A $\rho_{x,y} = 0$, or fully uncorrelated variables, implies that the the covariance is 0. A $\rho_{x,y} = 1.0$, or positively and fully correlated variables, means that the covariance is equal to the product of each variable's standard deviation.

$$\text{cov}(x, y) = \Delta_{x,y} = E\Big[\big(x - E(x)\big)\big(y - E(y)\big)\Big] \tag{6}$$

$$\rho_{x,y} = \frac{\Delta_{x,y}}{\Delta_x \Delta_y} \tag{7}$$

Thus for the random variables x_1 and x_2, Equations 3, 4, and 6 are used to calculate their corresponding mean values, variances, and the covariance between the variables. These values for x_1 and x_2 are shown in Table A.1.

Table A.1 – Expected values, variances, and covariance for the random variables x_1 and x_2.

	x_1	x_2
Expected Value, $E(x)$	$\frac{3}{2}$	4
Variance, Δ_x^2	$\frac{1}{12}$	$\frac{1}{3}$
Covariance, Δ_{x_1,x_2}	$\frac{1}{6}$	

A.2 Variance with Taylor Series Expansion

The DP method introduces error into the calculation of a function's variance because it is a first-order approximation. Using a Taylor series expansion to analytically calculate the variance is interesting because it highlights which terms are first order and which are second order, and thus it is easy to identify which terms are being neglected in the DP method's approximation. The Taylor series expansion for a function's variance is explained in this section and is later applied in Sections A.3 and A.4 to calculate the variances of the given linear and nonlinear examples.

The variance of a function of multiple random variables can be calculated with Equation 4 by using the function as the main argument x. However an alternative method using a Taylor series expansion can be done by supposing that there is a function x of at least two variables, u and v, shown in Equation 8. The function x has a most probable value, $\bar{x}$, that comes from the most probable values of its variables, $\bar{u}$ and $\bar{v}$, shown in Equation 9. The value $\bar{x}$ has an associated uncertainty due to the spread of its individual values, x_i shown in Equation 10, which is caused by the combination of the spread of its variables, u_i and v_i.

$$x = f(u, v, ...) \tag{8}$$

$$\bar{x} = f(\bar{u}, \bar{v}, ...) \tag{9}$$

$$x_i = f(u_i, v_i, ...) \tag{10}$$

In the limit of an infinite number of measurements, the distribution of x about its mean can be quantified by its variance, Δ_x^2, shown in Equation 11.

$$\Delta_x^2 = \lim_{N\to\infty}\left[\frac{1}{N}\sum(x_i - \bar{x})^2\right] \tag{11}$$

An expression for the variance as a function of the component variables, u and v, is desired rather than with the term $x_i - \bar{x}$, which is the error in that individual x_i value. This can be found by doing a Taylor series expansion on x, shown in Equation 12. This is done about the point of the averages of u and v, meaning that each partial derivative is evaluated while the other variable is fixed at its mean. This new expression for the error of x can then be plugged in to Equation 11 to calculate the variance seen in Equation 13 which is then expanded to Equation 14.

$$x_i - \bar{x} \approx (u_i - \bar{u})\frac{\delta x}{\delta u}\Big|_{\bar{u},\bar{y}} + (v_i - \bar{v})\frac{\delta x}{\delta v}\Big|_{\bar{u},\bar{y}} + \dots \tag{12}$$

$$\Delta_x^2 \approx \lim_{N\to\infty} \frac{1}{N}\left[(u_i - \bar{u})\frac{\delta x}{\delta u}\Big|_{\bar{u},\bar{y}} + (v_i - \bar{v})\frac{\delta x}{\delta v}\Big|_{\bar{u},\bar{y}} + \dots\right]^2 \tag{13}$$

$$\begin{aligned}\Delta_x^2 \approx \lim_{N\to\infty} \frac{1}{N}\Bigg[&(u_i - \bar{u})^2\Big(\frac{\delta x}{\delta u}\Big|_{\bar{u},\bar{y}}\Big)^2 + (v_i - \bar{v})^2\Big(\frac{\delta x}{\delta v}\Big|_{\bar{u},\bar{y}}\Big)^2 + \\ &2(u_i - \bar{u})(v_i - \bar{v})\frac{\delta x}{\delta u}\Big|_{\bar{u},\bar{y}}\frac{\delta x}{\delta v}\Big|_{\bar{u},\bar{y}} + \dots\Bigg]\end{aligned} \tag{14}$$

Next, the terms in Equation 14 can be replaced by the definitions for the variance of u and v, Δ_u and Δ_v, as seen in Equation 15, and for the covariance between u and v, $\Delta_{u,v}$, as seen in Equation 16. This gives a new expression, Equation 17, for the variance of x with only the first-order terms of the Taylor expansion shown. Equation 17 can then be used for functions that are represented by x to calculate the variance of the given function, which will be done for the example functions $f_1(x_1, x_2)$ and $f_2(x_1, x_2)$ in the following sections.

$$\begin{aligned}\Delta_u^2 &= \lim_{N\to\infty}\left[\frac{1}{N}\sum(u_i - \bar{u})^2\right] \\ \Delta_v^2 &= \lim_{N\to\infty}\left[\frac{1}{N}\sum(v_i - \bar{v})^2\right]\end{aligned} \tag{15}$$

$$\Delta_{uv} = \lim_{N\to\infty}\left[\frac{1}{N}\sum(u_i - \bar{u})(v_i - \bar{v})\right] \tag{16}$$

$$\Delta_x^2 \approx \Delta_u^2\Big(\frac{\delta x}{\delta u}\Big|_{\bar{u},\bar{y}}\Big)^2 + \Delta_v^2\Big(\frac{\delta x}{\delta v}\Big|_{\bar{u},\bar{y}}\Big)^2 + 2\Delta_{uv}\frac{\delta x}{\delta u}\Big|_{\bar{u},\bar{y}}\frac{\delta x}{\delta v}\Big|_{\bar{u},\bar{y}} + \dots \tag{17}$$

A.3 Linear Example: $f_1(x_1, x_2) = x_1 + x_2$

Presented in this section are the analytical, DP, and SS solutions for the variance of the function $f_1(x_1, x_2)$, or Equation 1. The variance is calculated for when the variables x_1 and x_2 are fully uncorrelated and positively, fully correlated. This example shows that the analytical, DP, and SS solutions for the variance of $f_1(x_1, x_2)$ are equivalent for a linear function.

A.3.1 Analytical Solution

The mean of $f_1(x_1, x_2)$ is calculated with Equation 1 and is shown as Equation 18. The variance of $f_1(x_1, x_2)$ is calculated using the Taylor series seen in Equation 17, evaluated at the means of x_1 and x_2. Because the function is linear, the Taylor series expansion has only first-order terms, as is shown in Equation 19. Evaluating the derivatives in Equation 19 leads to Equation 20 for the variance of $f_1(x_1, x_2)$. The mean and variance of $f_1(x_1, x_2)$ with correlated x_1 and x_2 variables are calculated using the values found in Table A.1 and are 5.50 and 0.75 respectively.

$$\bar{f_1}(x_1, x_2) = \bar{x_1} + \bar{x_2} \tag{18}$$

$$\Delta_{f_1}^2 = \Delta_{x_1}^2\Big(\frac{\delta f_1}{\delta x_1}\Big|_{\bar{x_1},\bar{x_2}}\Big)^2 + \Delta_{x_2}^2\Big(\frac{\delta f_1}{\delta x_2}\Big|_{\bar{x_1},\bar{x_2}}\Big)^2 + 2\Delta_{x_1,x_2}\frac{\delta f_1}{\delta x_1}\Big|_{\bar{x_1},\bar{x_2}}\frac{\delta f_1}{\delta x_2}\Big|_{\bar{x_1},\bar{x_2}} \tag{19}$$

$$\Delta_x^2 = \Delta_{x_1}^2 + \Delta_{x_2}^2 + 2\Delta_{x_1,x_2} \tag{20}$$

If the variables x_1 and x_2 are assumed to be uncorrelated and thus their covariance is 0, the $2\Delta_{x_1,x_2}$ term vanishes from Equation 20 leading to Equation 21. The variance calculated with Equation 21 is 0.42. The decreased variance from 0.75 to 0.42 shows that considering covariance (if it exists) between variables is very important in evaluating the uncertainty of a system.

$$\Delta_x^2 = \Delta_{x_1}^2 + \Delta_{x_2}^2 \tag{21}$$

A.3.2 Direct Perturbation Solution

With the DP method, the variance of $f_1(x_1, x_2)$ is taken from the output VCM obtained from the sandwich rule, or Equation 3.5. The sensitivity coefficient vector, $\mathbf{S}$, used in the sandwich rule is evaluated at the mean values for x_1 and x_2 as seen in Equation 22. The input VCM, $\mathbf{V_{in}}$, is made up of the variance and covariance terms of $f_1(x_1, x_2)$.

$$\mathbf{S} = \begin{bmatrix} \frac{\delta f}{\delta x_1}\Big|_{\bar{x_1},\bar{x_2}} & \frac{\delta f}{\delta x_2}\Big|_{\bar{x_1},\bar{x_2}} \end{bmatrix} \tag{22}$$

$$\mathbf{V_{in}} = \begin{bmatrix} \Delta_{x_1}^2 & \Delta_{x_1,x_2} \\ \Delta_{x_1,x_2} & \Delta_{x_2}^2 \end{bmatrix} \tag{23}$$

The evaluation of $\mathbf{S}$ for $f_1(x_1, x_2)$ gives Equation 24. The sandwich rule can then be applied for $f_1(x_1, x_2)$ and gives Equation 25. The solution for the variance seen in Equation 25 is identical to the analytical one seen in Equation 20. This shows that for this linear, fully and positively correlated function, the first-order approximation used with the DP method reproduces the analytical solution for the variance. The evaluation of Equation 25 using the values found in Table A.1 gives a variance of 0.75, equivalent to the analytically calculated variance.

$$\mathbf{S} = \begin{bmatrix} \frac{\delta f_1}{\delta x_1}\Big|_{\bar{x_1},\bar{x_2}} & \frac{\delta f_1}{\delta x_2}\Big|_{\bar{x_1},\bar{x_2}} \end{bmatrix} = \begin{bmatrix} 1 & 1 \end{bmatrix} \tag{24}$$

$$\mathbf{V_{out}} = \begin{bmatrix} 1 \\ 1 \end{bmatrix} \times \begin{bmatrix} \Delta_{x_1}^2 & \Delta_{x_1,x_2} \\ \Delta_{x_1,x_2} & \Delta_{x_2}^2 \end{bmatrix} \times \begin{bmatrix} 1 & 1 \end{bmatrix} = \Delta_{x_1}^2 + \Delta_{x_2}^2 + 2\Delta_{x_1,x_2} \tag{25}$$

If the variables are uncorrelated, the $\mathbf{V_{in}}$ matrix is simplified by making the covariance term, Δ_{x_1,x_2}, equal to 0. The sandwich rule is applied again to $f_1(x_1, x_2)$ with uncorrelated variables giving Equation 26. This solution is also identical to the analytical solution seen in Equation 21, showing again that the DP method reproduces the analytical solution. The evaluation of Equation 26 using the values found in Table A.1 gives a variance of 0.42, equivalent to analytically calculated variance.

$$\mathbf{V_{out}} = \begin{bmatrix} 1 \\ 1 \end{bmatrix} \times \begin{bmatrix} \Delta_{x_1}^2 & 0 \\ 0 & \Delta_{x_2}^2 \end{bmatrix} \times \begin{bmatrix} 1 & 1 \end{bmatrix} = \Delta_{x_1}^2 + \Delta_{x_2}^2 \tag{26}$$

A.3.3 Stochastic Sampling

Next the variance of $f_1(x_1, x_2)$ is evaluated using an implementation of the SS method in MATLAB. The correlation between the variables is important in determining how each

will be randomly sampled. If the samples are fully and positively correlated (i.e. the correlation coefficient, $\rho_{x,y} = 1.0$), they will use the same random number, u, as seen in Equation 27, where i is the i^{th} random sample from the sample set. The parameters α_x and β_x are the limits of the uniform distribution PDFs described in Section A.1, Equation 5. If the variables are fully uncorrelated (i.e. $\rho_{x,y} = 0$), separate random numbers, u_1 and u_2, for each variable must be generated as in Equation 28. Generating partially correlated, random uniform variables (i.e. $-1.0 < \rho_{x,y} < 0$ and $0 < \rho_{x,y} < 1.0$) is more difficult and requires the use of copulas to approximate the correlation during the random sampling. This is not done in this analysis.

$$x_1^i = \alpha_{x_1} + (\beta_{x_1} - \alpha_{x_1}) * u, \quad x_2^i = \alpha_{x_2} + (\beta_{x_2} - \alpha_{x_2}) * u \tag{27}$$

$$x_1^i = \alpha_{x_1} + (\beta_{x_1} - \alpha_{x_1}) * u_1, \quad x_2^i = \alpha_{x_2} + (\beta_{x_2} - \alpha_{x_2}) * u_2 \tag{28}$$

The MATLAB scripts for the simulations with fully correlated and fully uncorrelated variables are shown in Figures A.2 and A.3 respectively. The values for the mean and the variance of $f_1(x_1, x_2)$ produced with fully correlated variables are converging towards 5.5 and 0.75 after 1E6 samples. For the simulation with fully uncorrelated variables, the mean and variance converge towards 5.5 and 0.42 after 1E6 samples. This illustrates that for this linear example, the analytical, DP, and SS methods agree and both reproduce the analytical solution for the variance of the function.

```
n = 1e6;
alpha_x1 = 1;
beta_x1 = 2;
alpha_x2 = 3;
beta_x2 = 5;

for i = 1:n
   u = rand();
   x_1(i) = alpha_x1 + (beta_x1-alpha_x1)*u;
   x_2(i) = alpha_x2 + (beta_x2-alpha_x2)*u;
end

f_1 = x_1 + x_2;

fMean = mean(f_1)
fVar = var(f_1)
```

```
fMean =

    5.5014


fVar =

    0.7503
```

Figure A.2 – SS method applied to example $f_1(x_1, x_2)$ with fully correlated variables.

```
n = 1e6;
alpha_x1 = 1;
beta_x1 = 2;
alpha_x2 = 3;
beta_x2 = 5;

for i = 1:n
   u1 = rand();
   u2 = rand();
   x_1(i) = alpha_x1 + (beta_x1-alpha_x1)*u1;
   x_2(i) = alpha_x2 + (beta_x2-alpha_x2)*u2;
end

f_1 = x_1 + x_2;

fMean = mean(f_1)
fVar = var(f_1)
```

```
fMean =

    5.4991


fVar =

    0.4164
```

Figure A.3 – SS method applied to example $f_1(x_1, x_2)$ with fully uncorrelated variables.

A.4 Nonlinear Example: $f_2(x_1, x_2) = x_1 * x_2$

Presented in this section are the analytical, DP, and SS solutions for the variance of the function $f_2(x_1, x_2)$, or Equation 2. This example shows that for a simple, nonlinear function already there are divergences between the variance calculated analytically/with the SS method and the variance calculated by the DP method. Additionally, the time consuming analytical solution for the variance shows why the use of the DP and SS methods is valuable, especially if it were to be applied to more complicated, higher-order functions.

A.4.1 Analytical Solution

The mean of the product of two variables, for example xy, is described with the following derivation. First the terms Δx and Δy seen in Equation 29 are substituted for the values x and y as seen in Equation 30. Next in Equation 31, the expected value $E(xy)$ of the product of x and y is taken. Equation 31 is then simplified because the terms, $E(\Delta x)E(y)$ and $E(\Delta y)E(x)$ evaluate to zero as seen in Equation 32. Finally the mean of xy is given by Equation 33, with the covariance term, $\text{cov}(x, y)$, being described previously in Equation 6. This is then used to describe the mean of $f_2(x_1, x_2)$ as given by Equation 34, where the term Δ_{x_1,x_2} is the covariance between x_1 and x_2. For fully correlated and fully uncorrelated variables, the mean of $f_2(x_1, x_2)$ is 6.16 and 6.0 respectively.

$$\Delta x = x - E(x), \quad \Delta y = y - E(y) \tag{29}$$

$$xy = \big[\Delta x + E(x)\big]\big[\Delta y + E(y)\big] = \Delta x \Delta y + \Delta x E(y) + \Delta y E(x) + E(x)E(y) \tag{30}$$

$$E(xy) = E\big[\Delta x \Delta y\big] + E\big[\Delta x E(y)\big] + E\big[\Delta y E(x)\big] + E\big[E(x)E(y)\big] \tag{31}$$

$$E(\Delta x)E(y) = E\big[x - E(x)\big]E(y) = \big[E(x) - E(x)\big]E(y) = 0 \tag{32}$$

$$E(xy) = E(x)E(y) + E(\Delta x \Delta y) = E(x)E(y) + \mathrm{cov}(x, y) \tag{33}$$

$$\bar{f}_2(x_1, x_2) = \bar{x_1}\bar{x_2} + \Delta_{x_1,x_2} \tag{34}$$

Next the variance, $\Delta^2_{f_2}$, can be calculated with a Taylor series expansion, as seen in Equation 35. In this nonlinear case, the Taylor expansion around $\bar{x_1}$ and $\bar{x_2}$ includes second order terms, unlike in the linear Equation 19, which contains only first order terms. These second order terms are what will be later ignored in the DP method's prediction of the variance.

$$\begin{aligned}\Delta^2_{f_2} \approx \lim_{N\to\infty} \Bigg[&(x_{1,i} - \bar{x_1})\frac{\delta f_2}{\delta x_1}\Big|_{\bar{x_1},\bar{x_2}} + (x_{2,i} - \bar{x_2})\frac{\delta f_2}{\delta x_2}\Big|_{\bar{x_1},\bar{x_2}} + \\ &\frac{1}{2!}\Big[(x_{1,i} - \bar{x_1})^2\frac{\delta^2 f_2}{\delta x_1^2}\Big|_{\bar{x_1},\bar{x_2}} + (x_{2,i} - \bar{x_2})^2\frac{\delta^2 f_2}{\delta x_2^2}\Big|_{\bar{x_1},\bar{x_2}} + \\ &2(x_{1,i} - \bar{x_1})(x_{2,i} - \bar{x_2})\frac{\delta^2 f_2}{\delta x_1 x_2}\Big|_{\bar{x_1},\bar{x_2}}\Big]\Bigg]^2\end{aligned} \tag{35}$$

Expanding Equation 35 leads to Equation 36. For this function, the second derivative terms, $\frac{\delta^2 f_2}{\delta x_1^2}$ and $\frac{\delta^2 f_2}{\delta x_2^2}$, evaluate to zero and are not shown. This leaves only the first derivative terms, $\frac{\delta f_2}{\delta x_1}$ and $\frac{\delta f_2}{\delta x_2}$, and the mixed derivative term $\frac{\delta^2 f_2}{\delta x_1 x_2}$.

Then the definitions of variance and covariance given in Equations 15 and 16 are plugged in to Equation 36 to give Equation 37. Finally the derivatives are evaluated to give an analytical solution for the variance of $f_2(x_1, x_2)$ shown in Equation 38.

$$\begin{aligned}\Delta^2_{f_2} \approx \lim_{N\to\infty} \Bigg[&(x_{1,i} - \bar{x_1})^2\Big(\frac{\delta f_2}{\delta x_1}\Big|_{\bar{x_1},\bar{x_2}}\Big)^2 + (x_{2,i} - \bar{x_2})^2\Big(\frac{\delta f_2}{\delta x_2}\Big|_{\bar{x_1},\bar{x_2}}\Big)^2 + \\ &2(x_{1,i} - \bar{x_1})(x_{2,i} - \bar{x_2})\frac{\delta f_2}{\delta x_1}\Big|_{\bar{x_1},\bar{x_2}}\frac{\delta f_2}{\delta x_2}\Big|_{\bar{x_1},\bar{x_2}} + \\ &2(x_{1,i} - \bar{x_1})\frac{\delta f_2}{\delta x_1}\Big|_{\bar{x_1},\bar{x_2}}(x_{1,i} - \bar{x_1})(x_{2,i} - \bar{x_2})\frac{\delta^2 f_2}{\delta x_1 x_2}\Big|_{\bar{x_1},\bar{x_2}} + \\ &2(x_{2,i} - \bar{x_2})\frac{\delta f_2}{\delta x_2}\Big|_{\bar{x_1},\bar{x_2}}(x_{1,i} - \bar{x_1})(x_{2,i} - \bar{x_2})\frac{\delta^2 f_2}{\delta x_1 x_2}\Big|_{\bar{x_1},\bar{x_2}} + \\ &(x_{1,i} - \bar{x_1})^2(x_{2,i} - \bar{x_2})^2\Big(\frac{\delta^2 f_2}{\delta x_1 x_2}\Big|_{\bar{x_1},\bar{x_2}}\Big)^2\Bigg]\end{aligned} \tag{36}$$

$$\begin{aligned}\Delta^2_{f_2} = \Delta^2_{x_1}\Big(\frac{\delta f_2}{\delta x_1}\Big|_{\bar{x_1},\bar{x_2}}\Big)^2 + \Delta^2_{x_2}\Big(\frac{\delta f_2}{\delta x_2}\Big|_{\bar{x_1},\bar{x_2}}\Big)^2 + 2\Delta_{x_1,x_2}\frac{\delta f_2}{\delta x_1}\Big|_{\bar{x_1},\bar{x_2}}\frac{\delta f_2}{\delta x_2}\Big|_{\bar{x_1},\bar{x_2}} + \\ 2\Delta_{x_1}\Delta_{x_1,x_2}\frac{\delta f_2}{\delta x_1}\Big|_{\bar{x_1},\bar{x_2}}\frac{\delta f_2}{\delta x_1 x_2}\Big|_{\bar{x_1},\bar{x_2}} + 2\Delta_{x_2}\Delta_{x_1,x_2}\frac{\delta f_2}{\delta x_2}\Big|_{\bar{x_1},\bar{x_2}}\frac{\delta^2 f_2}{\delta x_1 x_2}\Big|_{\bar{x_1},\bar{x_2}} + \\ \Delta^2_{x_1}\Delta^2_{x_2}\Big(\frac{\delta^2 f_2}{\delta x_1 x_2}\Big|_{\bar{x_1},\bar{x_2}}\Big)^2\end{aligned} \tag{37}$$

$$\Delta^2_{f_2} = \Delta^2_{x_1}\bar{x_2}^2 + \Delta^2_{x_2}\bar{x_1}^2 + 2\Delta_{x_1,x_2}\bar{x_1}\bar{x_2} + \Delta^2_{x_1}\Delta^2_{x_2} \tag{38}$$

The variance of $f_2(x_1, x_2)$ is calculated to 4.11 with Equation 38 and the values found in Table A.1, assuming the variables x_1 and x_2 are fully correlated. If $f_2(x_1, x_2)$ is to have uncorrelated variables, the covariance term Δ_{x_1,x_2} is equal to zero and the variance of $f_2(x_1, x_2)$ reduces to Equation 39. The variance is then calculated to be 2.11. Again illustrated in this example is the importance of considering covariance in the system when calculating the variance. For this nonlinear case, the effect is large causing an increase of 2.00 in the variance by including covariance terms.

$$\Delta_{f_2}^2 = \Delta_{x_1}^2 \bar{x_2}^2 + \Delta_{x_2}^2 \bar{x_1}^2 + \Delta_{x_1}^2 \Delta_{x_2}^2 \tag{39}$$

A.4.2 Direct Perturbation

DP is applied to $f_2(x_1, x_2)$ with the sensitivity coefficient vector and input VCM taking the forms of Equations 40 and 41 respectively. The sensitivity coefficient vector $\mathbf{S}$, is evaluated at the mean values of x_1 and x_2. The output VCM is calculated by applying the sandwich rule as shown in Equation 42.

$$\mathbf{S} = \begin{bmatrix} \frac{\delta f_2}{\delta x_1}\Big|_{\bar{x_1},\bar{x_2}} & \frac{\delta f_2}{\delta x_2}\Big|_{\bar{x_1},\bar{x_2}} \end{bmatrix} = \begin{bmatrix} \bar{x_2} & \bar{x_1} \end{bmatrix} \tag{40}$$

$$\mathbf{V_{in}} = \begin{bmatrix} \Delta_{x_1}^2 & \Delta_{x_1,x_2} \\ \Delta_{x_1,x_2} & \Delta_{x_2}^2 \end{bmatrix} \tag{41}$$

$$\mathbf{V_{out}} = \begin{bmatrix} \bar{x_2} \\ \bar{x_1} \end{bmatrix} \times \begin{bmatrix} \Delta_{x_1}^2 & \Delta_{x_1,x_2} \\ \Delta_{x_1,x_2} & \Delta_{x_2}^2 \end{bmatrix} \times \begin{bmatrix} \bar{x_2} & \bar{x_1} \end{bmatrix} = \Delta_{x_1}^2 \bar{x_2}^2 + 2\bar{x_2}\bar{x_1}\Delta_{x_1,x_2} + \Delta_{x_2}^2 \bar{x_1}^2 \tag{42}$$

When the DP-calculated form of $\Delta_{f_2}^2$, Equation 42, is compared to the analytical solution of Equation 38, obvious is the missing second-order term $\Delta_{x_1}^2 \Delta_{x_2}^2$. When the variance is evaluated with the values in Table A.1, $\Delta_{f_2}^2$ is calculated to be 4.09, less than the analytically calculated value of 4.11. This procedure is repeated again for uncorrelated x_1 and x_2 variables with $\mathbf{V_{in}}$ taking the form of Equation 43 and the resulting variance expression after applying the sandwich rule taking the form of Equation 44. The variance calculated with Equation 44 is 2.08, smaller than the analytical variance of 2.11. From this example, it is easy to see the discrepancies that appear when the DP method is applied to nonlinear functions.

$$\mathbf{V_{in}} = \begin{bmatrix} \Delta_{x_1}^2 & 0 \\ 0 & \Delta_{x_2}^2 \end{bmatrix} \tag{43}$$

$$\mathbf{V_{out}} = \begin{bmatrix} \bar{x_2} \\ \bar{x_1} \end{bmatrix} \times \begin{bmatrix} \Delta_{x_1}^2 & 0 \\ 0 & \Delta_{x_2}^2 \end{bmatrix} \times \begin{bmatrix} \bar{x_2} & \bar{x_1} \end{bmatrix} = \Delta_{x_1}^2 \bar{x_2} + \Delta_{x_2}^2 \bar{x_1} \tag{44}$$

A.4.3 Stochastic Sampling

The SS method was again implemented in MATLAB with the methodology previously described in Section A.3.3 and is shown in Figure A.4 and A.5 for fully correlated and uncorrelated variables respectively. The script for the fully correlated variables converges upon a mean of ∼6.16 and a variance of ∼4.10, identical to the analytical solution for this function. The script with fully uncorrelated variables similarly reproduces the analytical values of the mean and variance at ∼6.0 and ∼2.11 respectively. This implementation

shows the power of SS when the given problem is non-linear. With 1E6 samples the variance is converging upon the analytical values of the variance. This accuracy is possible because unlike with DP, no approximations are made in the SS calculation.

```
n = 1e6;
alpha_x1 = 1;
beta_x1 = 2;
alpha_x2 = 3;
beta_x2 = 5;

for i = 1:n
   u = rand();
   x_1(i) = alpha_x1 + (beta_x1-alpha_x1)*u;
   x_2(i) = alpha_x2 + (beta_x2-alpha_x2)*u;
   f_2(i) = x_1(i)*x_2(i);
end

fMean = mean(f_2)
fVar = var(f_2)
```

```
fMean =

    6.1663


fVar =

    4.1011
```

Figure A.4 – SS MATLAB script for $f_2(x_1, x_2)$ with fully correlated variables.

```
n = 1e6;
alpha_x1 = 1;
beta_x1 = 2;
alpha_x2 = 3;
beta_x2 = 5;

for i = 1:n
   u1 = rand();
   u2 = rand();
   x_1(i) = alpha_x1 + (beta_x1-alpha_x1)*u1;
   x_2(i) = alpha_x2 + (beta_x2-alpha_x2)*u2;
   f_2(i) = x_1(i)*x_2(i);
end

fMean = mean(f_2)
fVar = var(f_2)
```

```
fMean =

    5.9971


fVar =

    2.1124
```

Figure A.5 – SS MATLAB script for $f_2(x_1, x_2)$ with fully uncorrelated variables.

A.5 Summary

This exercise, presenting a linear and nonlinear function, shows in a simple way the discrepancies that exist between the variance quantified by the SS and DP methods. The variance results are summarized for each example function in Table A.2 as calculated analytically and with the SS and DP methods. For the linear application $f_1(x_1, x_2)$, the analytical, SS, and DP variance results agree. When the function is linear, the first-order approximation introduces no error, as there are no higher-order terms being neglected.

For the nonlinear application $f_1(x_1, x_2)$, differences between the analytical and SS results and the DP results emerge. This is due to terms ignored in the first-order approximation used in the DP method. It is easy to project to more complicated, nonlinear functions that the DP method's error can become larger and larger.

Additionally the effect of correlation between the variables in the example function was investigated. If the variables are fully correlated vs fully uncorrelated, the magnitude of the variance changes, no matter the method used to calculate it. With fully correlated variables, the variance is larger at 0.75 and 4.11 for $f_1(x_1, x_2)$ and $f_2(x_1, x_2)$ respectively. Meanwhile, for the fully uncorrelated variables, the variance is 0.42 and 2.11 respectively. These differences show the importance of considering correlation between variables when quantifying the uncertainty associated with a system.

Table A.2 – Summary of variance calculation exercise.

	$f_1(x_1, x_2)$		$f_2(x_1, x_2)$	
	Corr.	Uncorr.	Corr.	Uncorr.
Analytical	0.75	0.42	4.11	2.11
SS	∼0.75	∼0.42	∼4.10	∼2.11
DP	0.75	0.42	4.09	2.08

Appendix B: Derivation of Criticality Parameters and Non-linearity Effects

B.1 Absolute Reactivity Worth

The neutron transport equation for a multiplying medium can be described in its lambda-eigenvalue form as Equation 45. In this equation, **L** and **P** are the loss and production operators respectively in the Boltzmann equation, ϕ is the neutron flux, and λ is the fundamental lambda-eigenvalue for the multiplying medium, which by definition takes the form of Equation 46, where k is k_{inf} or k_{eff}.

$$(\mathbf{L} - \lambda\mathbf{P})\phi = 0 \tag{45}$$

$$\lambda = \frac{1}{k} \tag{46}$$

During the LWR-PROTEUS Phase II campaign, samples were inserted into the core to measure change in the reactivity, $\Delta\rho$, due to burnup products. The system, the Proteus reactor, is in a reference state before a sample is inserted and has a reference lambda-eigenvalue of λ_{ref}. This reference state is when the reference sample of 3.5% enriched UO_2 is in the core. The reactivity at this reference state is defined as Equation 47. A perturbed state is then created when when the reference sample is removed and a burnt sample is inserted into the core. The different composition of the sample causes a change in the **L** and **P** terms in Equation 45. These changes in the loss and production of neutrons leads to a new lambda-eigenvalue, λ_{pert}, of the perturbed system. The static reactivity of this perturbed system is then Equation 48. The absolute change in reactivity between the reference and perturbed states is therefore described by Equation 49.

$$\rho_{ref} = 1 - \lambda_{ref} \tag{47}$$

$$\rho_{pert} = 1 - \lambda_{pert} \tag{48}$$

$$\Delta\rho = \rho_{pert} - \rho_{ref} = \lambda_{ref} - \lambda_{pert} \tag{49}$$

Equation 49 gives the *absolute reactivity worth* ($\Delta\rho$) which is a response parameter investigated in the experimental campaign and in the UQ/SA presented in this report. The UQ/SA analysis requires the calculation of sensitivity coefficients of $\Delta\rho$ (and thus of

k/λ as well) with respect to perturbations of an input parameter, α. Given a perturbation to α, the sensitivity coefficients of k and λ, $S_{k,\alpha}$ and $S_{\lambda,\alpha}$, to this perturbation are defined as Equations 50 and 51 respectively. Replacing k in Equation 50 with λ leads to the relation seen in Equation 52, that $S_{k,\lambda}$ is equal to but opposite of $S_{\lambda,\alpha}$.

$$S_{k,\alpha} = \frac{\alpha_0}{k_0}\frac{\delta k}{\delta \alpha}\bigg|_{\alpha_0} \tag{50}$$

$$S_{\lambda,\alpha} = \frac{\alpha_0}{\lambda_0}\frac{\delta \lambda}{\delta \alpha}\bigg|_{\alpha_0} \tag{51}$$

$$S_{k,\alpha} = \frac{\alpha_0}{k_0}\frac{\delta}{\delta \alpha}\Big(k\Big)\bigg|_{\alpha_0} = \alpha_0\lambda_0\frac{\delta}{\delta \alpha_0}\Big(\frac{1}{\lambda_0}\Big)\bigg|_{\alpha_0} = -\frac{\alpha_0\lambda_0}{\lambda_0^2}\frac{\delta \lambda}{\delta \alpha}\bigg|_{\alpha_0} = -\frac{\alpha_0}{\lambda_0}\frac{\delta \lambda}{\delta \alpha}\bigg|_{\alpha_0} = -S_{\lambda,\alpha} \tag{52}$$

B.1.1 $\Delta\rho$ sensitivity coefficient

The sensitivity coefficient of $\Delta\rho$, $S_{\Delta\rho,\alpha}$, is written in Equation 53. The outputs of CASMO-5 are the responses k_{inf} and k_{eff} and are thus only inputs into SHARK-X to calculate sensitivity coefficients. Therefore in order to calculate $S_{\Delta\rho,\alpha}$, Equation 53 needs to be rewritten in terms of k. To do this, the definition of $\Delta\rho$ given in Equation 49 is used in Equation 54 to obtain $S_{\Delta\rho,\alpha}$ in terms of the reference and perturbed sensitivity coefficients of k, $S_{k,\alpha}^{ref}$ and $S_{k,\alpha}^{pert}$ respectively. Equation 54 is what is implemented in SHARK-X to calculate $S_{\Delta\rho,\alpha}$ for use in UQ/SA.

$$S_{\Delta\rho,\alpha} = \frac{\alpha_0}{\Delta\rho_0}\frac{\delta\Delta\rho}{\delta\alpha}\bigg|_{\alpha_0} = \frac{\alpha_0}{\Delta\rho_0}\left(\frac{\delta\rho_{pert}}{\delta\alpha}\bigg|_{\alpha_0} - \frac{\delta\rho_{ref}}{\delta\alpha}\bigg|_{\alpha_0}\right) \tag{53}$$

$$S_{\Delta\rho,\alpha} = \frac{\alpha_0}{\Delta\rho_0}\left(\frac{\delta\lambda_{ref}}{\delta\alpha}\bigg|_{\alpha_0} - \frac{\delta\lambda_{pert}}{\delta\alpha}\bigg|_{\alpha_0}\right) = \frac{1}{\Delta\rho}\Big(\lambda_{0,pert}S_{k,\alpha}^{pert} - \lambda_{0,ref}S_{k,\alpha}^{ref}\Big) \tag{54}$$

B.1.2 Linearity of $\Delta\rho$

As seen in Appendix 7, the DP method introduces some error in the calculation of variance due the first-order approximation in its definition. Because of this, it is important to assess the degree of non-linearity in response of interest when doing UQ/SA. SA applied to representativity analysis in particular can only been done with the DP method because the sensitivity coefficients created with the SS method have often large degrees of uncertainty associated with them. This section assesses the degree of non-linearity of $\Delta\rho$. First the Taylor series expansion of $\Delta\rho$ about the reference state of the input parameter, α_0, is done and is shown truncated to the third order in Equation 55.

$$\Delta\rho(\alpha) - \Delta\rho(\alpha_0) = (\alpha-\alpha_0)\frac{\delta\Delta\rho}{\delta\alpha}\bigg|_{\alpha_0} + \frac{1}{2!}(\alpha-\alpha_0)^2\frac{\delta^2\Delta\rho}{\delta\alpha^2}\bigg|_{\alpha_0} + ... \tag{55}$$

The first and second derivatives of $\Delta\rho$ are given by Equations 56 and 57 respectively. The second derivative of $\Delta\rho$ requires the use of the product rule. In the DP method, the response of k is assumed to be linear with respect to α. The second derivative is therefore reduced to 58, as the $\frac{\delta^2 k_{pert}}{\delta\alpha^2}$ and $\frac{\delta^2 k_{ref}}{\delta\alpha^2}$ terms are zero in a linear system.

$$\frac{\delta\Delta\rho}{\delta\alpha} = -\frac{1}{k_{ref}^2}\frac{\delta k_{ref}}{\delta\alpha} + \frac{1}{k_{pert}^2}\frac{\delta k_{pert}}{\delta\alpha} \tag{56}$$

$$\frac{\delta^2\Delta\rho}{\delta\alpha^2} = \frac{2}{k_{ref}^3}\left(\frac{\delta k_{ref}}{\delta\alpha}\right)^2 - \frac{1}{k_{ref}^2}\frac{\delta^2 k_{ref}}{\delta\alpha^2} - \frac{2}{k_{pert}^3}\left(\frac{\delta k_{pert}}{\delta\alpha}\right)^2 - \frac{1}{k_{ref}^2}\frac{\delta^2 k_{ref}}{\delta\alpha^2} + \frac{1}{k_{pert}^2}\frac{\delta^2 k_{pert}}{\delta\alpha^2} \quad (57)$$

$$\frac{\delta^2\Delta\rho}{\delta\alpha^2} = \frac{2}{k_{ref}^3}\left(\frac{\delta k_{ref}}{\delta\alpha}\right)^2 - \frac{2}{k_{pert}^3}\left(\frac{\delta k_{pert}}{\delta\alpha}\right)^2 \quad (58)$$

The importance of the second-order term, or Equation 58, and thus the non-linearity of the response is considered by comparing the magnitude of the first-order term to the second-order term with example values for λ and $S_{k,\alpha}$. These values are given in Table B.1 for a reference state and two perturbed states, where the perturbations are done upon $^{238}\mathrm{U}/\sigma_c$ nuclide reaction pair, and thus the sensitivity coefficient is $S_{k,^{238}\mathrm{U}/\sigma_c}$.

Table B.1 – Typical values for λ and $S_{k,\alpha}$ values for $^{238}\mathrm{U}/\sigma_c$ for a reference state and two perturbed states.

State	λ	$S_{k,^{238}\mathrm{U}/\sigma_c}$
Reference	0.76182	-0.292
Pert1	0.76426	-0.290
Pert2	0.76245	-0.291

This comparison is shown in Figure B.1 for relative perturbations of -10% to 10% of $^{238}\mathrm{U}/\sigma_c$. The second derivative term of absolute reactivity is much smaller than the first derivative term in all ranges of perturbations. Therefore, despite having non-linearities in its formulation, the absolute reactivity response can be assumed to behave as a linear function for small perturbations of a given parameter α. Therfore in the UQ presented in this report, the SS and DP methods should return close UQ results for this response.

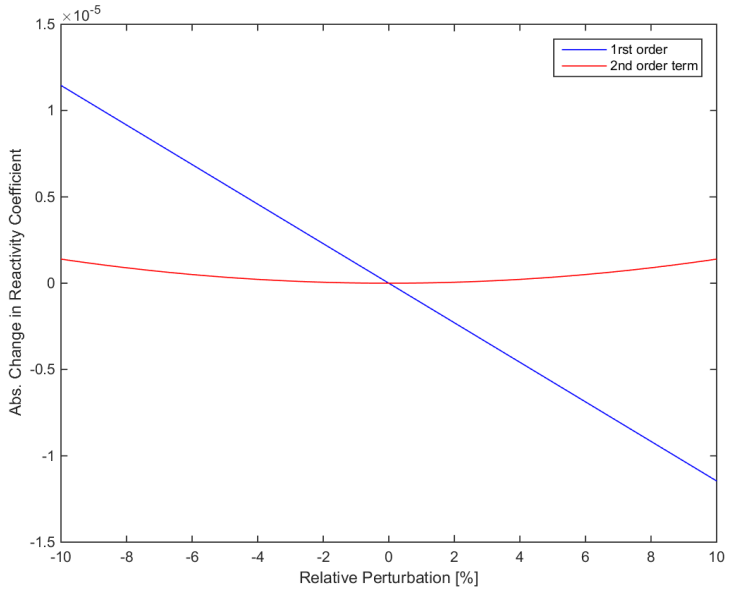

Figure B.1 – Evolution of the first and second order term of absolute reactivity's Taylor expansion with respect to the relative input uncertainty, for U-238 capture

B.2 Relative Reactivity Worth

During the experimental campaign, the absolute reactivity worth was normalized to a parameter called *relative reactivity worth* ($\Delta\rho^{rel}$) shown in Equation 2.2.

B.2.1 $\Delta\rho^{rel}$ Sensitivity Coefficient

The sensitivity coefficient of relative reactivity, $S_{\Delta\rho^{rel},\alpha}$, is also used in the UQ/SA done in this report. The SHARK-X utility calculates $S_{\Delta\rho^{rel},\alpha}$ from given the k_{inf} or k_{eff} response of the CAMSO-5 output. $S_{\Delta\rho^{rel},\alpha}$ is derived from Equation 3.2 and given as Equation 59, where α is a given input parameter that is perturbed from its reference state of α_0.

$$S_{\Delta\rho^{rel},\alpha} = \frac{\alpha_0}{\Delta\rho_0^{rel}} \frac{\delta\Delta\rho^{rel}}{\delta\alpha}\bigg|_{\alpha_0} \tag{59}$$

The derivative of term in $S_{\Delta\rho^{rel},\alpha}$ is given as Equation 60, where λ_r is from the reference state of the system, and λ_1 and λ_2 are two different perturbed states. The derivative is then evaluated using the quotient rule in Equation 61 and simplified to Equation 62

$$\frac{\delta\Delta\rho^{rel}}{\delta\alpha}\bigg|_{\alpha_0} = \frac{\delta}{\delta\alpha}\left(\frac{\lambda_r-\lambda_1}{\lambda_r-\lambda_2}\right)\bigg|_{\alpha_0} \tag{60}$$

$$\frac{\delta\Delta\rho^{rel}}{\delta\alpha}\bigg|_{\alpha_0} = \frac{1}{(\lambda_r-\lambda_2)^2}\left[(\lambda_{0,r}-\lambda_{0,2})\frac{\delta}{\delta\alpha}\left(\lambda_r-\lambda_1\right)\bigg|_{\alpha_0} - (\lambda_{0,r}-\lambda_{0,1})\frac{\delta}{\delta\alpha}\left(\lambda_r-\lambda_2\right)\bigg|_{\alpha_0}\right] \tag{61}$$

$$\frac{\delta\Delta\rho^{rel}}{\delta\alpha}\bigg|_{\alpha_0} = \frac{\lambda_{0,1}-\lambda_{0,2}}{(\lambda_r-\lambda_{0,2})^2}\frac{\delta\lambda_r}{\delta\alpha}\bigg|_{\alpha_0} + \frac{\lambda_{0,r}-\lambda_{0,2}}{(\lambda_r-\lambda_{0,2})^2}\frac{\delta\lambda_2}{\delta\alpha}\bigg|_{\alpha_0} - \frac{1}{(\lambda_{0,r}-\lambda_{0,2})}\frac{\delta\lambda_1}{\delta\alpha}\bigg|_{\alpha_0} \tag{62}$$

Equation 62 is then plugged into the definition of $S_{\Delta\rho^{rel},\alpha}$, or Equation 59, to obtain Equation 63. This allows for $S_{\Delta\rho^{rel},\alpha}$ to be calcualted in terms of λ. Next the sensitivity coefficient of λ, or Equation 51, and the definition of $\Delta\rho^{rel}$, Equation 2.2, are plugged into Equation 63 to obtain Equation 64. The relation between $S_{\lambda,\alpha}$ and $S_{k,\alpha}$ shown in Equation 52 is then used to obtain Equation 65. Equation 65 is implemented into SHARK-X to calculate the sensitivity coefficients for relative reactivity with DP.

$$S_{\Delta\rho^{rel},\alpha} = \frac{\alpha_0}{\Delta\rho_0^{rel}}\left[\frac{\lambda_{0,1}-\lambda_{0,2}}{(\lambda_{0,r}-\lambda_{0,2})^2}\frac{\delta\lambda_r}{\delta\alpha}\bigg|_{\alpha_0} + \frac{\lambda_{0,r}-\lambda_{0,2}}{(\lambda_r-\lambda_{0,2})^2}\frac{\delta\lambda_2}{\delta\alpha}\bigg|_{\alpha_0} - \frac{1}{\lambda_{0,r}-\lambda_{0,2}}\frac{\delta\lambda_1}{\delta\alpha}\bigg|_{\alpha_0}\right] \tag{63}$$

$$S_{\Delta\rho^{rel},\alpha} = \frac{\lambda_{0,r}(\lambda_{0,1}-\lambda_{0,2})}{(\lambda_{0,r}-\lambda_{0,1})(\lambda_{0,r}-\lambda_{0,2})}S_{\lambda_r,\alpha} - \frac{\lambda_{0,1}}{\lambda_{0,r}-\lambda_{0,1}}S_{\lambda_1,\alpha} + \frac{\lambda_{0,2}}{\lambda_{0,r}-\lambda_{0,2}}S_{\lambda_2,\alpha} \tag{64}$$

$$S_{\Delta\rho^{rel},\alpha} = -\frac{\lambda_{0,r}(\lambda_{0,1}-\lambda_{0,2})}{(\lambda_{0,r}-\lambda_{0,1})(\lambda_{0,r}-\lambda_{0,2})}S_{k_r,\alpha} + \frac{\lambda_{0,1}}{\lambda_{0,r}-\lambda_{0,1}}S_{k_1,\alpha} - \frac{\lambda_{0,2}}{\lambda_{0,r}-\lambda_{0,2}}S_{k_2,\alpha} \tag{65}$$

B.2.2 Linearity of $\Delta\rho^{rel}$

The definition of relative reactivity seen in Equation 2.2 shows that this parameter is nonlinear. Therefore there will be error introduced by the first-order approximation used in the DP method. The degree of this nonlinearity and the effect it has on the absolute value of $\Delta\rho^{rel}$ is investigated in this section. First, A Taylor series expansion of $\Delta\rho^{rel}(\alpha)$ truncated to the second order and evaluated at α_0 is done and is showed in Equation 66.

$$\Delta\rho^{rel}(\alpha) - \Delta\rho^{rel}(\alpha_0) = (\alpha-\alpha_0)\frac{\delta\Delta\rho^{rel}}{\delta\alpha}\bigg|_{\alpha_0} + \frac{1}{2!}(\alpha-\alpha_0)^2\frac{\delta^2\Delta\rho^{rel}}{\delta\alpha^2}\bigg|_{\alpha_0} + ... \tag{66}$$

$$\frac{\delta\lambda}{\delta\alpha}\bigg|_{\alpha} = -\lambda^2\frac{\delta k}{\delta\alpha}\bigg|_{\alpha} \tag{67}$$

The second derivative term in Equation 66 is redefined with the definition of relative reactivity, Equation 2.2, in Equation 68. The derivatives are then evaluated using the quotient rule and Equation 68 becomes Equation 69.

$$\frac{\delta^2\Delta\rho^{rel}}{\delta\alpha^2}\bigg|_{\alpha_0} = \frac{\delta^2}{\delta^2\alpha}\left(\frac{\Delta\rho_1}{\Delta\rho_2}\right)\bigg|_{\alpha_0} \tag{68}$$

$$\frac{\delta^2\Delta\rho^{rel}}{\delta\alpha^2}\bigg|_{\alpha_0} = \frac{1}{\Delta\rho_{0,2}}\frac{\delta^2\Delta\rho_1}{\delta\alpha^2}\bigg|_{\alpha_0} - \frac{\Delta\rho_{0,1}}{\Delta\rho_{0,2}^2}\frac{\delta^2\Delta\rho_2}{\delta\alpha^2}\bigg|_{\alpha_0} + 2\frac{\Delta\rho_{0,1}}{\Delta\rho_{0,2}^3}\left(\frac{\delta\Delta\rho_2}{\delta\alpha}\bigg|_{\alpha_0}\right)^2 \tag{69}$$

Using Equation 56 for the first derivative term of $\Delta\rho$ and Equation 58 for the second derivative terms, each of the derivative terms in Equation 69 are evaluated giving Equation 70

$$\begin{aligned}\frac{\delta^2\Delta\rho^{rel}}{\delta\alpha^2}\bigg|_{\alpha_0} = \frac{1}{\Delta\rho_{0,2}}\left(-\frac{2}{k_{0,1}^3}\left(\frac{\delta k_1}{\delta\alpha}\bigg|_{\alpha_0}\right)^2 + \frac{2}{k_{0,r}^3}\left(\frac{\delta k_2}{\delta\alpha}\bigg|_{\alpha_0}\right)^2\right) - \\ \frac{\Delta\rho_{0,1}}{\Delta\rho_{0,2}^2}\left(-\frac{2}{k_{0,2}^3}\left(\frac{\delta k_2}{\delta\alpha}\bigg|_{\alpha_0}\right)^2 + \frac{2}{k_{0,r}^3}\left(\frac{\delta k_r}{\delta\alpha}\bigg|_{\alpha_0}\right)^2\right) + \frac{2\Delta\rho_{0,1}}{\Delta\rho_{0,2}^3}\left(-\frac{1}{k_{0,2}^2}\frac{\delta k_2}{\delta\alpha}\bigg|_{\alpha_0} + \frac{1}{k_{0,r}^2}\frac{\delta k_r}{\delta\alpha}\bigg|_{\alpha_0}\right)\end{aligned} \tag{70}$$

The $\Delta\rho$ terms in Equation 70 can be then replaced by their expressions as a function of λ to give Equation 71.

$$\begin{aligned}\frac{\delta^2\Delta\rho^{rel}}{\delta\alpha^2} = -\frac{2\lambda_{0,1}^3}{(\lambda_{0,r}-\lambda_{0,2})}\left(\frac{\delta k_1}{\delta\alpha}\bigg|_{\alpha_0}\right)^2 + \frac{2\lambda_{0,2}^3}{(\lambda_{0,r}-\lambda_{0,2})}\left(\frac{\delta k_r}{\delta\alpha}\bigg|_{\alpha_0}\right)^2 \\ + \frac{2(\lambda_{0,r}-\lambda_{0,1})\lambda_{0,2}^3}{(\lambda_{0,r}-\lambda_{0,2})^2}\left(\frac{\delta k_2}{\delta\alpha}\bigg|_{\alpha_0}\right)^2 - \frac{2(\lambda_{0,r}-\lambda_{0,2})\lambda_{0,2}^3}{(\lambda_{0,r}-\lambda_{0,2})^2}\left(\frac{\delta k_2}{\delta\alpha}\bigg|_{\alpha_0}\right)^2 + \\ \frac{2(\lambda_{0,r}-\lambda_{0,1})}{(\lambda_{0,r}-\lambda_{0,2})^3}\left(\lambda_{0,2}^4\left(\frac{\delta k_2}{\delta\alpha}\bigg|_{\alpha_0}\right)^2\lambda_{0,2}^4\left(\frac{\delta k_r}{\delta\alpha}\bigg|_{\alpha_0}\right)^2 + 2\lambda_{0,2}^4\left(\frac{\delta k_2}{\delta\alpha}\bigg|_{\alpha_0}\right)^2 + \lambda_{0,r}^2\lambda_{0,2}^2\frac{\delta k_2}{\delta\alpha}\bigg|_{\alpha_0}\frac{\delta k_r}{\delta\alpha}\bigg|_{\alpha_0}\right)\end{aligned} \tag{71}$$

$$\alpha_0^2\frac{\delta^2\Delta\rho^{rel}}{\delta\alpha^2} = \frac{2}{\lambda_r-\lambda_2}\left(\lambda_r S_{k_r}^2 - \lambda_1 S_{k_1}^2\right)^2 + \frac{2\lambda_r\lambda_2(\lambda_r-\lambda_1)}{(\lambda_r-\lambda_2)^3}\left(\lambda_r S_{k_r} - \lambda_2 S_{k_2}\right) \tag{72}$$

The importance of the second-order term of $\Delta\rho^{rel}$ and thus the non-linearity of the response is considered by comparing the magnitude of the first-order term to the second-order term with example values for λ and $S_{k,\alpha}$ previously seen in Table B.1. Using these values, the magnitude of the first and second order terms of Equation 66 are evaluated to be 1.5 and -31.6 respectively for a 1% perturbation to the $^{238}U/\sigma_c$ pair. Additionally the behaviour of these terms for perturbations of -10% to 10% is shown in Figure B.2. The second derivative term is significant even for small perturbation (1%) with respect to its first derivative term. This means that the relative reactivity response is not behaving as a linear function for small perturbations and therefore errors will be introduced when the UQ is performed for this term with the DP method. Thus the SS and DP methods will calculate different UQ results for relatice reactivity.

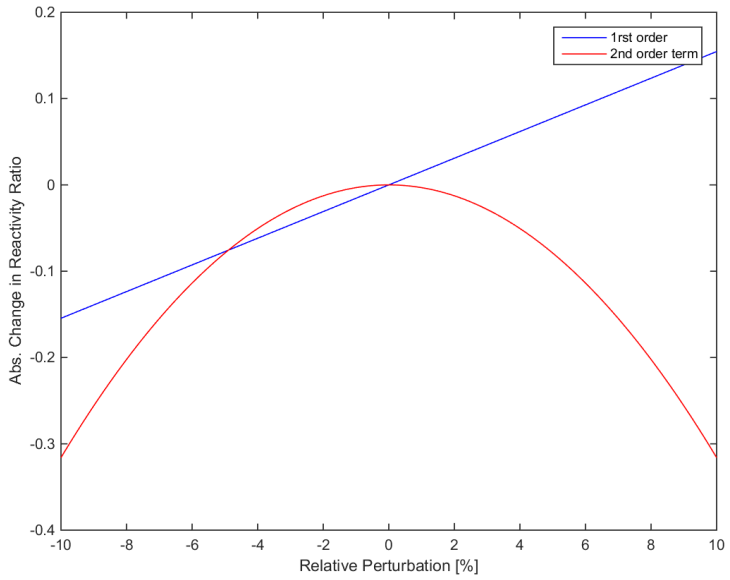

Figure B.2 – Evolution of the first and second order term of relative reactivity's Taylor expansion with respect to the relative input uncertainty, for U-238 capture.

Appendix C: Numerical Precision of Sensitivity Coefficients and Representativity Indices

CASMO-5 has numerical precision to the fifth digit after the decimal point, or at 1 pcm if the given value is k_{eff}. Sensitivity coefficients and representativity indices are derived from k_{eff}, and will therefore have the numerical uncertainty associated with k_{eff} propagated to their values. These numerical uncertainties had to be considered when results were reported in this analysis.

A simple exercise was done to propagate the uncertainty associated with k_{eff} at the sixth decimal place through to sensitivity coefficients and representativity indices. To do this, two systems were chosen, called 1 and 2. Both systems start at a reference k_{eff} value, k_{ref}, of 1.00000. Hypothetical perturbations were then applied to 1 and 2 that changed their k_{eff} value to $k_1 = 0.99940$ and $k_2 = 0.99910$. The sensitivity coefficient is then calculated as seen in Equation 3.2 for a given relative perturbation.

Next a uniform distribution probability density function (PDF) was assumed to exist from [0, 1E-6] that describes the probability of the value that the sixth digit after the decimal point will assume. The PDF was then randomly sampled 1,000 times using Equation 73 to generate the sixth digit of k_{eff}, x^i, for k_{ref}, k_1, and k_2. Here 1,000 random numbers, u^i, were generated and the limits of the uniform distribution $\alpha = 0$ and $\beta =$ 1E-6 were used. This created a sample set of 1,000 k_{eff} values for each k_{eff} parameter. Equation 3.2 is then used with these sample sets to create two sets of 1,000 sensitivity coefficients for k_{eff}, S^i. The relative perturbations were arbitrarily chosen to be 1.00%, 5.00%, 10.00%, and 0.10%.

$$x^i = \alpha + (\beta - \alpha) * u^i \tag{73}$$

The mean and standard deviation of the sensitivity coefficients were then calculated and are presented in Table C.1. Seen is that the magnitude of absolute uncertainty, σ, associated with the the sensitivity coefficients is dependent on the size of the perturbation. Because in the DP method in SHARK-X the perturbations are the order of 1.00-10.00%, the quoted uncertainty for sensitivity coefficients was chosen to be reported at the third digit after the fourth digit after the decimal.

Table C.1 – Uncertainty associated with SC with varying relative perturbations for systems 1 and 2.

	k_1		k_2	
Rel. Pert.	SC	1σ	SC	1σ
1.00%	0.06000	0.00125	0.09000	0.00082
5.00%	0.01200	0.00025	0.01800	0.00016
10.00%	0.00600	0.00013	0.00900	0.00008
0.10%	0.60000	0.01251	0.90000	0.00817

Next the representativity of systems 1 to itself and to system 2 was evaluated using Equation 3.13, where i and j are systems 1 and 1 or systems 1 and 2 respectively. Because the two systems are fully uncorrelated, the covariance term $\sigma_{i,j}$ in the numerator is equal to the multiplication term of the standard deviations term, $\sigma_i\sigma_j$ in the denominator and c_k evaluates to 1.0. Therefore the uncertainty associated with c_k is just that associated with the propagation of the the sensitivity coefficients through the sandwich rule to calculate σ_1 and σ_2. This was done assuming an input uncertainty of 10.00% (which is used in the input VCM in the sandwich rule) and the results for each perturbation are shown in Table C.2. Evident is that for c_k, uncertainty is given to the third digit after the decimal place on its value. Additionally the uncertainties are independent of the perturbation size for these simple, uncorrelated systems.

Table C.2 – Calculated c_k for each system with varying relative perturbations.

Rel. Pert.	k_1 vs. k_1 c_k 1σ	k_1 vs. k_2 c_k 1σ
1.00%	0.00293	0.00260
5.00%	0.00293	0.00260
10.00%	0.00293	0.00260
0.10%	0.00293	0.00260